5.4.2.3.1 Phase Partitioning—Typically, VOCs in the vadose zone will partition into all phases, seeking an equilibrium condition. The relative amount of chemical in two neighboring phases in equilibrium is described by partition coefficients. Partitioning between vapor and aqueous phases is described by Henry's law. Henry's Law coefficients, shown in Table 5-2, are simply the vapor pressure of pure compound divided by the aqueous solubility.

Partitioning of VOCs between the aqueous and solid phases often is described using a distribution coefficient, which assumes sorption is linear and reversible. The distribution coefficient for VOCs is simply the product of the organic carbon partition coefficients (mL/g) and the fraction of organic carbon in the soil (dimensionless). The amount of sorption, therefore, depends strongly on the type of geologic material (especially the amount of organic carbon), and the type of chemical constituents dissolved in water. In the model, sorption was assumed to occur in sediment, based on an organic carbon content value of 0.05% reported by Colwell (1988). Sorption in basalt was considered negligible. Organic carbon partition coefficients are shown in Table 5-2.

5.4.2.3.2 Gaseous Transport—Gaseous- or vapor-phase migration in the vadose zone is typically much more rapid than aqueous transport. The rate of vapor transport strongly depends on soil-moisture content. Soil moisture will retard vapor migration by reducing the pore space available for vapor movement and through partitioning of the vapor phase into the aqueous phase. The relatively dry nature of the SDA suggests that vapor transport is an important transport mechanism.

Vapor diffusion in porous media is described by Fick's first law, which states that the contaminant flux is proportional to the concentration gradient. The proportionality constant is called the effective diffusion coefficient. In a porous medium, contaminant molecules must travel longer diffusion paths because of the structure of the medium and moisture in the pore space. To account for the longer diffusion paths, the effective diffusion coefficient is the product of the free-air diffusion coefficient and the gas- or air-filled porosity, divided by a parameter of the medium called the tortuosity. Free-air diffusion coefficients are presented in Table 5-2. Gaseous-phase tortuosity values were an important calibration parameter. Initial estimates of tortuosity were calculated using an expression derived by Millington (1959). These values were adjusted as part of the model calibration process and are discussed in Section 5.4.4.2.

Table 5-2. Volatile organic compound chemical and transport properties.

Property	Carbon Tetrachloride	Tetrachloroethylene	Methylene Chloride	1,4-Dioxane
Molecular weight (g/mole)	154	166	85	88
Density (kg/m^3)	1,584	1,631	1,335	1,033
Henry's constant (nondim)	0.75	0.442	0.058	0.00021
Organic carbon partition coefficient, K_{oc} (mL/g)	439	364	8.8	1.23
Free Air diffusion coefficient (m^2/day)	0.72	0.69	0.87	1.98

Vapor-phase advection can result from pressure, density, and thermal gradients in the subsurface. Pressure gradients can be caused by barometric pressure fluctuations, positive-pressure air drilling, and vapor extraction operations. To implement barometric pressure fluctuations in TETRAD, only low-frequency variations associated with passage of pressure fronts were considered. According to Auer et al. (1996), these low-frequency variations have a much larger impact on subsurface gas transport than the high-frequency variations caused by diurnal temperature fluctuations and local wind gusts. Another approximation consisted of representing actual pressure variations that are somewhat sinusoidal with a square wave. This was done for convenience and to preclude extremely long run times due to time-step limitations. An examination of barometric pressure at the SDA over several months showed a period for low-frequency perturbations of approximately 10 days. The average pressure during this period was 845 mb (84.5 kPa) with an average deviation (amplitude) of approximately ±7 mb (0.7 kPa). Figure 5-23 illustrates the square-wave fit to the barometric pressure data for a 2-month interval from the examination period. In TETRAD, the air pressure at land surface was alternately increased 14 mb for 10 days and then decreased 14 mb for 10 days for the entire simulation. Although barometric pressure fluctuations were included in the calibration, they could not be included in the base-case simulations due to extremely long simulation times caused by the short time step limitation. The effects of not including barometric pressure are discussed in Section 5.4.7.

Pressure gradients resulting from air injection during well drilling have the potential to move vapor-phase VOCs because of the high pressures involved and the permeable basalt subsurface. Many wells in the vicinity of the SDA have been drilled with air to bring drill cuttings to the surface. Since 1994, reverse-air circulation, which uses a dual-wall drill stem, has been used because it recovers most of the injected air. Before 1994, more than 40 wells were drilled without reverse-air circulation. A survey of SDA drill logs indicates that, for most of these wells, circulation (i.e., air recovery) was partially or totally lost below about 18 m (60 ft). This meant that a large volume of air had been pumped into the subsurface at high pressures.

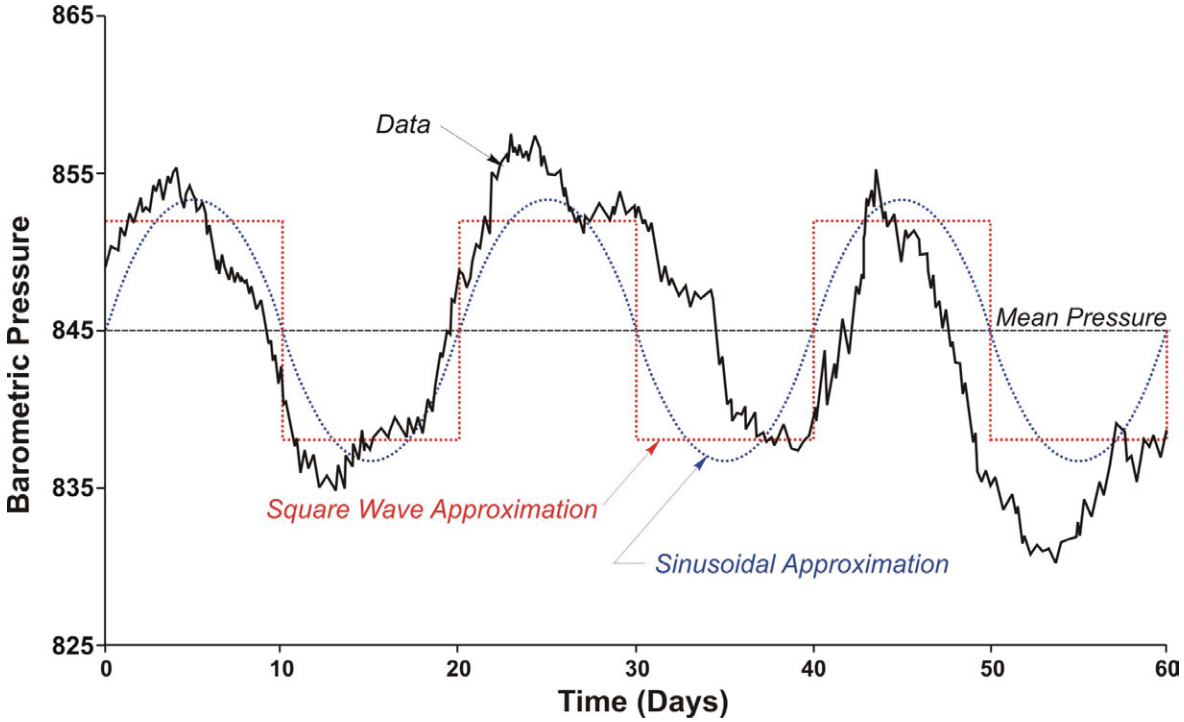

Figure 5-23. Barometric pressure data with square-wave approximation as implemented in the carbon tetrachloride calibration simulation.

Figure 5-24 shows the location of air-drilled wells with a depth greater than 18 m (60 ft) that did not use reverse-air circulation. Drill dates, depths, and drill methods for these wells are listed in Table 5-3. An examination of the drilling logbooks shows that the wells in Table 5-3 were typically drilled at speeds of about 9 m (30 ft) per day at air pressures of 125 to 250 psi and injection rates of 750 to 1,100 cfm. In TETRAD, either the pressure or the injection rate may be specified with a limit put on the one that is not specified. The air injection rate was set to 1,000 cfm with no limit on the pressure. The length of the injection interval was increased in steps of approximately 9 m (30 ft) each day until the terminal depth was reached and air was injected over the entire length of the interval each day.

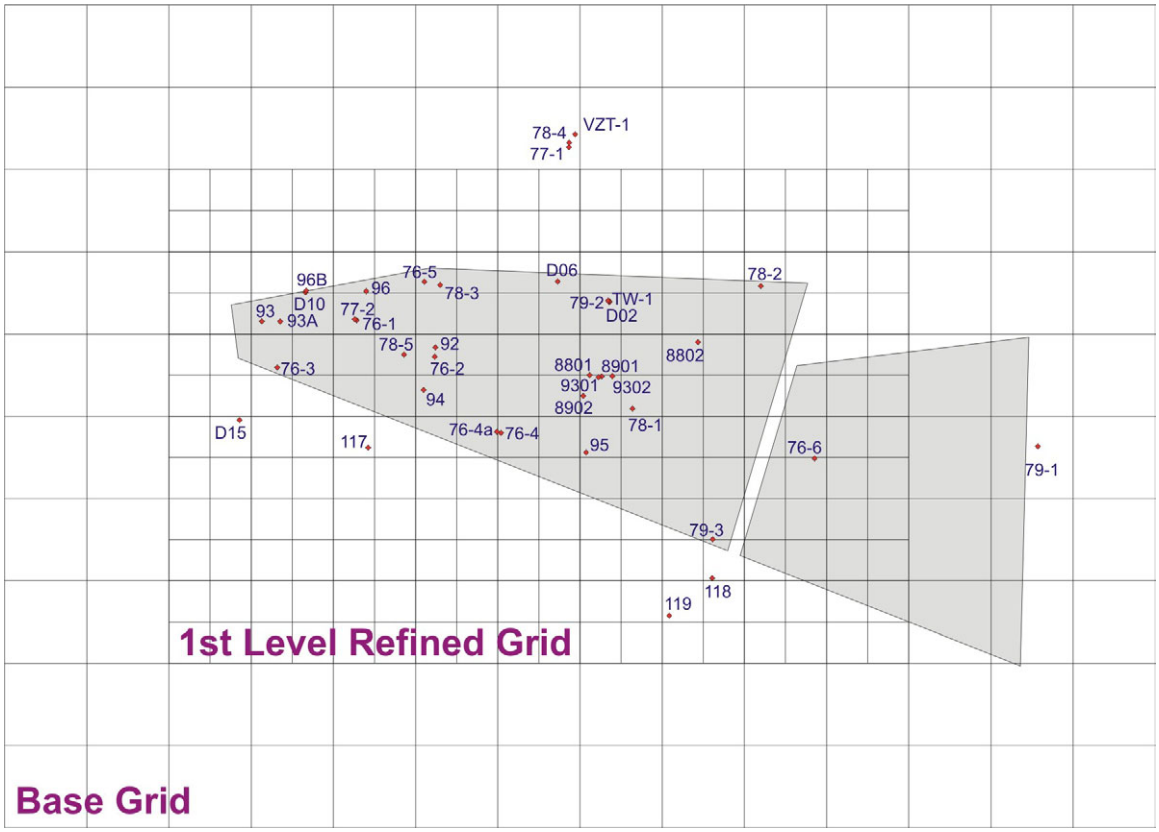

Figure 5-24. Locations of air-drilled wells (excluding reverse-air-rotary) in the vicinity of the Subsurface Disposal Area with a depth of greater than 18 m (60-ft).

Table 5-3. Information on air-drilled wells at the Subsurface Disposal Area with a depth greater than 18 m (60 ft), excluding wells drilled using reverse-air circulation.

Well	Year	Depth (ft)	Drill Method
USGS-92	1972	247	Air rotary/core
USGS-93	1972	246	Air rotary/core
USGS-93A	1972	233	Air rotary/core
USGS-94	1972	302	Air rotary/core
USGS-95	1972	246	Air rotary/core
USGS-96	1972	236	Air rotary/core

Table 5-3. (continued).

Well	Year	Depth (ft)	Drill Method
USGS-96B	1975	229	Air rotary/core
76-1	1976	228	Air rotary/tricone/core
76-2	1976	253	Air rotary/core
76-3	1976	240	Air rotary/core
76-4	1976	215	Air rotary/tricone/core
76-4A	1976	254	Air rotary/tricone/core
76-5	1976	245	Air rotary/core
76-6	1976	244	Air rotary/core
77-1	1977	600[a]	Air rotary/core/water
77-2	1977	87	Air rotary/core
78-1	1978	82	Air rotary/core
78-2	1978	253	Air rotary/core
78-3	1978	248	Air rotary/core
78-4	1978	350	Air rotary/tricone
78-5	1978	250	Air rotary/core
79-1	1979	244	Air rotary/core
79-2	1979	223	Air rotary/core
79-3	1979	262	Air rotary/tricone/core
D02	1986	243	Air rotary/tricone/core
D06	1986	126	Air rotary/tricone/core
D10	1987	239	Air rotary/core
D15	1987	252	Air rotary/tricone/core
TW-1	1987	238	Air rotary/tricone/core
USGS-117	1987	655	Tricone/air
USGS-118	1987	622	Air rotary/core
USGS-119	1987	705	Tricone/air
USGS-120	1987	705	Tricone/air
8801	1988	245	Air rotary/core
8802	1988	221	Air rotary/core
VZT-1	1988	132	Air rotary
8901	1989	249	Air rotary/tricone/core
8902	1990	245	Tricone/air

Table 5-3. (continued).

Well	Year	Depth (ft)	Drill Method
9301	1993	238	Air rotary
9302	1993	238	Air rotary

a. Drilled to 272 ft with air, drilled to 600 ft with water.

Vapor vacuum extraction is simulated in the model similar to the way air injection is handled. One difference with extraction is that phases are extracted rather than components. In this case, the gaseous phase is extracted, which is mostly air but can also include any water vapor or VOC vapor. Also, extraction is simpler because extraction intervals do not change the way injection intervals changes when the well is drilled. Three historic vapor extraction tests were included in the calibration and base-case simulations, including the 1989 2-week test, the 1990 4-month test, and the 1993 Organic Contamination in the Vadose Zone Project treatability study. All of these tests pumped from Well 8901.

In 1996, Operable Unit 7-08 began operation of a large-scale VVET system to remove vapor-phase VOCs from the vadose zone. The system consisted of three thermal oxidizer (i.e., treatment) units (i.e., Units A, B, and C) and multiple extraction wells with different length extraction intervals at different depths. Since beginning operations, the units have essentially been shutdown only for maintenance or when breakdowns occur. The original units have been upgraded with more efficient and reliable treatment units (i.e., Units D, E, and F) and additional extraction wells have been drilled. Actual VVET operations from January 1996 through January 2005 were included for base-case simulations. Base-case simulations also included future vapor extraction activities through the year 2010 and assumed extraction from six wells (two per treatment unit) for 10 months a year.

To implement vapor extraction in the model, a volumetric removal rate of gas and vapor was assigned to the extraction interval for each well that was connected to a VVET unit. The original VVET units (i.e., A, B, and C) only monitored total flow into the unit; therefore, if extraction was from multiple wells, assumptions had to be made regarding the division of flow between each well. Fortunately, however, the number of viable extraction wells were limited and most of the time the units were only connected to one well. In 2002 to 2003, several new extraction wells were drilled and flow meters have been installed at each wellhead. Since that time, the recorded flow rates for each well have been used in the model. For future operations from 2005 to 2010, the VVET system was assumed to operate in the same configuration as was being used at the beginning of 2005. In that configuration, Unit D was removing 160 scfm from Well SE6, and 240 scfm from Well IE6; Unit E was removing 200 scfm each from Wells SE7 and 8901; and Unit F was removing 200 scfm each from Wells SE8 and 7E. Figure 5-25 shows the locations of current vapor extraction wells that may be used by Operable Unit 7-08. Figure 5-26 shows the depth of the extraction intervals. Extraction in the model took place from gridblocks that corresponded to the location and depth of the extraction interval. The operating time for each of the extraction units is shown graphically in Figure 5-27. Not shown in Figure 5-27 are the wells that were connected to the units while they were operating.

Vapor density gradients caused when high molecular weight compounds, such as CCl_4, are vaporized into the surrounding air, also cause vapor advection. Falta et al. (1989) and Mendoza and Frind (1990a, 1990b) suggest that density driven gas flow will be significant where total gas density exceeds ambient gas density by more than 10% and the gas-phase permeability is greater than $1 \times 10\text{-}7$ cm^2, which is within the range of fractured basalt permeability. Density driven flow is likely to be important immediately below the source where concentrations are highest. Table 5-2 contains molecular weights of the VOCs.

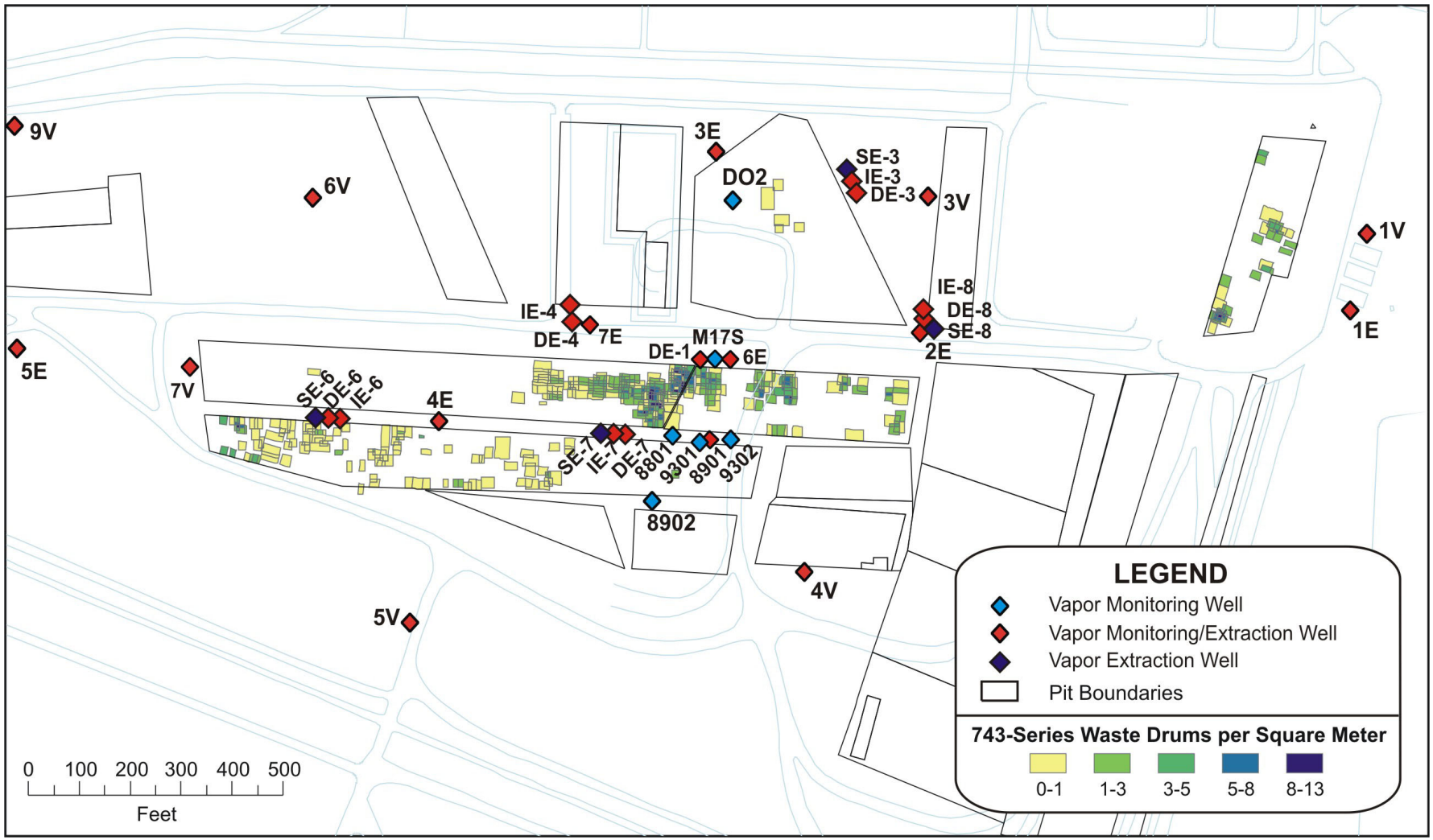

Figure 5-25. Operable Unit 7-08 vapor extraction and vapor monitoring well locations.

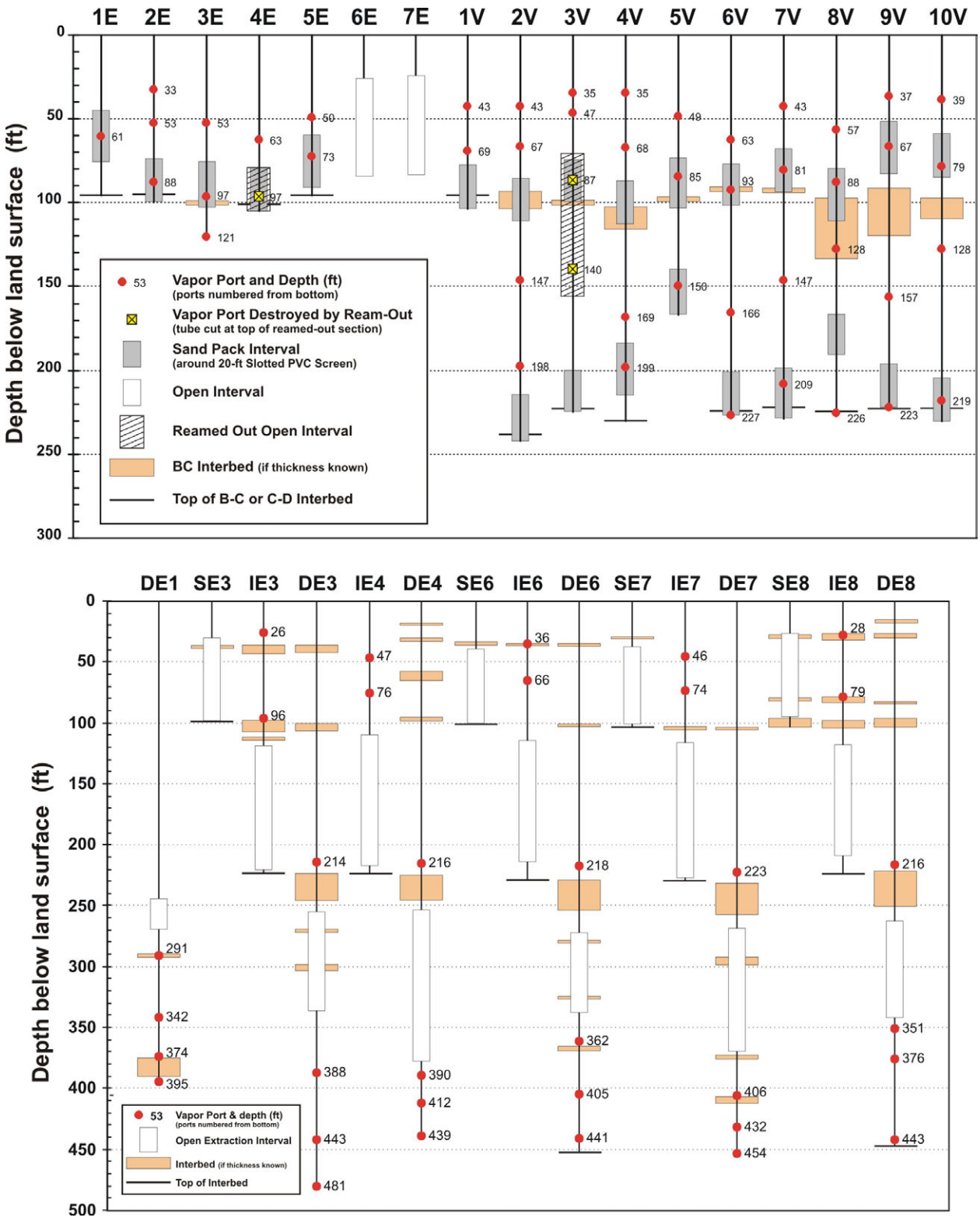

Figure 5-26. Depth of vapor ports and extraction intervals in Operable Unit 7-08 wells.

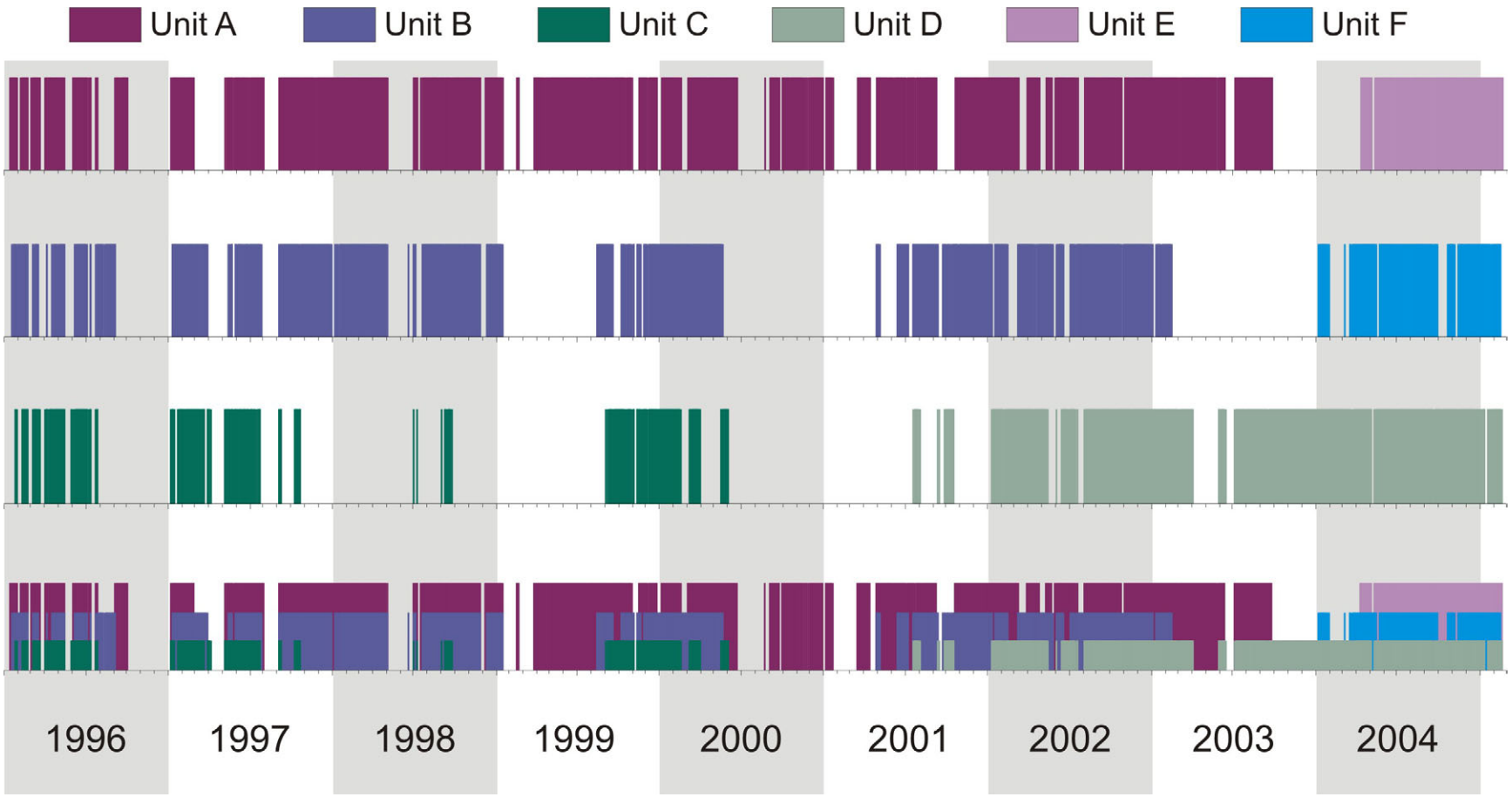

Figure 5-27. Operable Unit 7-08 vapor vacuum extraction with treatment unit operation history.

Vapor advection caused by thermal gradients is not likely to be significant and was not included in the simulation study. The subsurface was assumed to be isothermal.

5.4.2.3.3 Aqueous Transport—Aqueous transport of VOCs can take place as a result of advection and diffusion, even though advection is typically much more rapid. Dissolved VOCs are transported by aqueous advection whenever water moves in the subsurface. Section 4 contains an extensive discussion of water movement in the vadose zone and aquifer. Aqueous diffusion acts the same as vapor diffusion, but aqueous-diffusion coefficients are usually four to five orders of magnitude less than vapor-diffusion coefficients. Aqueous-diffusion coefficients used in the RI/FS model were assigned a value four orders of magnitude less than the free-air-diffusion coefficients (Table 5-2).

5.4.2.3.4 Degradation—Although degradation of CCl_4 has probably occurred in the SDA subsurface, it was not included in simulations because of uncertainty regarding the rate and mechanism. In the environment, CCl_4 is degraded more readily under anaerobic conditions. In the SDA subsurface, aerobic conditions likely dominate; however, anaerobic conditions may occur in isolated locations, allowing for CCl_4 degradation.

The presence of chloroform, a transformation product of CCl_4, is evidence that reductive dechlorination has occurred in the SDA subsurface. Historical records do not indicate chloroform disposal in the SDA, but chloroform has been detected in the groundwater and soil gas beneath the SDA. Neglecting degradation is conservative because byproducts of CCl_4 degradation (i.e., chloroform, methylene chloride, and chloromethane) have transport properties similar to CCl_4, yet they are less toxic (i.e., have higher risk-based concentrations).

5.4.2.4 Interface from the Vadose Zone Model to Aquifer Model. Section 4.3.7.4 describes the process for transferring dissolved-phase simulation results from the vadose zone model to the aquifer model. In that case, the flux of water and the aqueous flux of contaminants from the fractured basalt were transferred from the vadose zone to the aquifer on a grid-by-grid basis. Because the VOC model has the added complexities of being dual continua, it was necessary to capture the flux of contaminant within the matrix domain. No gaseous-phase flux of contaminants is present in either the fracture or matrix domain because vapor-phase contaminants partition into the aqueous phase as water saturations increase near the water table and then advect out the bottom of the model domain. Direct partitioning from the vapor phase into the aquifer across the water table is not considered. Since contaminant mass advects out the bottom of the model domain without being influenced by contaminant mass already present in the aquifer, this approach is conservative because it maximizes aquifer concentrations. Direct partitioning would decrease overall as concentrations increased in the aquifer.

5.4.3 Volatile Organic Compound Model Calibration Methodology

Calibration was achieved through a trial-and-error process of adjusting particular parameters within reasonable uncertainty ranges until model results adequately agreed with observations of CCl_4 in vadose zone soil-gas and aqueous concentrations in the aquifer. Carbon tetrachloride was chosen because it has the largest inventory and available data set for comparison, and documentation of its disposal history and origin is better when compared to other VOCs. Given the high degree of subsurface heterogeneity, the goal of calibration was to match observed general trends and not be overly concerned with matching values at specific points. Comparison of model results to observed data was both qualitative and subjective, relying primarily on visual observations of plots that compare model results to data.

Calibration focused primarily on data collected through 1995, before the start of full-scale VVET operations by Operable Unit 7-08. By doing this, calibration focused on matching data and trends that resulted from natural, ambient processes and not on artificial processes (e.g., vapor extraction).

Comparisons were made of actual VOC mass removed to simulated mass removed, but parameter adjustments were not warranted based on the level of agreement.

5.4.4 Volatile Organic Compound Transport Model Calibration

As part of the IRA model calibration (Magnuson and Sondrup 1998), several model inputs were modified to improve calibration. Some modifications were small deviations from the original value and others were significant. Parameter values that were modified only slightly were kept the same for model calibration. These include the fraction of organic carbon (f_{oc}), which affects sorption, the basalt matrix porosity, the duration of air drilling, and barometric pressure amplitude and wavelength.

For the VOC model calibration, source-release and tortuosity values were the only inputs initially intended to be used as part of calibration. However, in an effort to improve the match between simulated and observed data, other parameters or features of the model were modified. Each of these calibration steps are discussed in the following subsections.

5.4.4.1 Source Release. Source releases are calculated external to the VOC transport model, using the computer code DUST-MS (Anderson and Becker 2006). Inputs to the source model include source inventory, drum-failure rates, and diffusivity of VOCs in sludge. Table 5-4 lists the best available data for the source model inputs.

Table 5-4. Best available data for volatile organic compound source-release model inputs.

Model Input	Value	Source
Carbon tetrachloride inventory	7.9E+05 kg	Miller and Varvel (2005)
Dumped drum corrosion-failure rate	11.7 years[a]	Anderson and Becker (2006)
Stacked drum corrosion-failure rate[b]	22.6 years[a]	Anderson and Becker (2006)
Initial drum-failure rate	28.5%	Anderson and Becker (2006)
Carbon tetrachloride diffusivity in sludge	2.5E-06 cm^2/s	Lowe et al. (2003)

a. Expressed as a mean-time-to-failure, using a normal distribution with a standard deviation of one-half the mean time to failure.
b. Very small percentage of the Series-743 sludge drums was stacked.

To help constrain the source model, Sondrup et al. (2004) attempted to estimate the amount of CCl_4 remaining in the pits by using chlorine data obtained from neutron-gamma logging of waste. Vapor sampling of Type B vapor probes and nuclear logging of Type A probe holes suggest a substantial amount of VOCs remain in the pits even after 40 years of burial. Although a defensible quantitative estimate could not be obtained, Sondrup et al. (2004) used other information and recommended that 50% of VOCs remaining in year 2000 be used for modeling purposes as a target for the source-release model.

In order to determine feasible combinations of source model inputs that could produce a release where 50% of the source remained in the pits in the year 2000, three cases of source-model simulations were run by varying the three parameters that control release: (1) initial drum-failure rate, (2) corrosion-failure rate for dumped drums, and (3) diffusivity of VOCs in sludge. In each case, two of the three values were held fixed, and the other value was varied over a predetermined range. The corrosion-failure rate for stacked drums was not examined because nearly all of the Series-743 drums were dumped. Table 5-5 shows the range of values examined for each of the three parameters. Figure 5-28 shows graphical results for the three cases in terms of percent of original mass remaining in the year 2000.

Table 5-5. Ranges of volatile organic compound source-release model inputs examined.

Case	Model Input	Best Available Value	Range of Values Examined
1	Dumped drum corrosion mean-time-to-failure	11.7 years[a]	10 to 60 years[a]
2	Initial drum-failure rate	28.5%	0 to 50%
3	Carbon tetrachloride diffusivity in sludge	2.5E-06 cm^2/s	2.5E-10 to 2.5E-05

a. Standard deviation was half the mean-time-to-failure.

In Case 1, a value of 50% mass remaining was achieved with a drum mean-time-to-failure of approximately 45 years. In Case 2, with the mean-time-to-failure fixed at 11.7 years and the diffusivity fixed at 2.5E-06 cm^2/s, there were no values of initial failure rate that would keep 50% mass remaining in the year 2000. Even the extreme case of an initial failure rate of 0% (i.e., corrosion-failure only) resulted in only 6% of the original mass remaining in the year 2000. This is because the other two parameters (i.e., mean-time-to-failure = 11.7 years, diffusivity = 2.5E-06 cm^2/s) allow the mass to be released much too rapidly. Therefore, to test the source-release dependence on initial drum-failure rate, a mean-time-to-failure value of 45 years was used. Forty-five years was the value from Case 1 that resulted in 50% of the mass remaining in the source. Using this value, an initial drum-failure rate of 0% resulted in 70% of the mass remaining in the year 2000 and a value of 50% resulted in half of that (35%). The results are linear.

For Case 3, the mean-time-to-failure was fixed at 11.7 years as recommended by Anderson and Becker (2006), and the initial-failure rate at 28.5%. In order to achieve 50% mass remaining in the year 2000 for Case 3, the sludge diffusivity must be approximately 3E-10 cm^2/s. This is more than four orders of magnitude greater than the value suggested by Lowe et al. (2003). The exercise of varying source parameters to achieve a remaining mass of 50% suggests that (1) the mean-time-to-failure of 11.7 years as proposed by Anderson and Becker (2006) is too short for Series-743 sludge drums, or (2) the sludge diffusivity determined by Lowe et al. (2003) is too large (i.e., diffusion too rapid), or (3) some combination of 1 or 2 is correct. The answer is more likely that the mean-time-to-failure for the drums is too large, or more likely that bagging is preventing release of VOCs and no credit is being taken for bagging. Visual observations of waste during the Glovebox Excavator Method Project retrieval (Olson 2004) indicated that while many of the drums had corroded, many of the polyethylene bags within the drums appeared to be intact and acted as a barrier to VOC release. Therefore, a longer mean-time-to-failure for the drums would be more representative of an effective container-failure rate that includes influence of the bags. Thus, the mean-time-to-failure for the VOC source-release model was chosen to be 45 years, while the other parameters were assigned the best available values shown in Table 5-5.

5.4.4.2 Tortuosity Values. Before calibration, initial tortuosity values were estimated from an empirical formula determined by Millington (1959). The Millington formulation relates tortuosity (τ), to porosity (θ) and water saturation (S_w) as shown below:

$$\tau = \frac{\theta_T^{\,2}}{\left[\theta_T\left(1 - S_w\right)\right]^{7/3}} \quad . \tag{5-2}$$

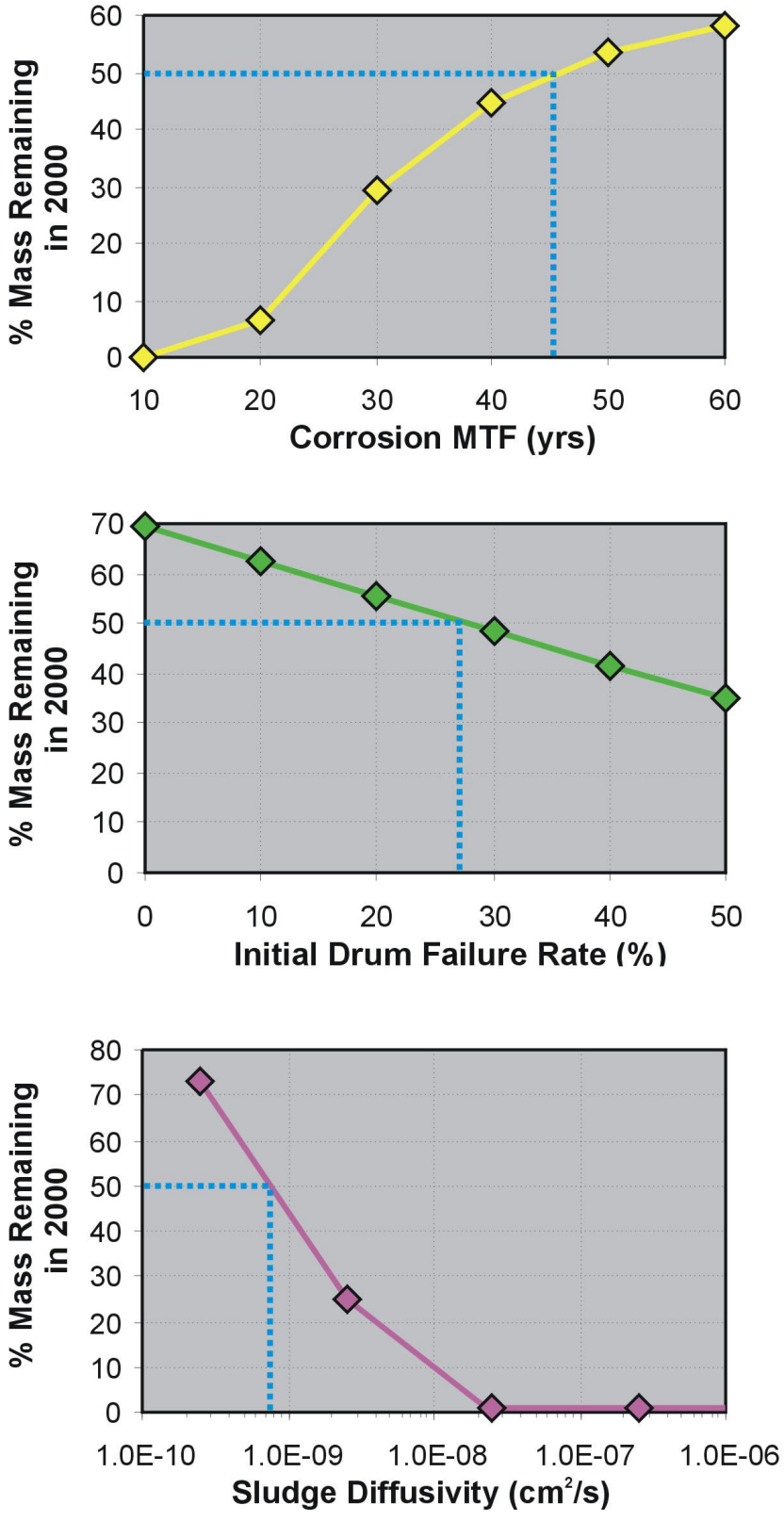

Figure 5-28. Results of carbon tetrachloride source-release parameter variations showing combinations that result in 50% of the original mass remaining in the year 2000.

Table 5-6 lists initial tortuosity values used in the VOC model calibration, using average saturation and porosity values from the ABRA model.

Table 5-6. Initial tortuosity values for the different material types used in the model.

Material Type	Tortuosity
Surficial sediment	6
A-B interbed	10
B-C interbed	7
C-D interbed	7
Fractured basalt	3[a]
Matrix basalt	9

a. Final value changed to 1 as a result of the calibration.

During the calibration process, numerous simulations with different tortuosity values were performed in an attempt to improve the match to observed data. The values investigated for each material type ranged from 1 up to as high as 30. In the end, however, the original values shown in Table 5-6 produced the best overall results with one exception. Early during the calibration process, it was clear that a tortuosity value of 3 for fractured basalt was too high and that a value of 1 produced the best overall match to vadose zone vapor and groundwater concentrations. Except for that change, the other values remained the same. Figure 5-29 shows a cross section of results for CCl_4 vadose zone vapor concentrations using the final tortuosity values.

Larger interbed tortuosity values were investigated in an attempt to cause more spreading of the vadose zone plume. The tortuosity values in Table 5-6 resulted in a general underestimation of the vadose zone vapor concentrations and aquifer concentrations at some of the outlying wells (e.g., M6S and M7S). Although the larger tortuosity values created the favorable effect of a broader vadose zone plume, they overly restricted the downward movement of VOCs near the SDA and caused an underestimation of the groundwater concentrations close to the SDA.

Other variations of tortuosity were attempted to improve calibration. The first variation was a direct implementation of the Millington formulation in the model. Equation (5-2) was programmed into the TETRAD model and the tortuosity values for each gridblock were calculated at each time step, based on the porosity and phase saturations. However, the simulation with the Millington formulation within TETRAD was not successful in terms of computational feasibility and desired effect. At many locations, water saturations approached saturated conditions (S_w=1) and the Millington tortuosity values approached infinity. This creates a computational burden, but one that is not overwhelming. The larger problem is that the tortuosity values are so large that transport is overly retarded and the match of simulated to observed data, especially in the aquifer, is very poor. Figure 5-30 compares simulation results using tortuosity values calculated by the model according to the Millington formulation against those using the final calibration tortuosity values shown in Table 5-6.

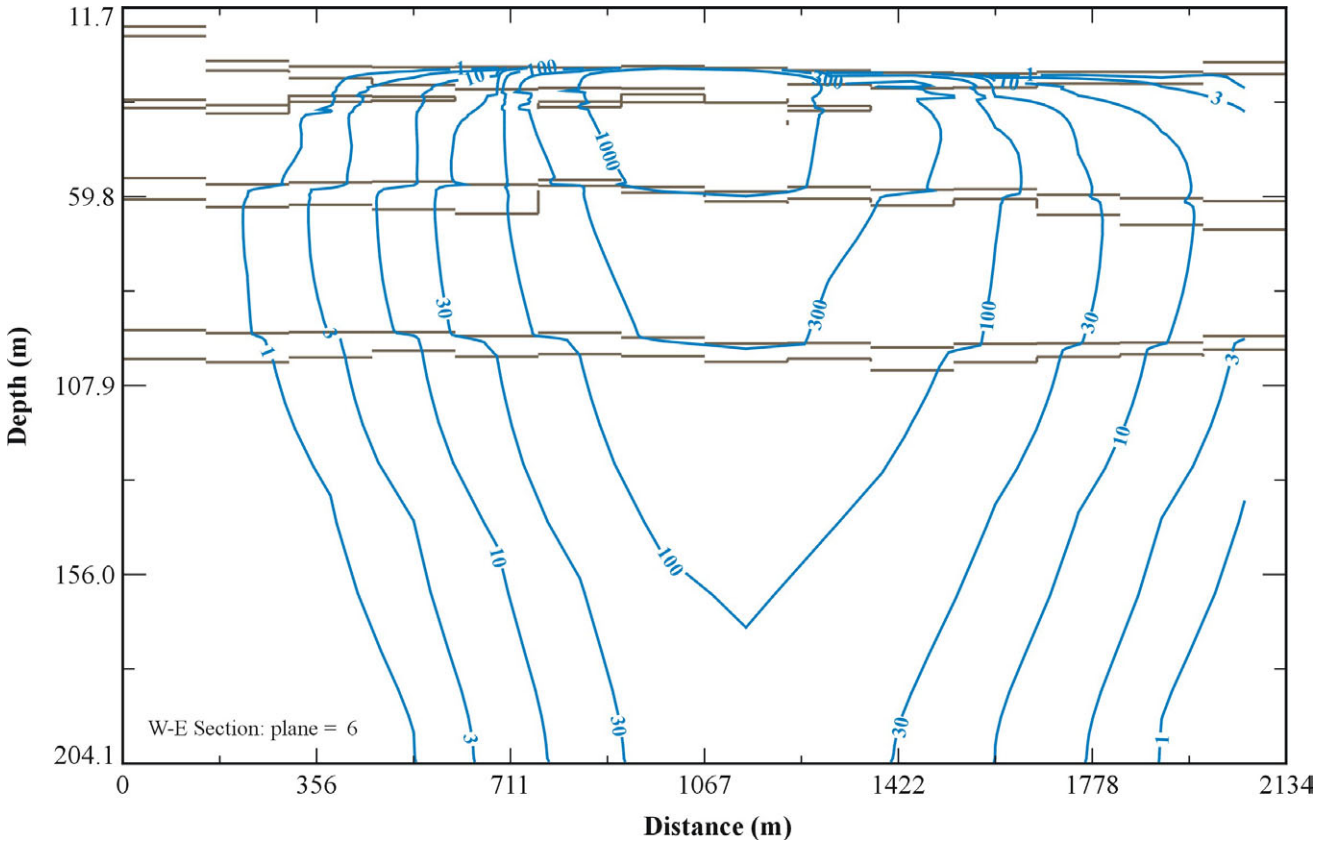

Figure 5-29. Carbon tetrachloride vapor concentration contours on a west-east cross section of the base model grid through the center of the Subsurface Disposal Area. Surface sediment and A-B, B-C, and C-D interbed locations are shown with horizontal lines.

The other tortuosity variation was a compromise between simulations that used single tortuosity values for the different material types and simulations that used the built-in Millington formulation. These additional simulations were performed with the values shown in Table 5-6, but with the added complication that smaller zones within some of the sediment layers were assigned slightly larger tortuosity values to account for the higher moisture contents. The higher moisture contents are the result of higher infiltration rates within the SDA. Results of these simulations were not significantly better than simulations with homogeneous values for the sediment layers.

5.4.4.3 Other Calibration Modifications. One limitation of the model is that it does not produce the amount of lateral spreading indicated by monitoring data. During the calibration process, three other model parameters were modified in an attempt to increase spreading of the VOC plume in the vadose zone and aquifer. The first change was to increase the fractured basalt permeability horizontal to vertical anisotropy ratio from the value of 30:1 used in the IRA and ABRA models to a value of 300:1. This change produced a better match of the observed spreading of CCl_4 in the vadose zone. Section 6.4.7 contains additional details on this parameter modification.

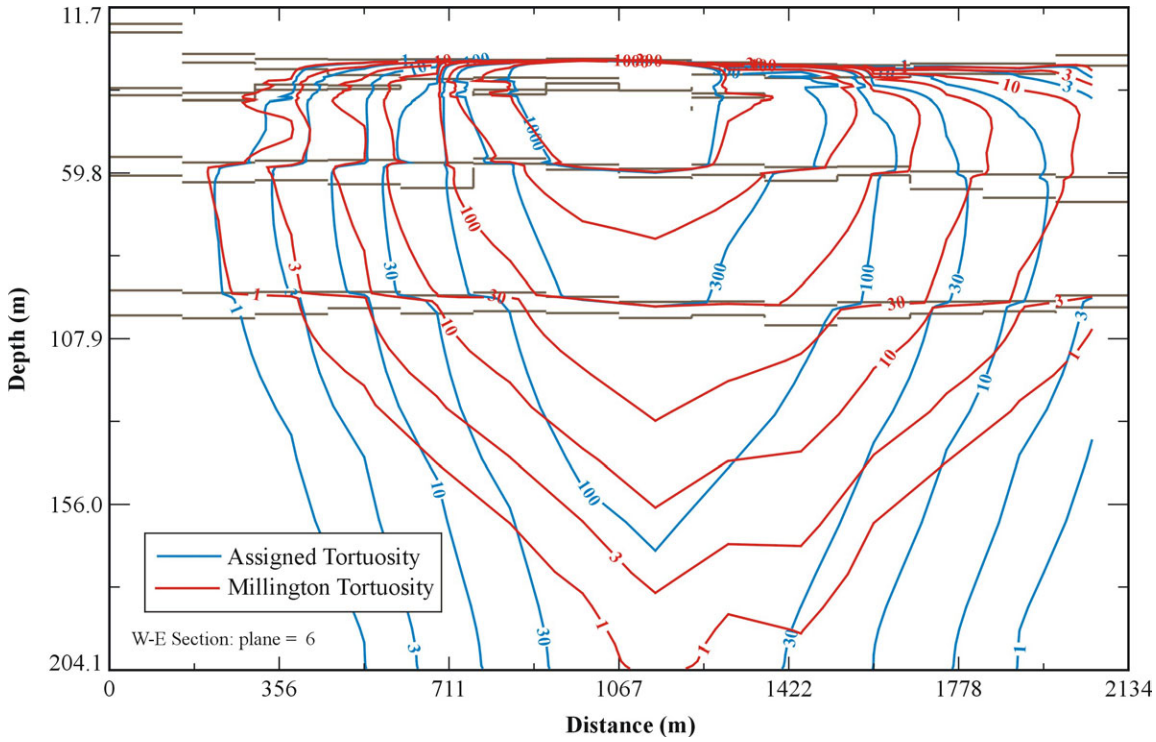

Figure 5-30. Comparison of simulated vapor concentration results using assigned tortuosity values (Table 5-6) and tortuosity values calculated by the model for each gridblock using the Millington formulation. Results are shown on a west-east cross section of the base model grid through the center of the Subsurface Disposal Area. Surface sediment and A-B, B-C, and C-D interbed locations are shown with horizontal lines.

The second parameter modification that helped increase lateral spreading of the plume was to increase the basalt matrix characteristic block length from the value of 2 m (6.6 ft) used in the IRA and ABRA models to a value of 20 m (65.6 ft). The larger matrix block length forces more of the flow and contaminant to be moved through the high-permeability fractures.

The third modification implemented to increase lateral movement of VOCs was to increase the number of low-permeability, low-porosity layers on the interbeds from 1 to 3. The rationale for this is discussed in Section 4.3.4.1. In the IRA and ABRA models, the top gridblock of each of the interbeds was assigned low-permeability, low-porosity properties. When the RI/FS model was created, it was noticed that the finer discretization around the basalt-interbed interfaces resulted in low-permeability, low-porosity gridblocks that were approximately one-third the thickness of those used in the IRA and ABRA model. Simulations were performed where the number of low-permeability, low-porosity gridblocks was increased to 2 and 3. The simulation using three gridblocks produced the best match to observed data. It also made the RI/FS model similar to the IRA and ABRA models in terms of the thickness of the low-permeability, low-porosity layer.

Each of these modifications by themselves helped to improve lateral spreading, but the model still could not match the overall breadth of the vadose zone plume. The inability of the model to reproduce this condition is more likely a result of neglecting historical impacts on water flow in the vadose zone and aquifer flow due to infiltration into the spreading areas, and the inability to characterize and incorporate heterogeneity into the model on an appropriate scale. However, this should not be viewed as a fundamental deficiency. The amount of VOCs in the outer fringes of the plume is a very small percentage

of the total mass. Matching the concentrations in this region was secondary to obtaining a good match to concentration trends in the interior of the plume. The calibration produced a good match to vadose zone concentrations near to and below the burial pits where the majority of the mass exists and enters the aquifer.

5.4.5 Final Calibration Results

At each step of the calibration process, simulated results were compared to (1) time-averaged, vapor concentration, vertical profiles at each vapor monitoring well, (2) vapor concentration time histories at each vapor port, and (3) aquifer concentration time histories at each aquifer well. This section contains selected vapor concentration comparisons at different locations and depths to represent the entire vadose zone plume. The full set of results is contained in Appendix G. All aquifer results are shown in this section.

In this section, vapor- or gas-phase concentrations are given in ppm (i.e., parts per million), which is a volume/volume ratio and is the same as ppmv. Aquifer or aqueous concentrations are given in μg/L (i.e., mass of contaminant/volume of aqueous solution). For low concentrations, μg/L is the same as ppb (parts per billion), which is a mass/mass (e.g., μg/kg) ratio.

5.4.5.1 Carbon Tetrachloride Vapor Concentration Vertical Profiles. Figure 5-31 shows a comparison of simulated concentrations at the simulation time of January 1, 1994 to time-averaged vertical profiles of the CCl_4 concentration at selected wells. The measured data are the average of data collected over a 4-year period from January 1, 1992 to January 1, 1996. An average was taken because the concentration at a single point can vary considerably with time. Horizontal bars through each averaged data point indicate plus or minus 1 standard deviation for data at that port over the 4-year period. The 4-year averaging period was somewhat arbitrary, but was made large to represent as much data as possible, and remove influence of short-term events like vapor extraction during the 1993 treatability study. Also, many monitoring wells were being drilled over this period, which can cause short-term variations in the data.

Data from wells near the center of the SDA were deemed to be more important for calibration, and more effort was focused on matching the profile of these wells. The model results compared well with measured concentrations in these wells below the B-C interbed. However, above the B-C interbed, specifically toward land surface, the concentrations predicted by the model are greater than the measured data in many cases. This deviation is primarily due to discretization around the source areas (i.e., pits). In the model grid, monitoring wells are located in the same gridblocks that are designated as source gridblocks (i.e., pits). Because wells in the model were located as if they were drilled through the center of source pits, they showed a high concentration near land surface where the pits are located, especially because the source is still active (i.e., releasing mass). In reality, monitoring wells are located next to or between pits and concentrations near the surface would be lower than if the monitoring wells were drilled in the pits. At depth, differences in port locations and pit locations become less important because of the vertical distance from the source location.

Again, the simulation results and data compare quite well at locations inside and near the SDA. However, at wells such as Well M7S (approximately 914 m [3,000 ft] from the northeastern corner of the SDA), the simulation results are much lower than the data. In general, lateral spreading was less in the simulation results than is apparent in the data. This is one of the reasons that the larger basalt permeability anisotropy ratio of 300:1 was investigated and selected over the previously used 30:1. The larger horizontal-to-vertical permeability ratio was helpful in causing more lateral spreading in the model, but it was still not enough to produce the degree of spreading apparent in the data. However, as previously stated, matching concentrations in this region was secondary to obtaining a good match to concentration

trends at the interior of the plume. Calibration produced a good match to vadose zone concentrations near to and below the burial pits where the majority of the mass exists and enters the aquifer.

5.4.5.2 Carbon Tetrachloride Vapor Concentration Time Histories. Figure 5-32 shows time-history comparisons for CCl_4 vapor concentrations at several selected vapor ports in and around the SDA. Simulated data are plotted in the most refined grid that contains the monitoring port. In general, simulation results are in good agreement with measured data. The best agreement was obtained for ports closer to the source areas.

Perturbations in the modeled concentrations are due to air injection during well drilling and VVET operations. In the model, data were saved roughly every 500 days (i.e., 1.4 years), except during some well-drilling events and VVET events. In these cases, data were saved more often in an attempt to capture the higher frequency changes that occur as a result of the event. Variation in measured data is due to VVET operations, well drilling, and barometric pressure fluctuations. Because it is not feasible to include actual barometric data in the simulation, changes in measured concentrations caused by these data cannot be matched. Therefore, the purpose was to match the magnitude of the measured data.

5.4.5.3 Carbon Tetrachloride Aquifer Concentration Time Histories. Simulation results used for comparison to measured aquifer data were taken from the second gridblock down in the aquifer model. The second gridblock extends from 8 to 16 m (26 to 52 ft) from the top of the model, which represents the water table. This depth interval corresponds to the depth of the screened interval in most of the monitoring wells near the SDA. The only exception is Well M4D, which is open from approximately 61 to 70 m (200 to 230 ft) below the water table. For this well, simulation results from a corresponding gridblock deeper in the model are used for comparison.

Figure 5-33 shows how the screened interval of several monitoring wells near the SDA corresponds to the vertical grid in the aquifer model. The elevation of the pumps is within the second gridblock from the top of model for most of the wells. In Figure 5-33, the top of the model grid was placed at the average elevation of the water table based on measurements from 2005. If the top of the model grid were placed 3 m (10 ft) higher, reflective of the water table elevation 10 years ago, nearly all of the pumps would fall within the second or third gridblock from the top.

Figure 5-34 compares the time history of measured CCl_4 concentrations to simulation results for aquifer wells in the vicinity of the SDA. The same data and well locations are shown on Figure 5-35. Model results and measured data are shown through the year 2005. Although the calibration focused on data collected before 1996, it is doubtful whether VVET operations have impacted aquifer results significantly by 2005. In addition, some wells were drilled or began being monitored after 1995 (i.e., Wells M14S, M15S, M16S, M17S, and OW2); therefore, no data for these wells exist from before 1995 to use for comparison.

Model results are a mixture of underpredictions, overpredictions, and good matches of the measured data. Only in a few cases do the model results and measured data compare well in magnitude and trend. This is not surprising because of the highly irregular and unpredictable distribution of CCl_4 in the aquifer. The model underpredicts concentrations at Wells M3S, M6S, M7S, M16S, A11A31, USGS-88, USGS-120, and the RWMC Production Well. However, the model matches the magnitude and trend of measured data quite well at Wells M1S, M4D, USGS-87, USGS-89, and USGS-90. The match is reasonable, but not quite as good, at Wells M14S, M15S and OW2. The model overpredicts concentrations at Wells USGS-117 and USGS-119, and considerably overpredicts concentrations at Well M17S, which is the only aquifer well inside the SDA boundary. However, the measured concentrations at Well M17S seem unreasonably low given the close proximity of the well to the VOC sources.

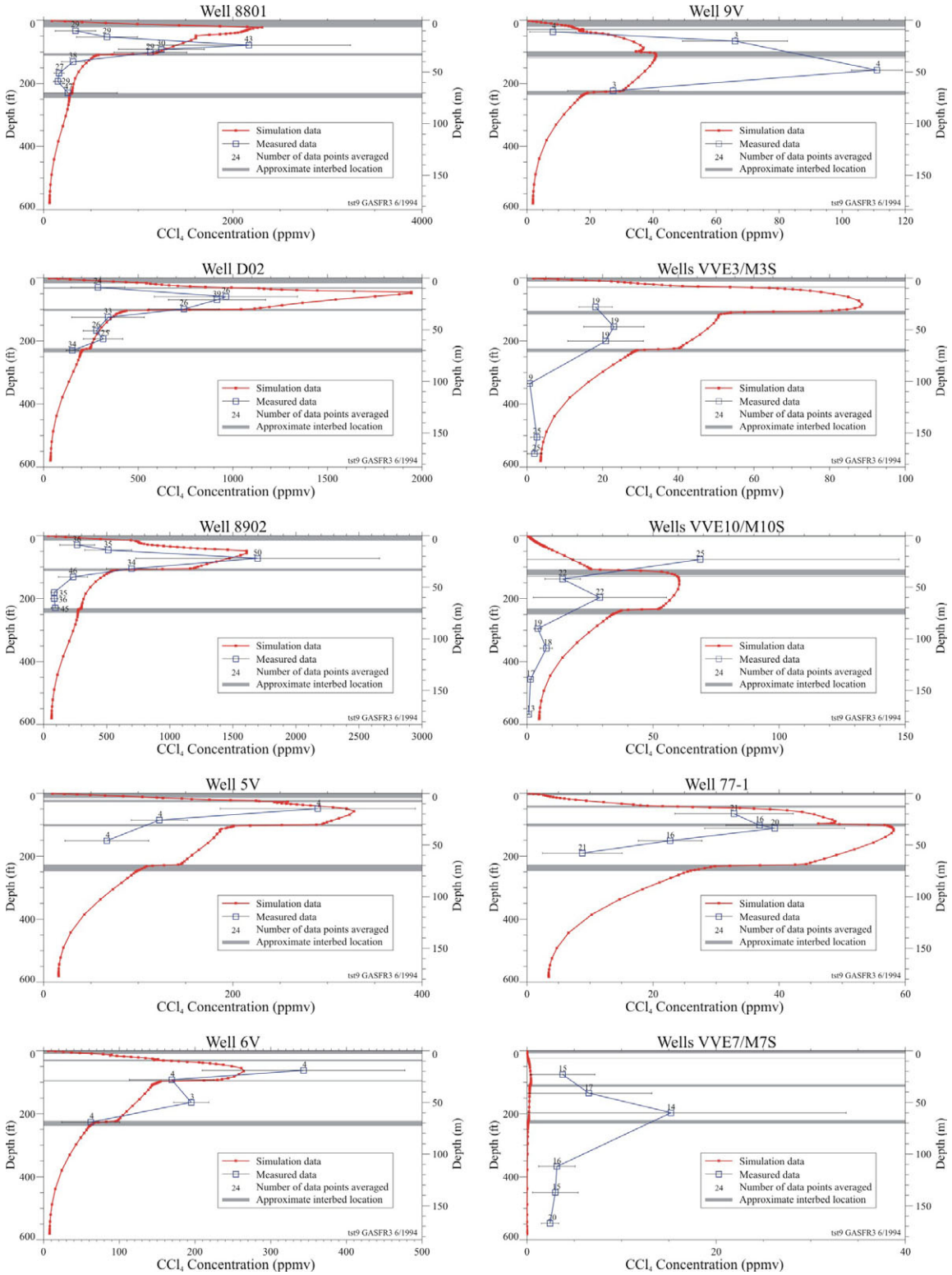

Figure 5-31. Comparison of simulated and measured carbon tetrachloride vapor concentration vertical profiles for select vapor-monitoring wells in the vicinity of the Subsurface Disposal Area. The simulated data are from June 1994. The measured data were averaged over a 4-year period from January 1, 1992 to January 1, 1996. Error bars on the measured data represent plus or minus 1 standard deviation.

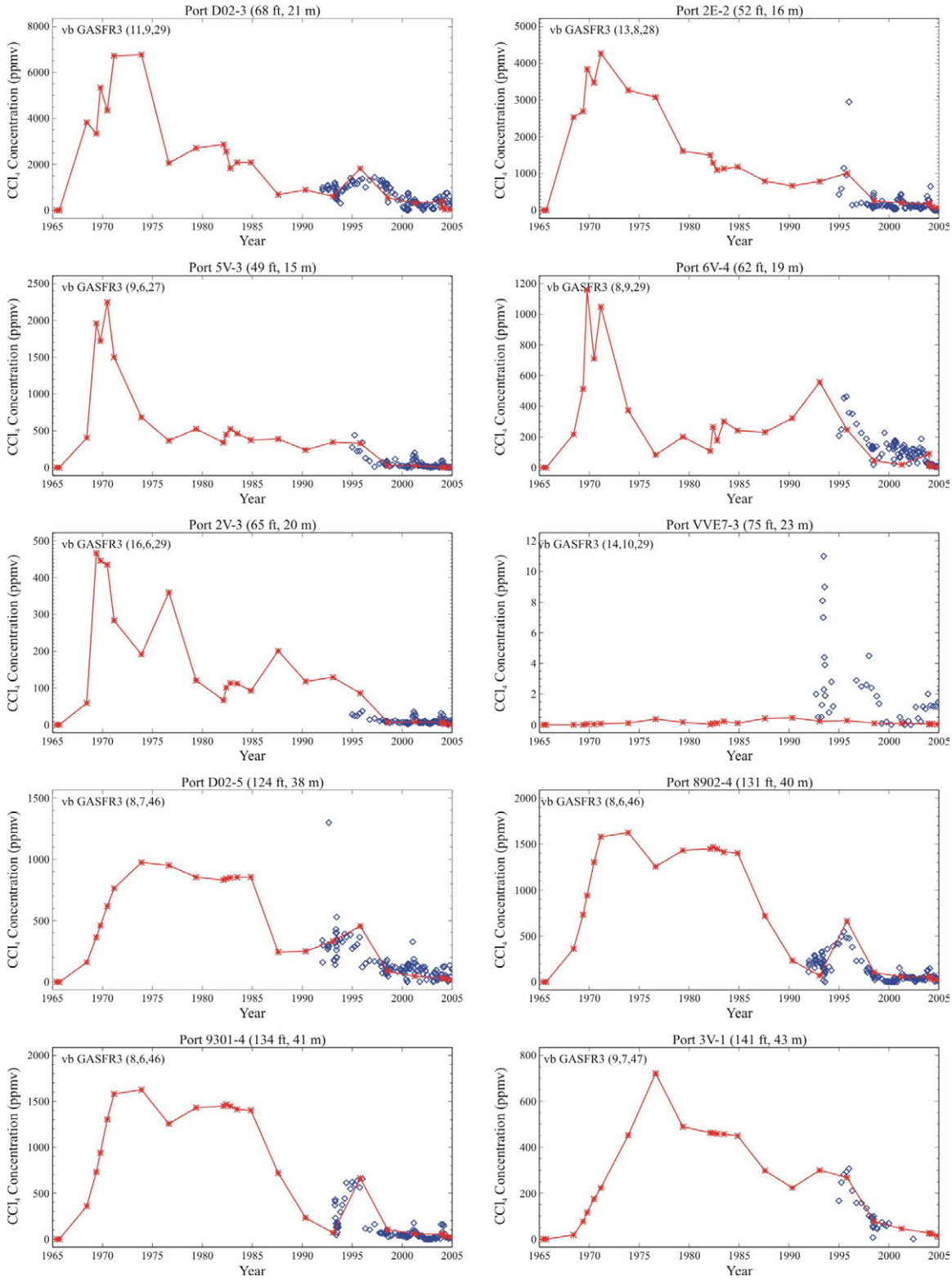

Figure 5-32. Comparison of simulated (stars) and measured (diamonds) carbon tetrachloride vapor concentration time histories for select vapor-monitoring ports in the vicinity of the Subsurface Disposal Area through the year 1995. The port name and depth below land surface is indicated above each graph.

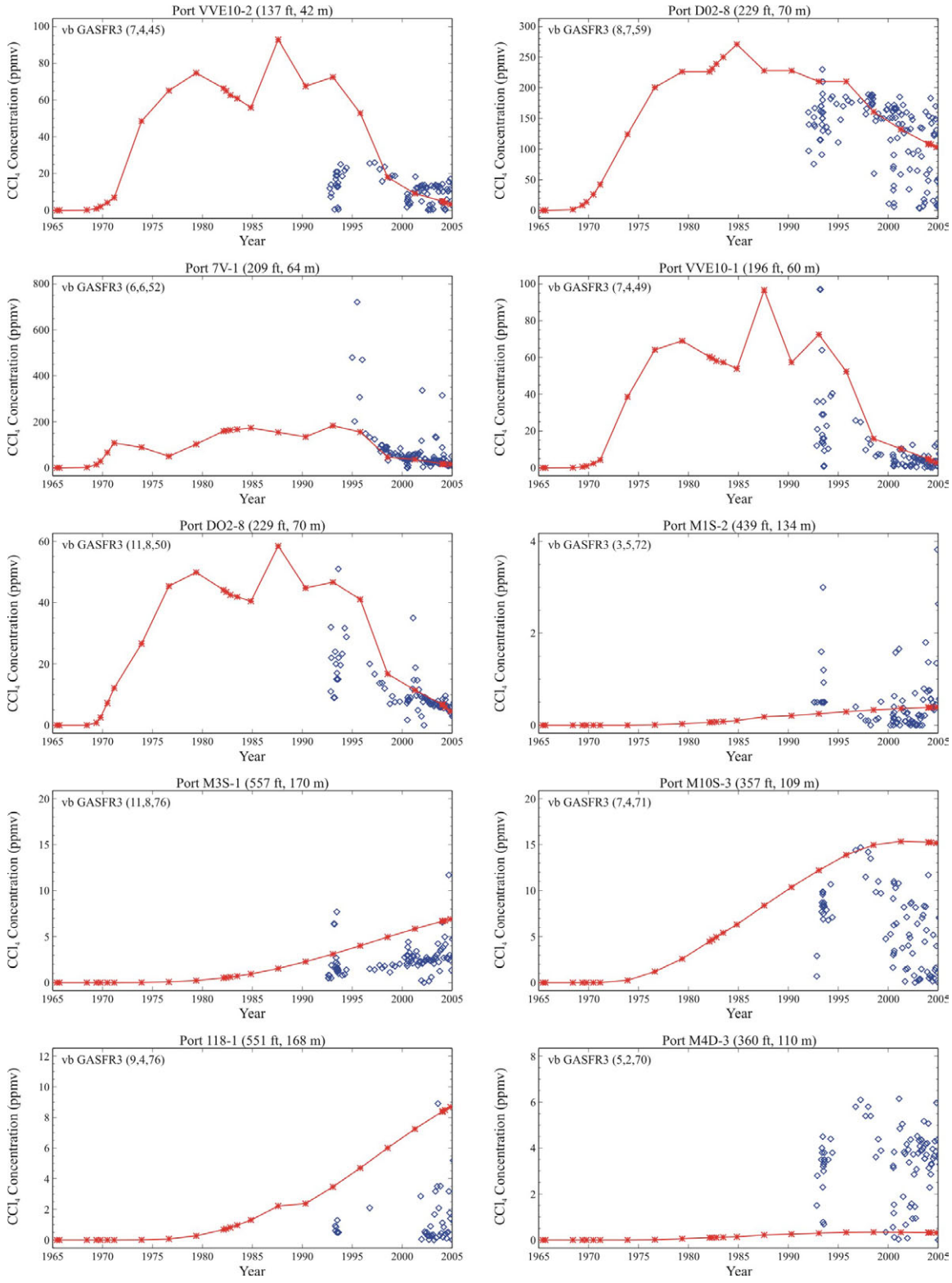

Figure 5-32. (continued).

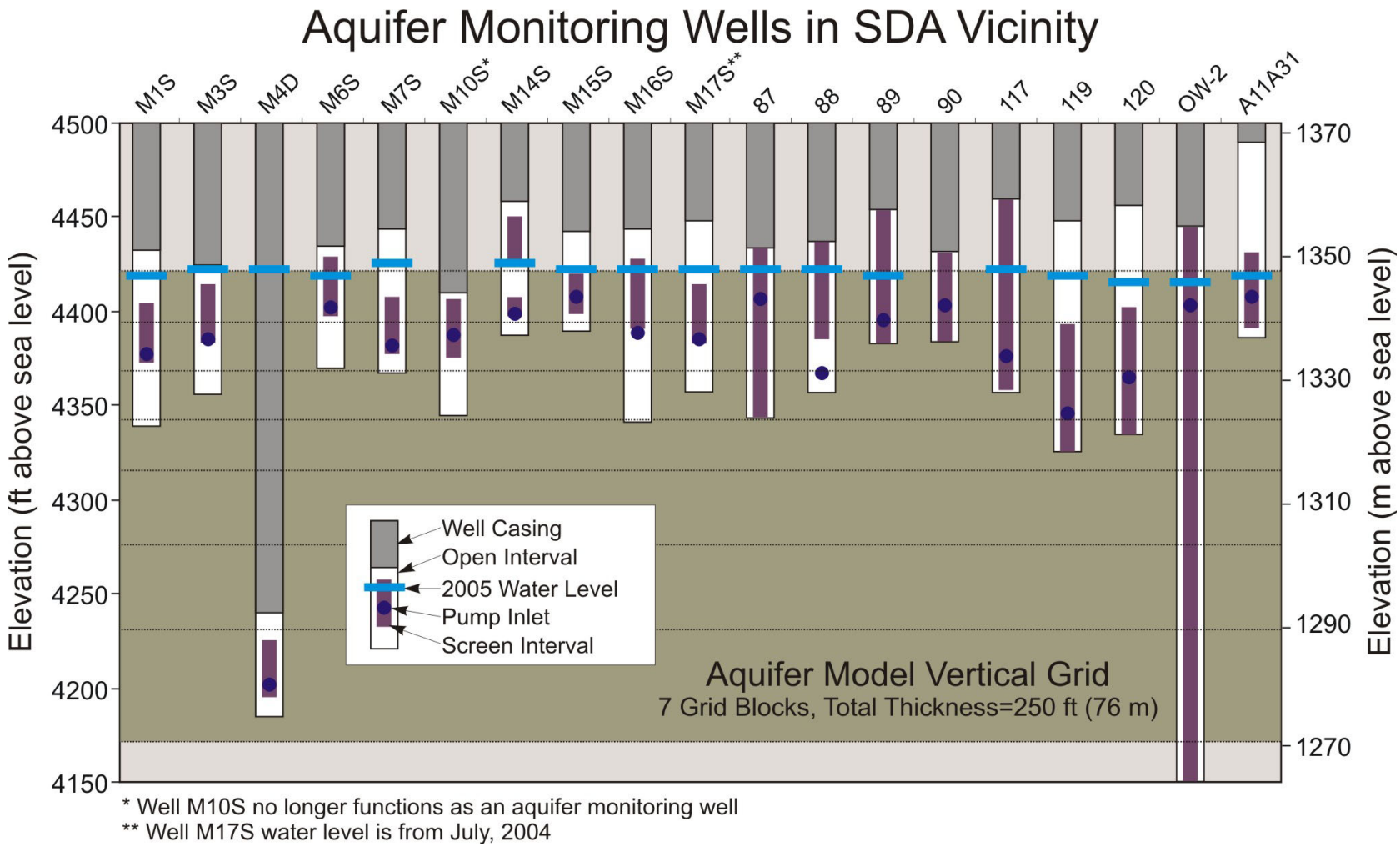

Figure 5-33. Screen intervals for aquifer monitoring wells in relation to vertical aquifer model grid discretization. The top of the model grid is placed at the average 2005 water table elevation of the wells shown.

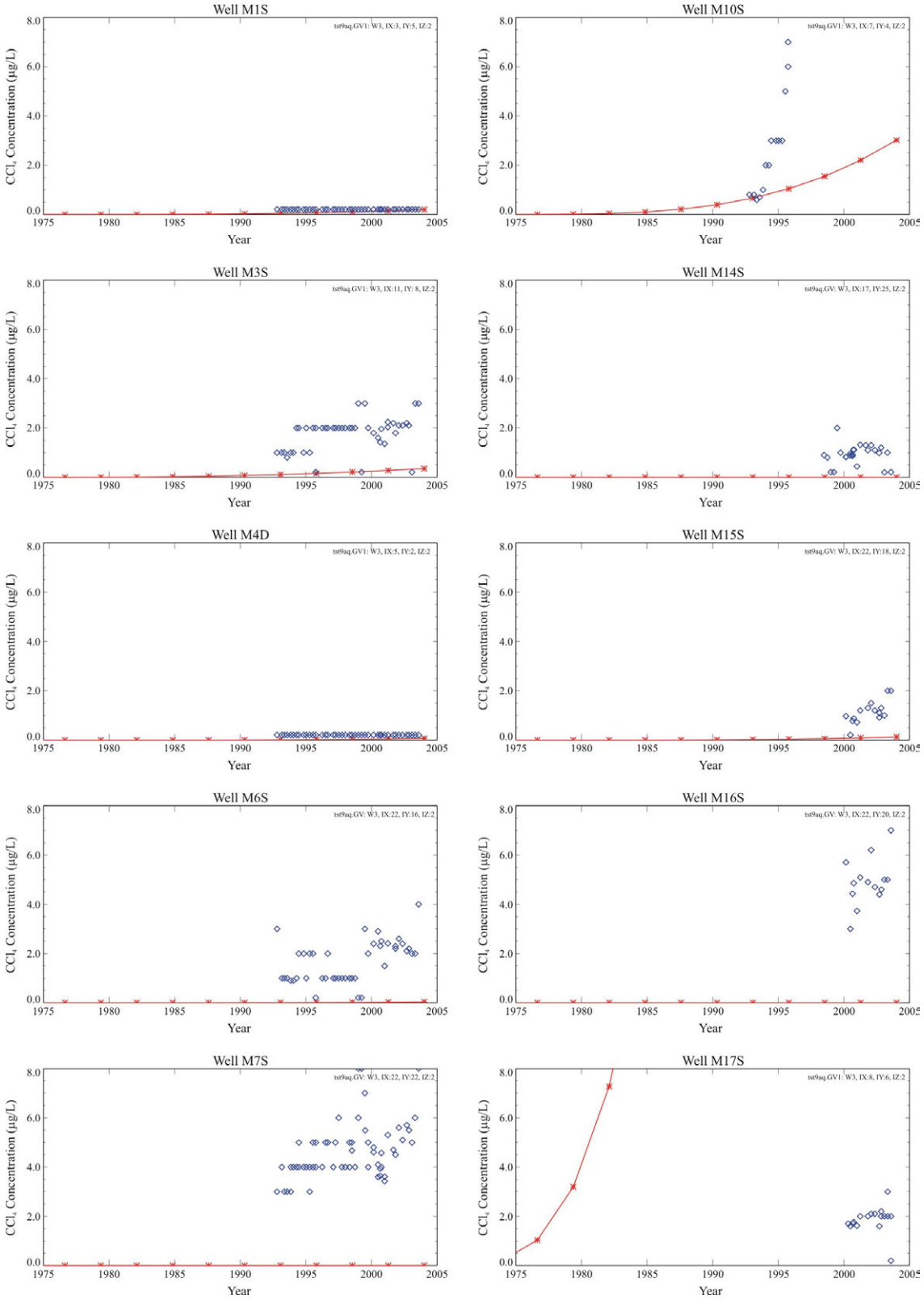

Figure 5-34. Time-history comparison of simulated (stars) and measured (diamonds) carbon tetrachloride concentrations in the aquifer at wells in and around the Subsurface Disposal Area through the year 2005.

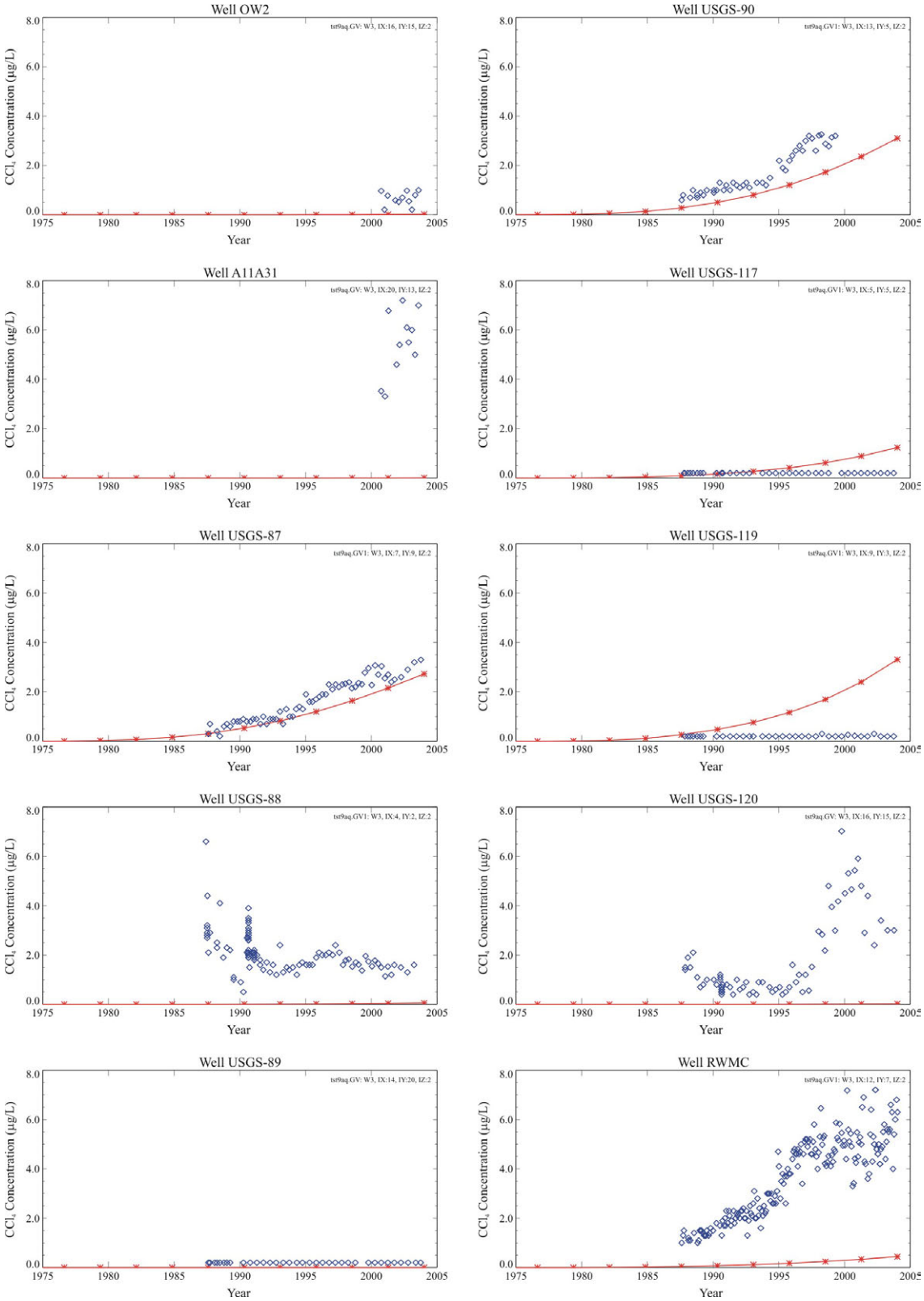

Figure 5-34. (continued).

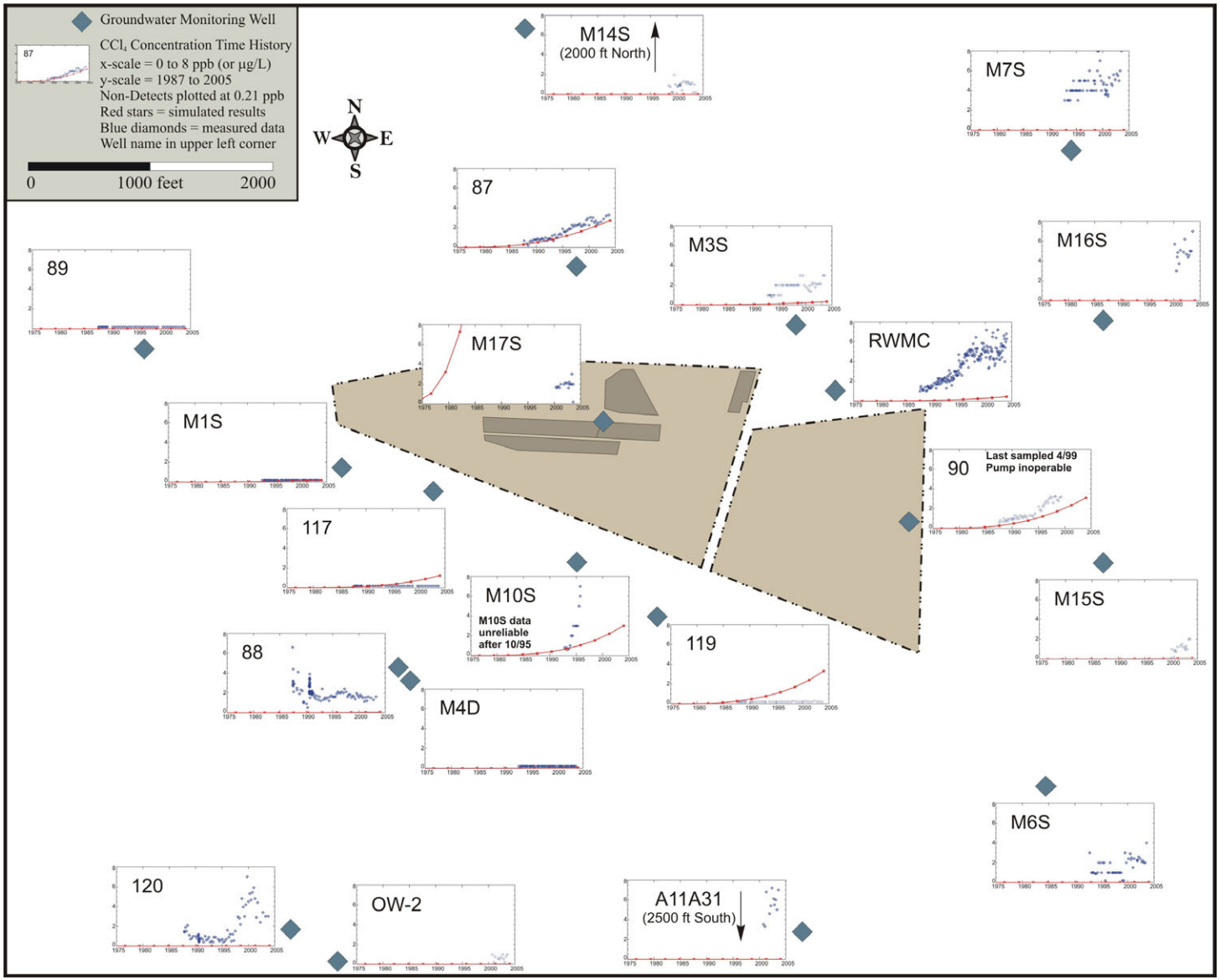

Figure 5-35. Time history of measured and simulated carbon tetrachloride concentrations in aquifer at wells in and around the Subsurface Disposal Area. The source pits shaded in the Subsurface Disposal Area are the primary carbon tetrachloride source pits.

In general, the RI/FS model results are similar to the IRA model results for the aquifer. Interim Risk Assessment model results at the RWMC Production Well agreed better because more VOCs in the IRA model were assigned to Pit 9, which is closer to the RWMC Production Well. However, knowledge of VOC waste burial locations has vastly improved since the IRA model, and it is likely that if the current distribution of VOC waste were used in the IRA model, the results would be similar to the results obtained for the RI/FS model.

5.4.6 Volatile Organic Compound Transport Model Calibration Summary

Numerous source and transport model simulations were performed in order to create a model that would adequately reproduce the observed migration of CCl_4 from the SDA, and predict, with a relatively high degree of confidence, future concentrations of VOCs and other contaminants that are transported in a vapor phase. The effort was aided considerably by modeling work performed for the IRA and other modeling efforts (e.g., Sondrup 1998).

The first step of calibration was to establish an appropriate source-release model that was compatible with the estimate of CCl_4 mass remaining in the pits. This involved investigation of several source-release parameter combinations. In the end, only one of the combinations that produced the desired result seemed reasonable. The next step was to calibrate the transport model by adjusting tortuosity values of the different material types in the model. Although numerous combinations of tortuosity values were investigated, the final tortuosity values were the same as the initial estimated values, except for a change in the fracture basalt tortuosity.

In general, the simulated results matched the observed data quite well close to the SDA, with one prominent exception—the model greatly overpredicted the aquifer concentrations at Well M17S. However, low concentrations in this well do not seem representative, given its proximity to the source. Also, the model did not do a very good job of matching the spread of contamination in the vadose zone. Other parameters of the model (e.g., fracture basalt anisotropy ratio, matrix basalt characteristic block length, and thickness of the low-permeability, low-porosity layer) were modified to increase spreading, and, although each by themselves improved the result, the model still could not match the overall breadth of the vadose zone plume. However, since the amount of CCl_4 on the outer fringes of the plume is a very small percentage of the total mass entering the aquifer, matching concentrations away from the SDA was a less critical part of calibration. Because of good agreement of simulated data to measured data within and near the SDA in both the vadose zone and the aquifer, the calibration was deemed successful.

5.4.7 Impact of Fluctuating Barometric Pressure Boundary Condition

Simulations were performed to quantify the impact of a fluctuating barometric pressure boundary condition. Figure 5-36 shows the mass flux of CCl_4 to the aquifer both with and without a fluctuating barometric pressure boundary condition. The results show that when barometric pumping is not included in the simulation, the flux to the aquifer increases. The increase is approximately 40% in the year 2000 and 30% in the year 2125, when the flux to the aquifer peaks. The results for flux to the atmosphere are similar, but in this case the flux decreases when barometric pumping is not included. Therefore, not including barometric pumping is conservative for the groundwater pathway, but is not conservative for the air pathway.

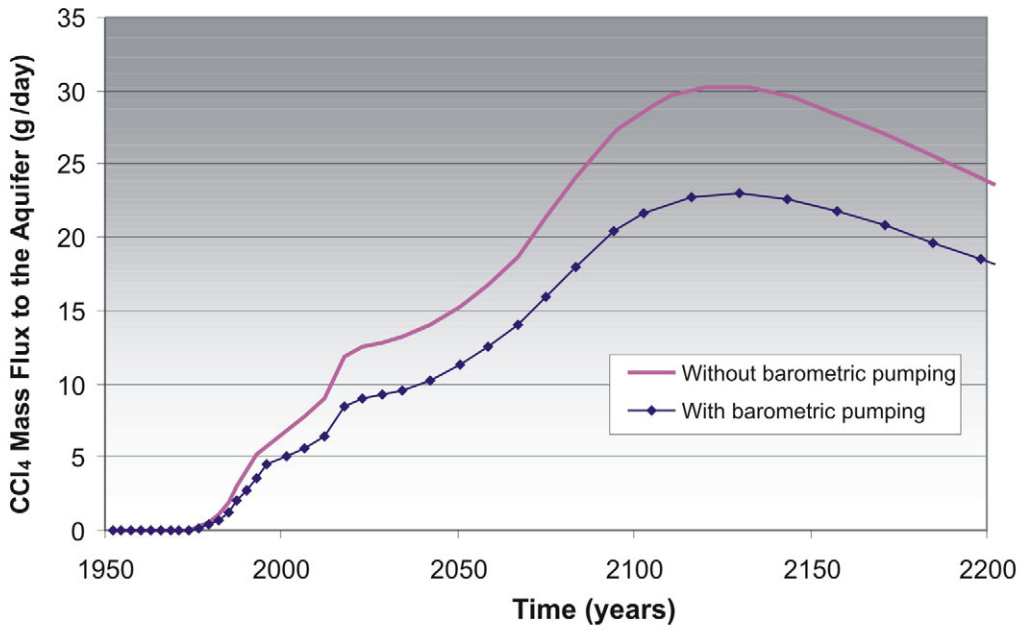

Figure 5-36. Time-history comparison of simulated carbon tetrachloride mass flux to the aquifer, with and without surface barometric pressure fluctuations.

5.5 Dual-Phase Carbon-14 Simulations

In the ABRA, C-14 was simulated as a strictly dissolved-phase contaminant. This meant that C-14 could not partition into the gaseous phase and undergo additional transport processes (e.g., diffusion in the gaseous phase). Therefore, C-14 could not diffuse out through the upper surface of the simulation domain (land surface). This was a conservative approach that maximized C-14 concentrations in the groundwater pathway. However, in the ABRA, the C-14 concentrations in the groundwater pathway were overpredicted by two to three orders of magnitude due to this conservatism when compared to currently observed concentrations from contaminant monitoring.

For the RI/FS model, the simulation of C-14 was modified to allow C-14 to partition into the gaseous phase. This means that C-14 existed in both the aqueous and gaseous phase and underwent transport in both phases simultaneously. This approach to simulating C-14 was most easily accommodated by adopting the dual-continua model implemented for the VOC modeling previously described. Before simulating C-14 with the full-scale dual-continua vadose zone model, two interim simulation efforts were conducted to determine the appropriate partitioning parameters and the possible effect of increased diffusion to land surface in the immediate vicinity of the beryllium blocks, which contain a large fraction of the C-14 inventory. These two interim studies are briefly described first, followed by the implementation of C-14 in the dual-continua vadose zone model developed for VOCs.

5.5.1 Carbon-14 Partitioning from Column Experiment

A simulation study was conducted to determine the correct partitioning for C-14 in a combined aqueous- and gaseous-phase system. This simulation study used experimental data from a 3-m (9.8-ft) high × 0.9-m (3-ft)-diameter mesoscale column where an aqueous-phase tracer (i.e., bromide), a gaseous-phase tracer (i.e., SF_6), and C-14, which partitioned into both phases, was monitored. The column experiment was designed to mimic conditions in the waste zone at the SDA and had a constant

low flux of water applied at the surface. The column experiment also allowed gaseous-phase diffusion out the surface. Inverse modeling was applied to this set of column data to match both the aqueous- and gaseous-phase transport. This inverse modeling study is documented in Martian (2003).

Parameters describing partitioning of C-14 comprise the primary output from the inverse study used in RI/FS modeling. In Martian (2003), C-14 was treated as if it were carbon dioxide, with the partitioning estimated from Henry's Law. The resulting TETRAD input parameter A was 2.9×10^4 kPa and is essentially the inverse of the effective Henry's Law constant, assuming constant temperature and pressure.

The inverse modeling application resulted in excellent matches to observed water flux, breakthrough of the bromide and SF_6 tracers, and breakthrough of C-14 from the column in both the aqueous and gaseous phases. Because of this good agreement, a conclusion was made that effective Henry's Law partitioning adequately described the partitioning of C-14 in the column and could be used, with the normal cautions on upscaling, for the RI/FS vadose zone modeling.

5.5.2 Carbon-14 Beryllium Block Near-Field Simulation

A significant portion of C-14 buried in the SDA is in beryllium reflector blocks. As beryllium corrodes, C-14 and tritium are released and partition into the aqueous and gaseous phases. With contaminant release concentrated in a small area within the surficial sediment, higher gaseous-phase concentration gradients would be established between release sites and the short distance to land surface, where movement of air maintains a gaseous-phase concentration of essentially zero. A hypothesis that this increased concentration gradient could result in additional release of C-14 from the subsurface was tested in a study documented in Nalla (2004). Subsurface and atmospheric sampling from an instrumented location in the SDA was used in an inverse modeling study.

Even with the less-than-desired match to observed C-14 and tritium migration behavior, it was concluded that a substantial fraction, on the order of 80% of the C-14 mass, is released to land surface through diffusion. This indicated that it was indeed important to include diffusional loss through land surface in the RI/FS model. The Nalla (2004) recommendation to reduce C-14 release from beryllium reflector blocks by 80% for use in the subsurface model was not implemented; that implementation would have resulted in accounting doubly for the release to the atmosphere because surface diffusional losses also were included in the RI/FS model.

5.5.3 Operable Unit 7-13/14 Model Carbon-14 Implementation

The VOC dual-continua model described in Section 5.4 was used to simulate transport of C-14. Use of this dual-continua model takes advantage of additional calibration achieved in VOC modeling. The assigned contaminant mass locations for C-14 were different from locations for the strictly aqueous-phase contaminants, as discussed in Section 4.3.7.3.

5.5.3.1 Carbon-14 Model Boundary Conditions. The aqueous-phase boundary conditions were kept the same as the RI/FS VOC dual-continua model. Two changes were made to the gaseous-phase boundary conditions. First, the lateral zero-concentration boundaries were omitted because they were unnecessary for simulation of C-14. They were unnecessary because the C-14 contaminant mass did not reach the boundaries in appreciable quantities, as it did for VOC contaminants. Second, similar to VOC modeling, barometric-pressure fluctuations at land surface were eventually neglected in C-14 modeling. They were neglected primarily for computational expediency, because including barometric fluctuations required using a minimum 10-day time step, which resulted in long run times—on the order of 2 months of computer processing time—to achieve approximately 700 years of simulation time (the radionuclide

simulations for the base case and sensitivity simulations were all planned to be simulated to 1,000 years into the future, and out to peak concentrations within 10,000 years). This was not feasible within even the most generous time constraints. Fortunately, the effect of neglecting barometric fluctuations was conservative, because more C-14 mass was retained in the simulation domain and migrated through the groundwater pathway.

The effect of not including barometric fluctuations was tested by making comparative simulations, with and without barometric pumping. These comparisons used the sensitivity simulation of the comparative base case (i.e., B4ng_g8), which comprised no removal of Pit 4 inventory and no grouting of beryllium blocks. Figure 5-37 shows a comparison of the maximum simulated aquifer concentration as a function of time at a depth of 12 m (39.3 ft) anywhere in the simulation domain, with and without barometric pumping. Concentrations for each simulation are extracted for both anywhere in the model domain and anywhere in the domain outside the SDA fence. The effect of not including barometric-pressure fluctuations for locations outside the SDA fence was to increase the simulated aquifer concentration by approximately 20%. It was slightly larger inside the SDA, with an approximate 25% increase. Implementing C-14 simulations without barometric-pressure fluctuations brought back some of the conservatism that had been reduced by simulating gaseous-phase partitioning.

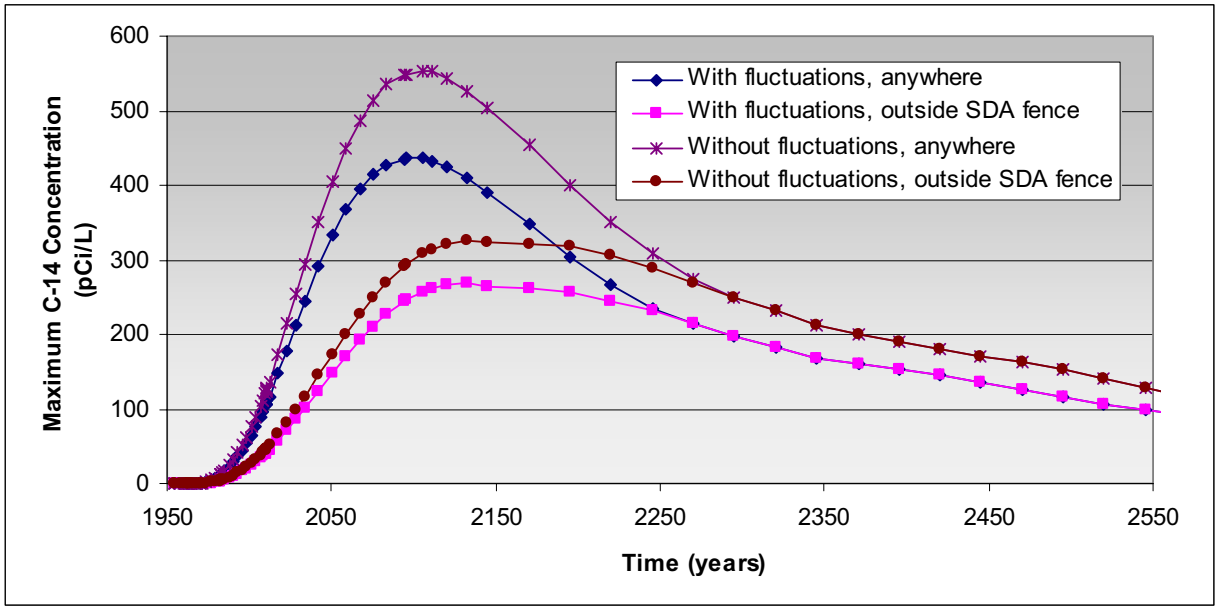

Figure 5-37. Maximum simulated aquifer carbon-14 concentration, anywhere in the simulation domain, at a depth of 12 m (39.3 ft), with and without surface barometric pressure fluctuations.

5.5.3.2 Carbon-14 Comparison without Gaseous-Phase Partitioning. To demonstrate the effect of including gaseous-phase partitioning in the RI/FS model, an additional simulation was performed where C-14 source release was imposed on the single-continua model used for contaminants that migrated strictly in the aqueous phase, essentially reverting to the method used in the ABRA for simulating C-14 migration. Figure 5-38 shows a comparison of the maximum simulated concentration anywhere in the aquifer for case B4ng_g8 with gaseous partitioning in the vadose zone model and diffusion at land surface to the same simulation where gaseous-phase partitioning is not included. In the case where gaseous partitioning is not allowed, no diffusive loss to land surface occurs. The results are presented with both a linear and logarithmic scale concentration axis because the difference is so large (i.e., approximately two orders of magnitude).

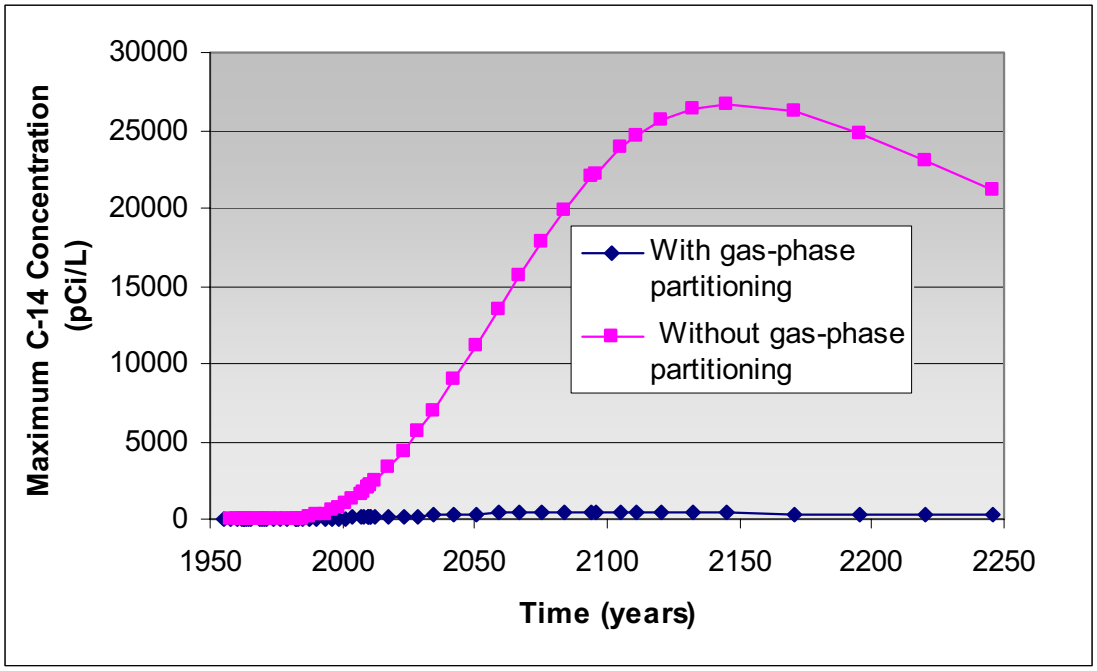

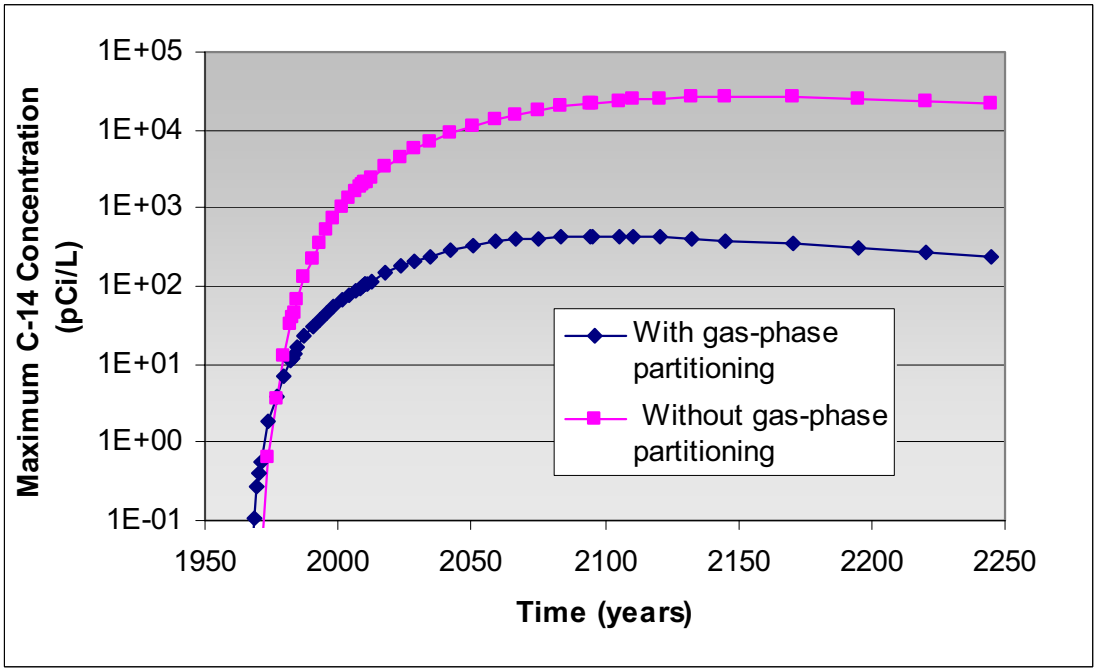

Figure 5-38. Maximum simulated concentration anywhere in the aquifer, with and without gaseous-phase partitioning in the vadose zone transport model.

5.5.3.3 Carbon-14 Model Remedial Investigation and Baseline Risk Assessment Base-Case Simulation Results. The base-case final simulation for C-14 did not include barometric-pressure fluctuations. No consistently elevated concentrations or trends have been in evidence for C-14 monitoring in the vadose zone. One location that has shown detections is the perched water in Well USGS-92 above the C-D interbed. Figure 5-39 shows a comparison of the simulated C-14 aqueous-phase concentration at the gridblock representing this location to the monitoring results. No

background concentration is added to the simulation results. Even with inclusion of gaseous-phase partitioning and diffusional losses to land surface, the simulated concentrations still overpredict the sporadic observed values, indicating the simulation result is still conservative.

The simulated aquifer concentration time histories for C-14 at locations containing aquifer-monitoring wells are shown in Figure 5-40. Monitoring results for C-14 that represent 3σ detections, or greater, are included as blue diamonds on the time-history plots along with a whisker-style indication of their associated 1σ uncertainties. Results show the sporadic nature of detections and demonstrate that simulation results are conservative because they overpredict measured groundwater concentrations in Wells M17S and USGS-119, though not nearly to the degree recorded in the ABRA. The overprediction at Well M17S is consistent with CCl_4 results in that the model overpredicts measured data. Figure 5-41 shows simulated aquifer C-14 concentrations in the first-level refined grid for the aquifer domain. The simulated elevated concentrations are more centrally located beneath the southeastern corner of the SDA when compared to other contaminants (e.g., nitrate).

5.5.4 Summary

There is a substantial reduction in simulated concentration results when gaseous-phase partitioning of C-14 is included in the RI/FS model. Excluding barometric pressure fluctuations at land surface was conservative since the simulated groundwater concentrations were higher than they would have been had barometric pressure fluctuations been included. However, conservatism is slight and does not negate the reason for including gaseous-phase partitioning in the first place.

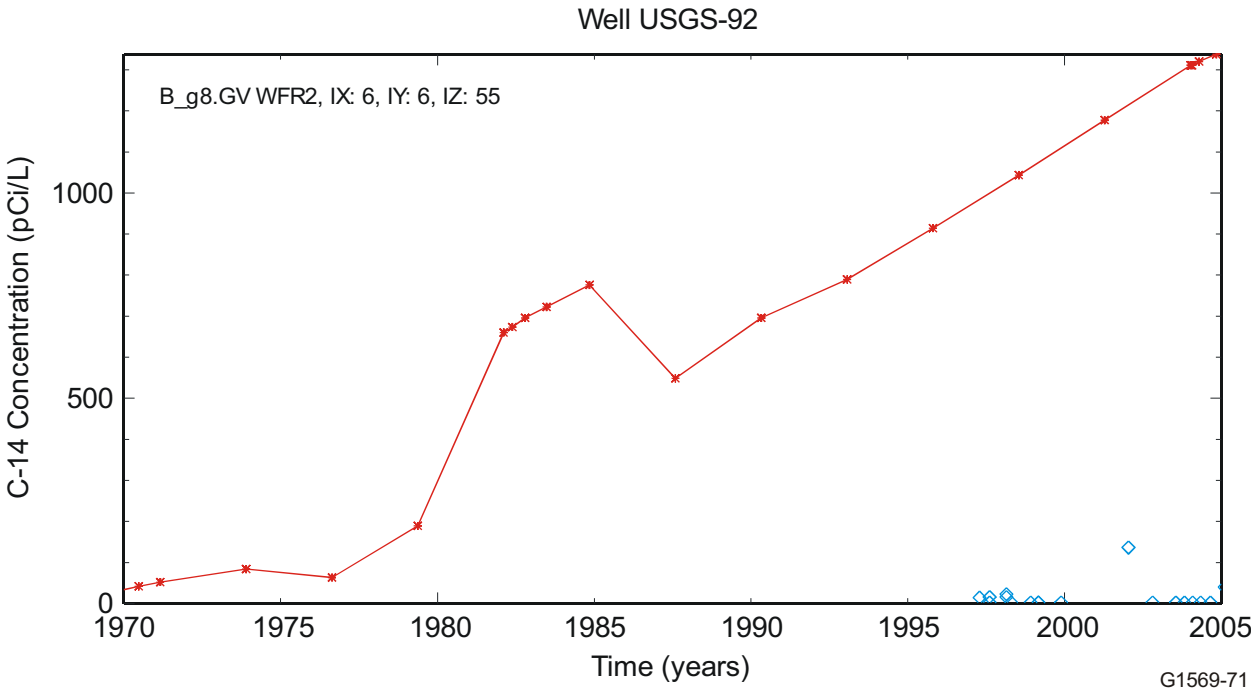

Figure 5-39. Time history of simulated (red line) and observed (blue diamonds) carbon-14 aqueous-phase concentrations at Well USGS-92.

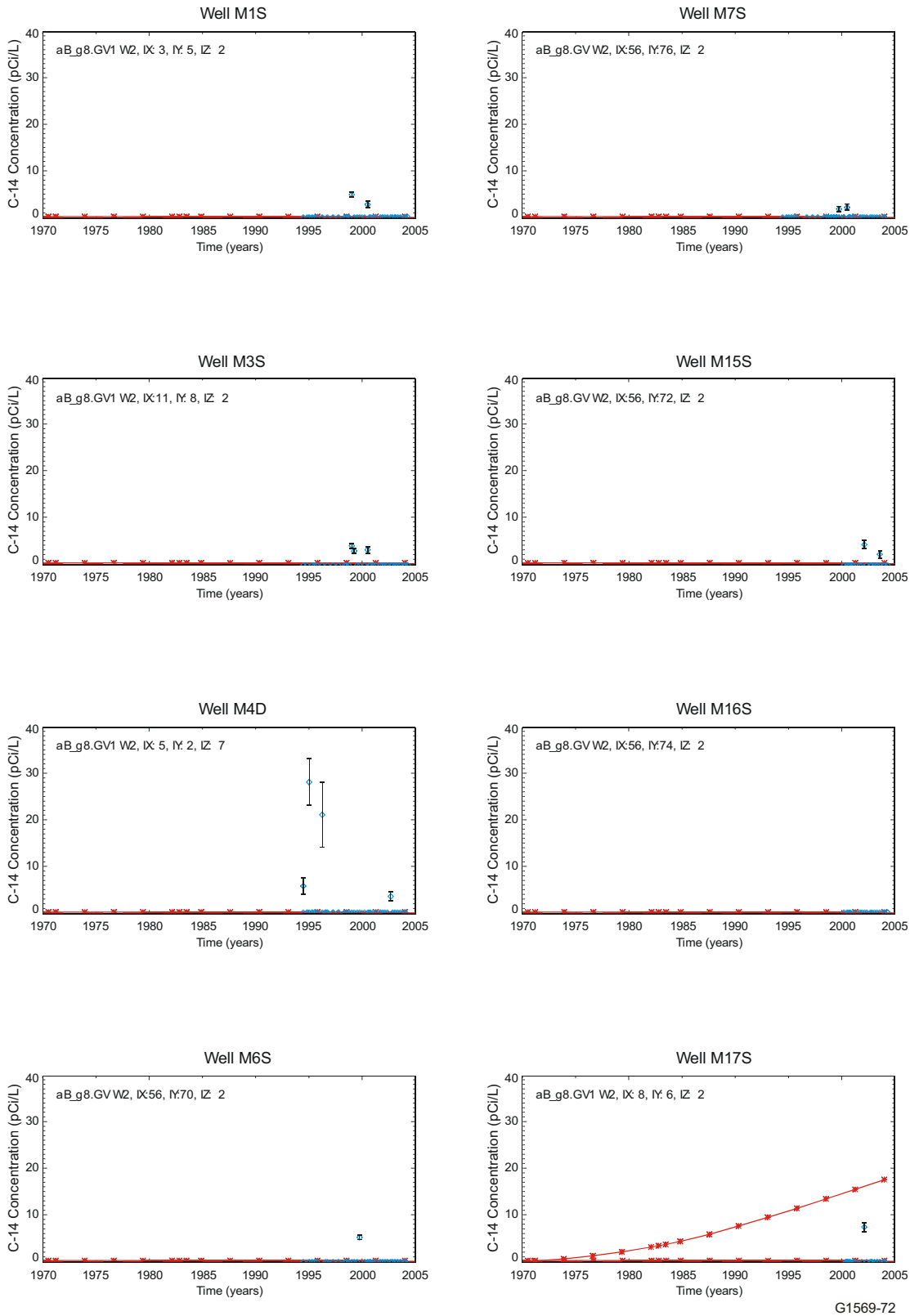

Figure 5-40. Comparison of time histories for simulated carbon-14 concentrations (red line) to observed monitoring results (blue diamonds) for aquifer monitoring wells in the vicinity of the Subsurface Disposal Area.

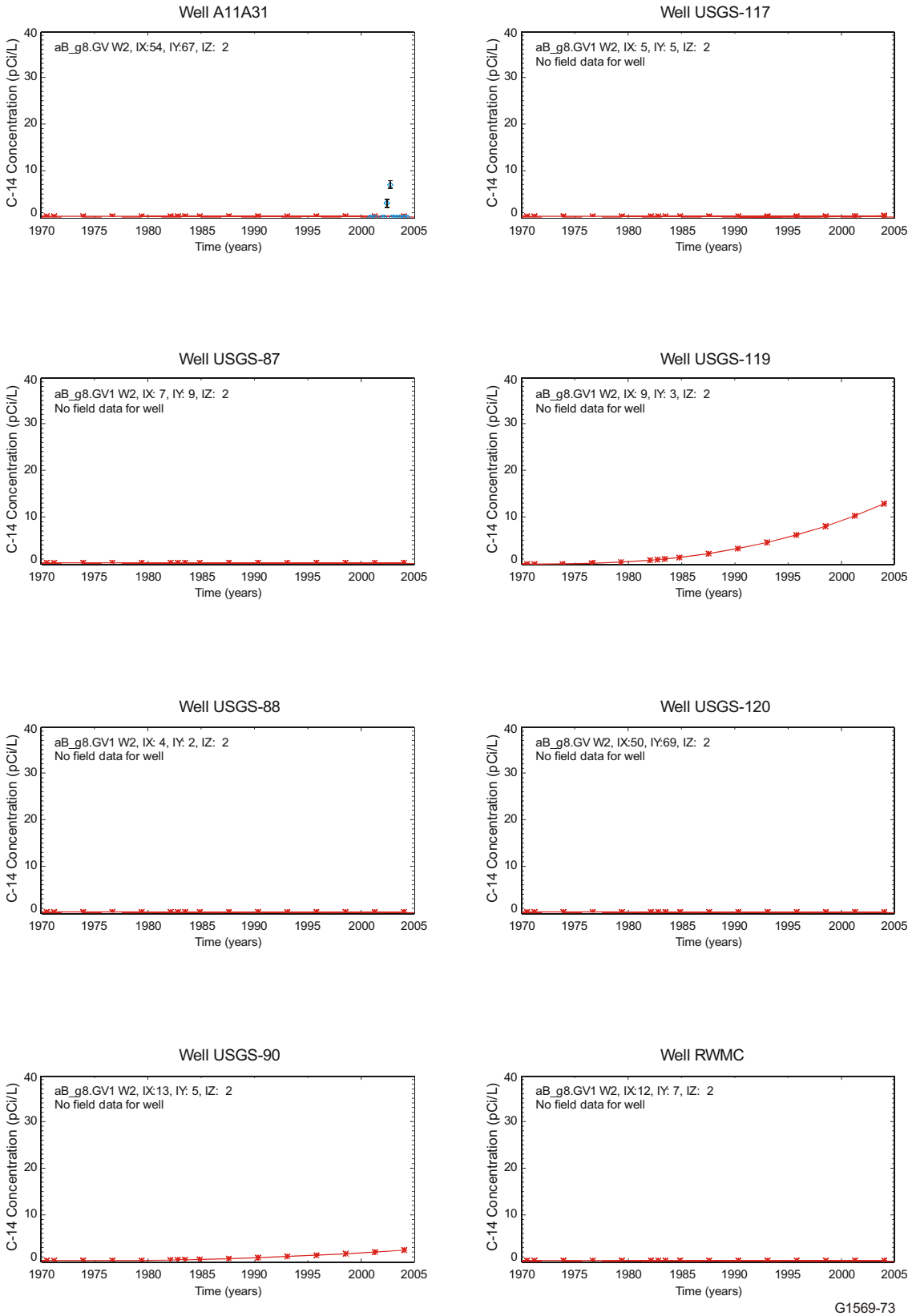

Figure 5-40. (continued).

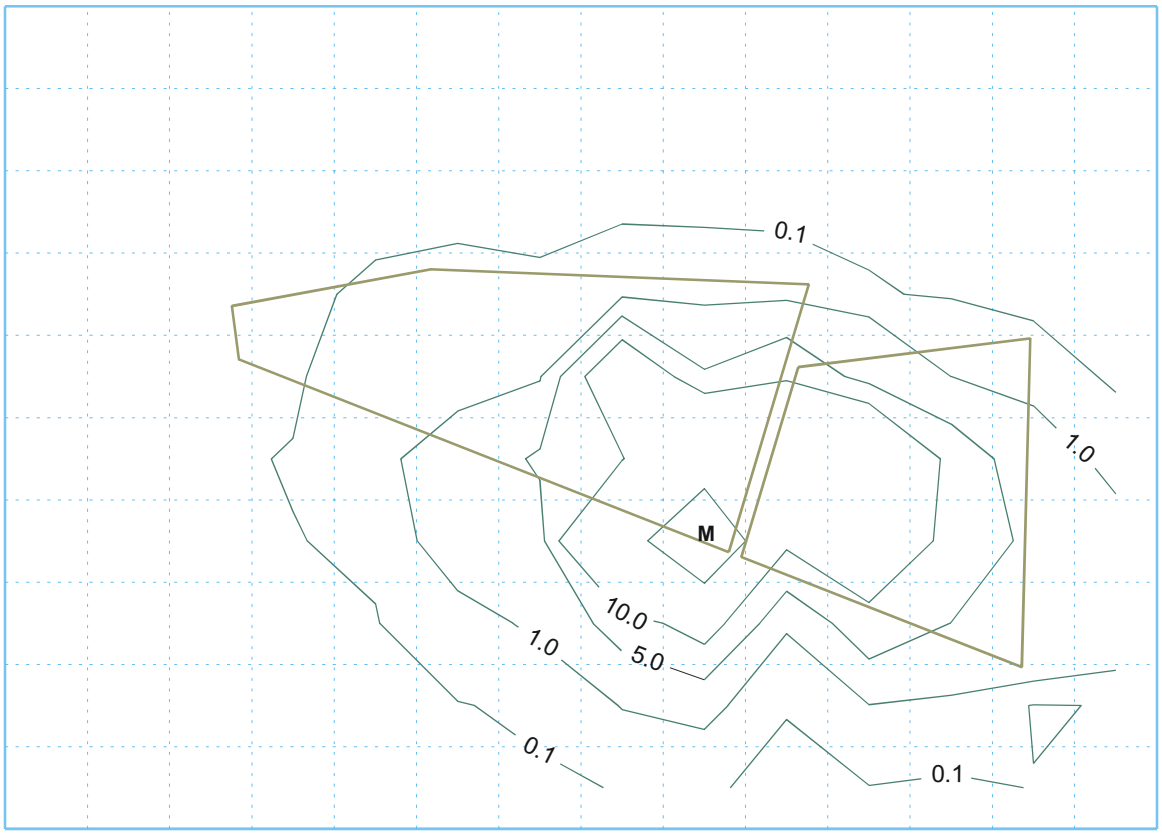

Figure 5-41. Simulated aquifer carbon-14 concentrations (pCi/L) at the 12-m (39.3-ft) depth for the year 2004.

6. OPERABLE UNIT 7-13/14 FATE AND TRANSPORT MODEL RESULTS

This section presents comparisons of the base-case model to contaminant monitoring results, describes sensitivity simulations performed for the draft RI/BRA, and describes simulations performed for the feasibility study.

6.1 Baseline Risk Assessment Base-Case Simulation with Comparison to Monitoring Results

The numerical model, implemented as discussed in Sections 4 and 5, was used to simulate each COPC for the RI/BRA base case. The source-release model provided contaminant inputs to the vadose zone model. This section presents comparisons of simulated results with observed concentrations for selected contaminants to illustrate transport model performance. These comparisons are presented in sequence for the vadose zone from 0 to 10.7 m (0 to 35 ft), the deeper vadose zone from 10.7 to 76.2 m (35 to 250 ft) that contains the B-C and C-D interbeds, and the aquifer. The comparisons are primarily time histories and aquifer concentration contours at points in time. The contaminants, for which simulation results are presented in the vadose zone, are U-238, Tc-99, and nitrate. These contaminants were identified in Section 4 of the draft RI/BRA as showing either elevated concentrations relative to background or significant increasing trends. In the aquifer, the presentation focuses on simulation results for nitrate and chromium, because those contaminants can be discerned above background aquifer concentrations. Additionally, time histories are presented for all radionuclide contaminants with any detections. Simulation time histories for CCl_4 were presented previously in Section 5.4.5. The full set of CCl_4 results is contained in Appendix G.

6.1.1 Vadose Zone: 0 to 10.7 m (0 to 35 ft)

This section focuses on the U-238, Tc-99, and nitrate simulation results for those locations showing elevated concentrations or trends in the vadose zone at depths less than 10.7 m (35 ft). In general, this region encompasses the waste zone and surficial sediment down to the first basalt interface. Because there can be multiple lysimeters at different elevations for an individual well location, lysimeters are referred to in this section using a combined well name-lysimeter number identifier.

6.1.1.1 Uranium-238. From Section 4 of the draft RI/BRA, lysimeters at Wells PA01, PA02, W08, and W23 show substantially elevated concentrations relative to an estimated background concentration of 1.1 pCi/L for the vadose zone. This background concentration is added onto simulation results in the following time histories. The first set of time histories shown in Figure 6-1 is for lysimeters at Wells PA01, PA02, W08, 98-4, and W25; all five wells are located in the east-central portion of the SDA. At first impression, the simulation results show almost no agreement; however, this difference is explained by the relationship of the gridblocks containing the lysimeters to the locations where U-238 is released from the source model into the vadose zone model. The locations of the lysimeters can be seen in Figure 6-3. For example, Figure 6-1 also shows a simulated concentration time history for U-238 for a gridblock that is one gridblock north of the location containing Well PA02-L16. This latter gridblock location is assigned the Pad A waste stream. The time history at this location shows better agreement with observed monitoring results. The concentrations are slightly underpredicted, but are well within the same order of magnitude. Lysimeters in Wells PA01 and W08 also are not in gridblock locations that have a U-238 source release superimposed on them; for similar reasons, these wells show poor agreement with observed concentrations. Lysimeters in Wells 98-4 and W25 show similar behavior, with location relative

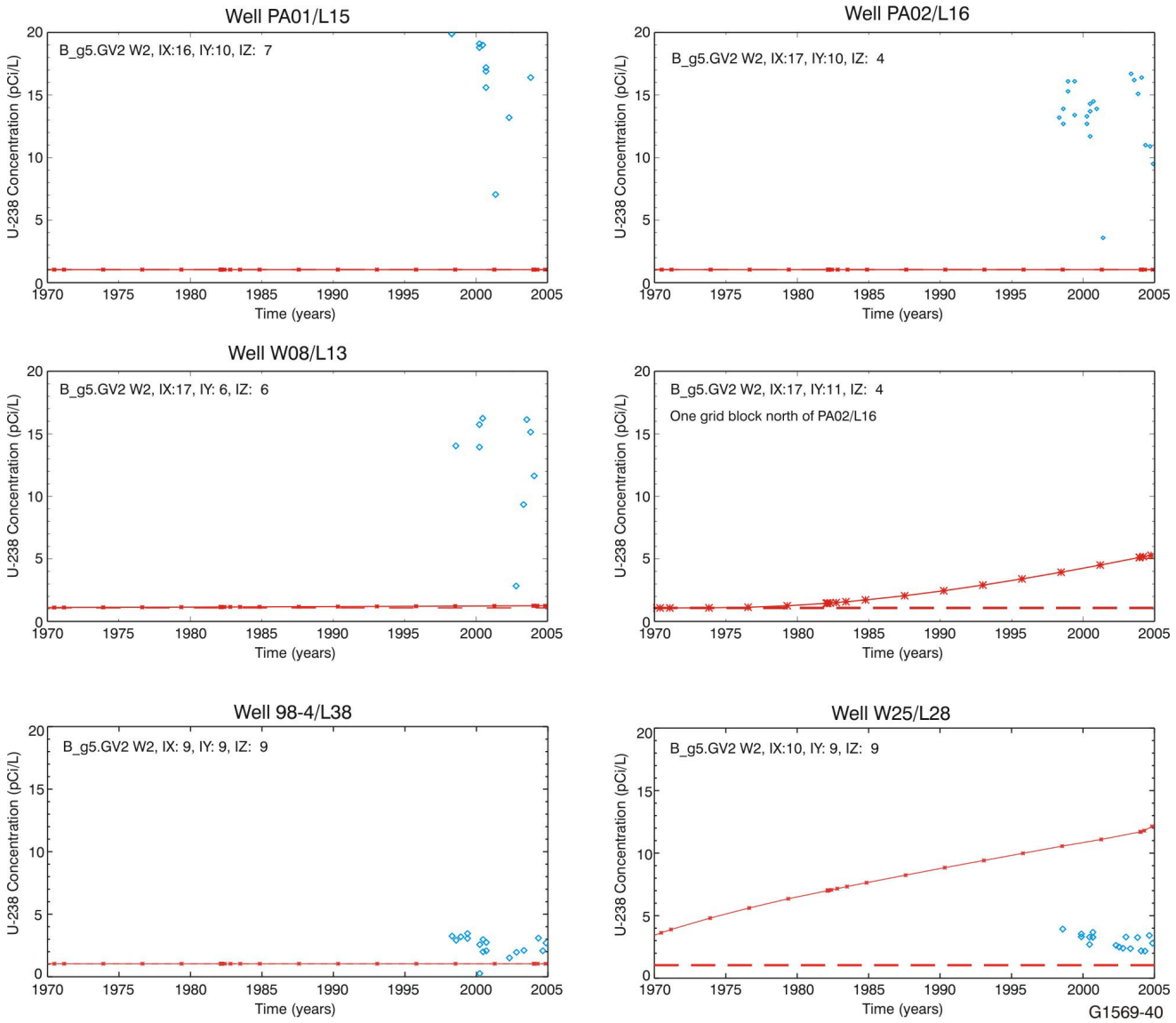

Figure 6-1. Time-history comparison of simulated (red line) and observed (blue diamonds) concentrations for uranium-238 in the lysimeters at Wells PA01, PA02, and W08. Background concentration is indicated by the dashed line.

to gridblocks where waste streams are applied as being important. The lysimeter in Well 98-4 corresponds to the gridblock one cell west of the Pit 4 waste stream and shows reasonable agreement with monitoring data, which is similar to the estimated background. The lysimeter in Well W25, however, just barely corresponds to the westernmost gridblock receiving the Pit 4 waste stream, and the simulated results overpredict monitoring results, which again are similar to the estimated background concentration. With a model as coarsely discretized as the RI/FS model, some locations will show good agreement and some locations will not, depending on where mass is loaded into the vadose zone model from the source model. Also, simulated concentrations represent an average for the entire gridblock, whereas monitoring results represent point data that will vary spatially.

The simulated concentration time history shown in Figure 6-2 is for the three lysimeters in Well W23, located in the western portion of the SDA. This gridblock corresponds to the source-release area of Trenches 1 through 10, which does have U-238 mass imposed on it. As a result, simulated concentrations are nonzero for this location and, although low compared to the observed concentrations, are within an order of magnitude of the monitoring results.

To avoid giving the erroneous impression that U-238 is underpredicted everywhere, vertical cross sections, which include source-release locations in the second-level refined grid, are presented in Figure 6-3. Figure 6-3 shows the locations of the cross sections—two west-east and one south-north. The additional blue shading on the locations of the cross sections indicates source-release gridblocks, with the darker shading showing those locations with higher source-release fluxes and the lighter shading showing those locations with lower source-release fluxes. Figure 6-4 shows cross sections from the indicated locations for a simulation time corresponding to Calendar Year 2004. Monitoring results from this time period are posted on the plot at their approximate location. Also posted beneath these two values is the number of monitoring results that were available from this lysimeter from an arbitrary 2-year period before and after the indicated time. Only samples with detections are posted. Lithologic divisions can be discerned in the cross sections. Land surface is the uppermost solid line and shows slight variations in surface elevation. Solid lines also indicate the bottom of the surficial sediment and the A-B interbed.

The effects of discretization and where U-238 mass is assigned in the model can be clearly seen in the cross sections shown in Figure 6-4. The effect of the U-238 mass assignment, relative to the location of Well PA02, also can be seen in the cross sections. The southernmost Pad A waste stream gridblock shows up in cross sections of both the W-E Section: Plane 11, and in the S-N Section: Plane 17. Well PA02 is in the gridblock just to the south, and it shows very little simulated U-238 mass in contrast to monitoring results for Well PA02, which show U-238 is elevated. In addition, simulation results in the cross sections show that the majority of the U-238 remains within the lower part of the surficial sediment and selectively migrates downward, with some influence from gaps in the A-B interbed.

6.1.1.2 Technetium-99. Only one vadose zone location in the 0- to 10.7-m (0- to 35–ft) depth zone shows an increasing trend for Tc-99. This location is Well W23 and Figure 6-5 shows the simulated results compared to monitoring results for this location. The estimated background concentration for Tc-99 in the vadose zone is 0 pCi/L; therefore, it is not added to the time-history simulation results. Time histories in Figure 6-5 are presented using a logarithmic scale for concentration due to Tc-99 being substantially overpredicted at this location, as well as almost everywhere else in the simulations. Figure 6-6 shows a west-east cross section from the second-level refined grid for simulated Tc-99 concentrations in Calendar Year 2004. The Tc-99 overprediction in the vadose zone model is probably caused by the source-release model overpredicting the release of Tc-99.[d]

d. A task to improve the source-release and fate and transport modeling for Tc-99 is ongoing for incorporation into the Operable Unit 7-13/14 feasibility study to provide a better basis for remedial decisions.

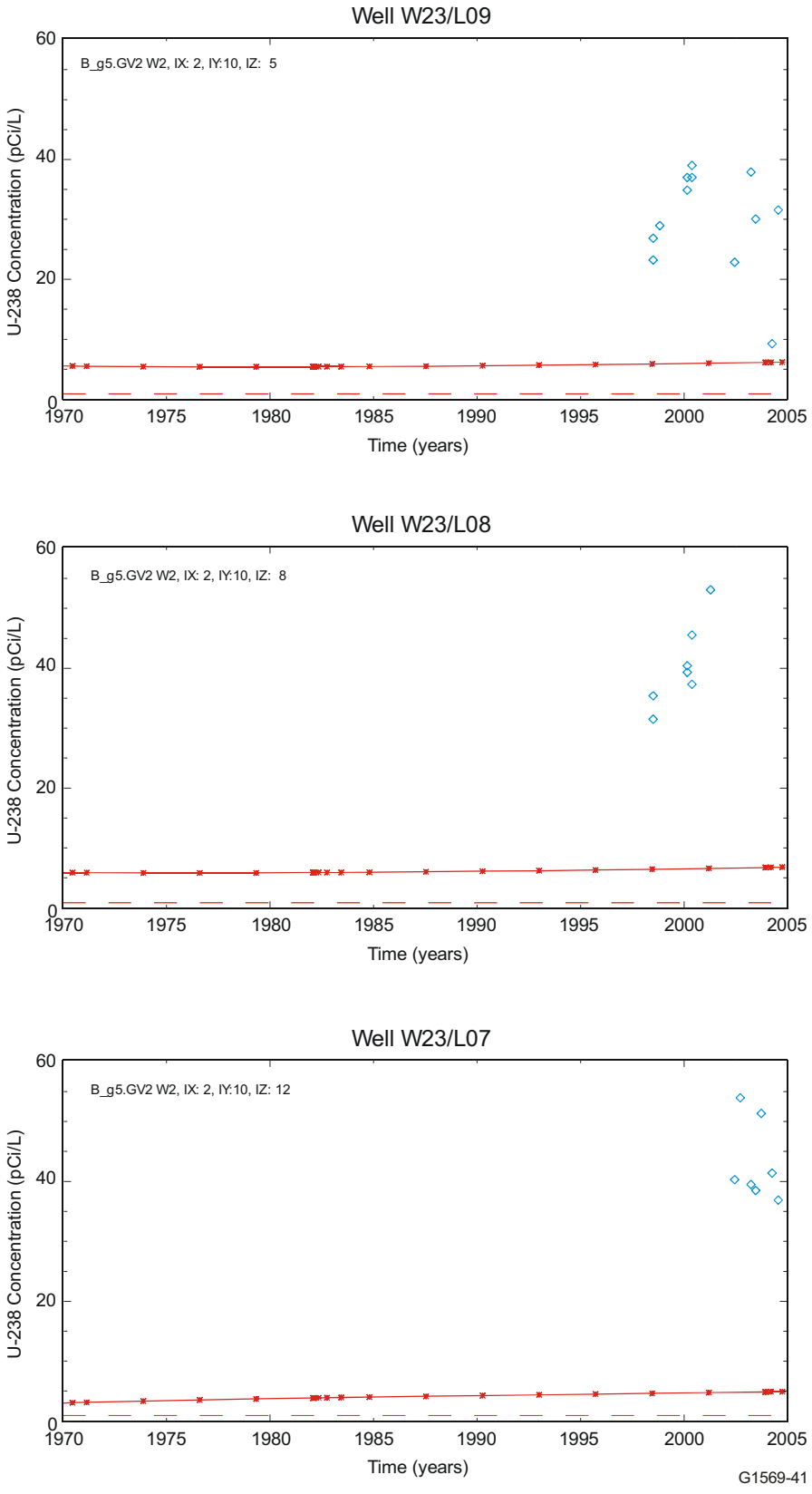

Figure 6-2. Time-history comparison of simulated (red line) and observed (blue diamonds) concentrations for uranium-238 in the lysimeters at Well W23. Background concentration is indicated by the dashed line.

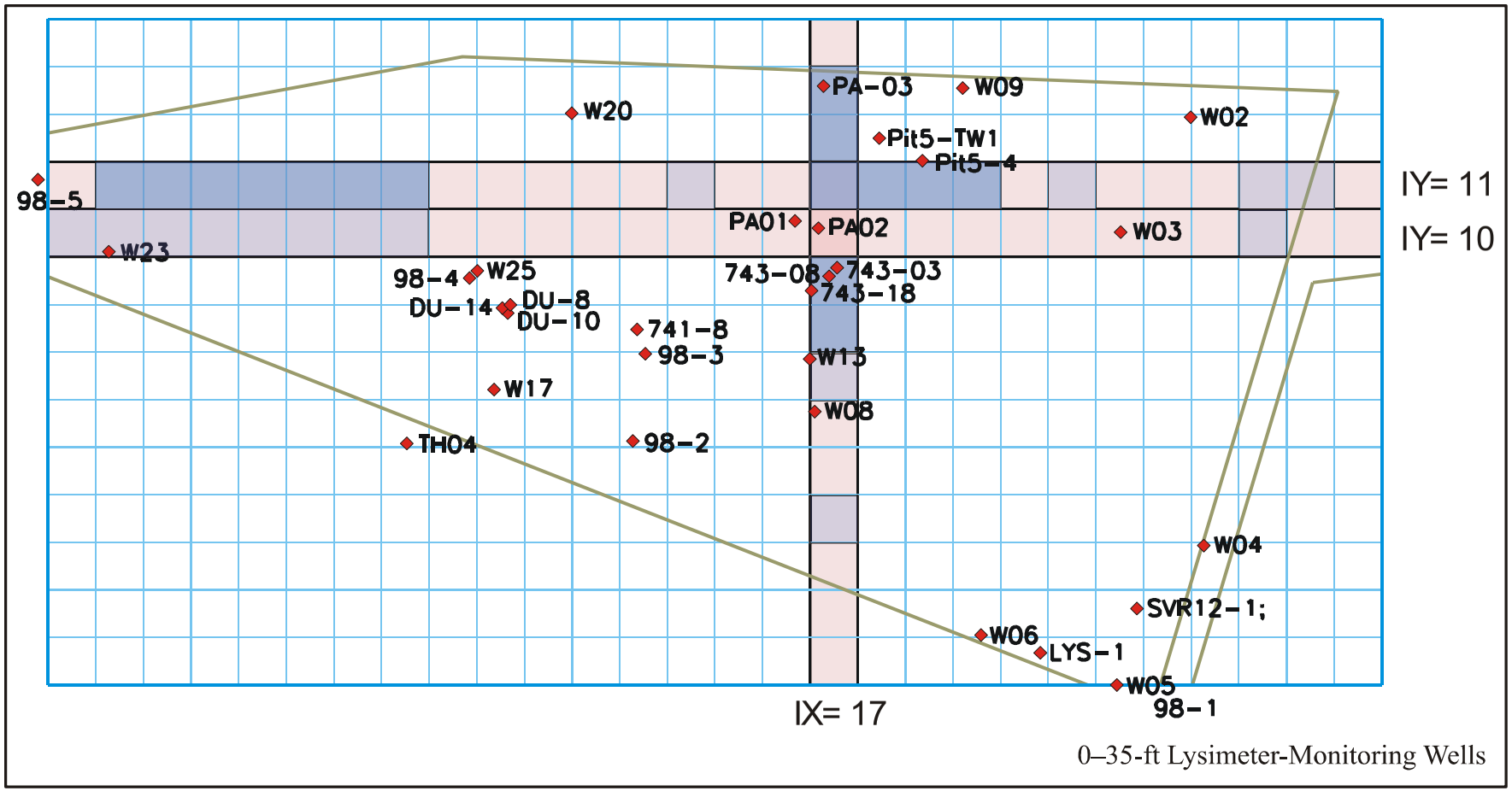

G1569-17

Figure 6-3. Cross sections in the second-level refined grid vadose zone domain. Darker blue shaded gridblocks indicate locations of primary uranium-238 mass loading from the source-release model.

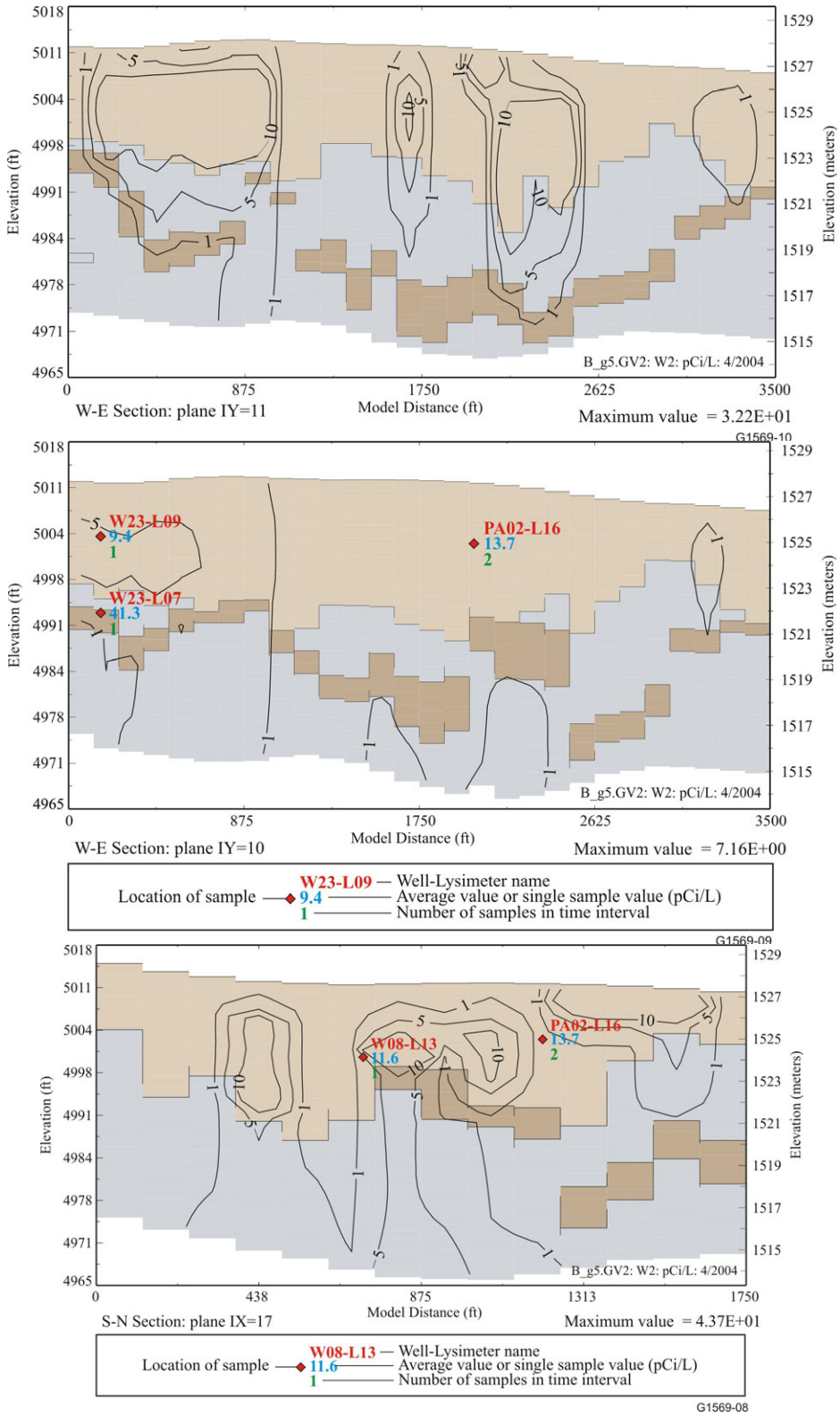

Figure 6-4. Cross sections showing simulated uranium-238 aqueous concentrations in Calendar Year 2004 (see Figure 6-3 for the location of the cross section).

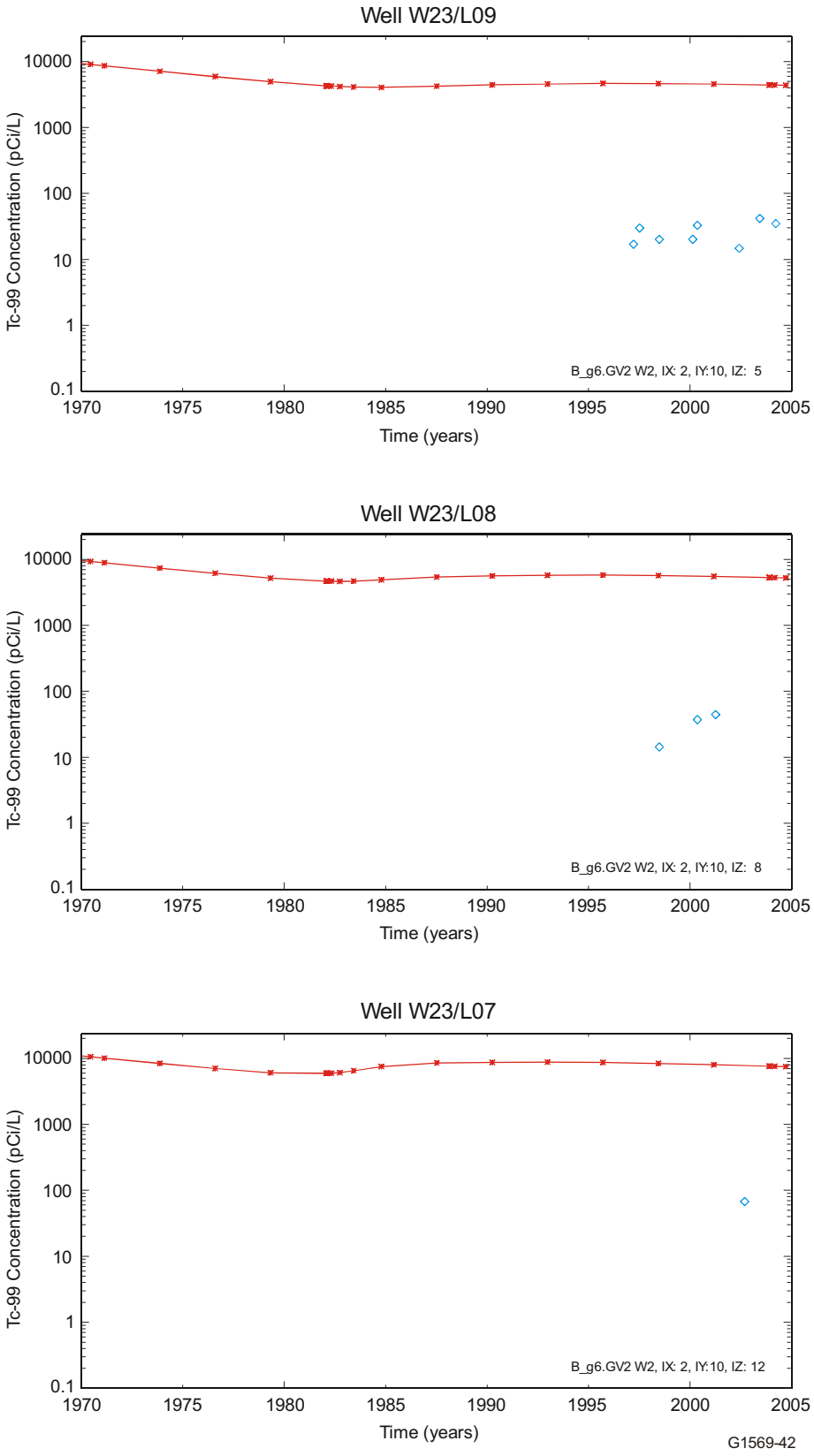

Figure 6-5. Time-history comparison of simulated (red line) and observed (blue diamonds) concentrations for technetium-99 in the lysimeters at Well W23.

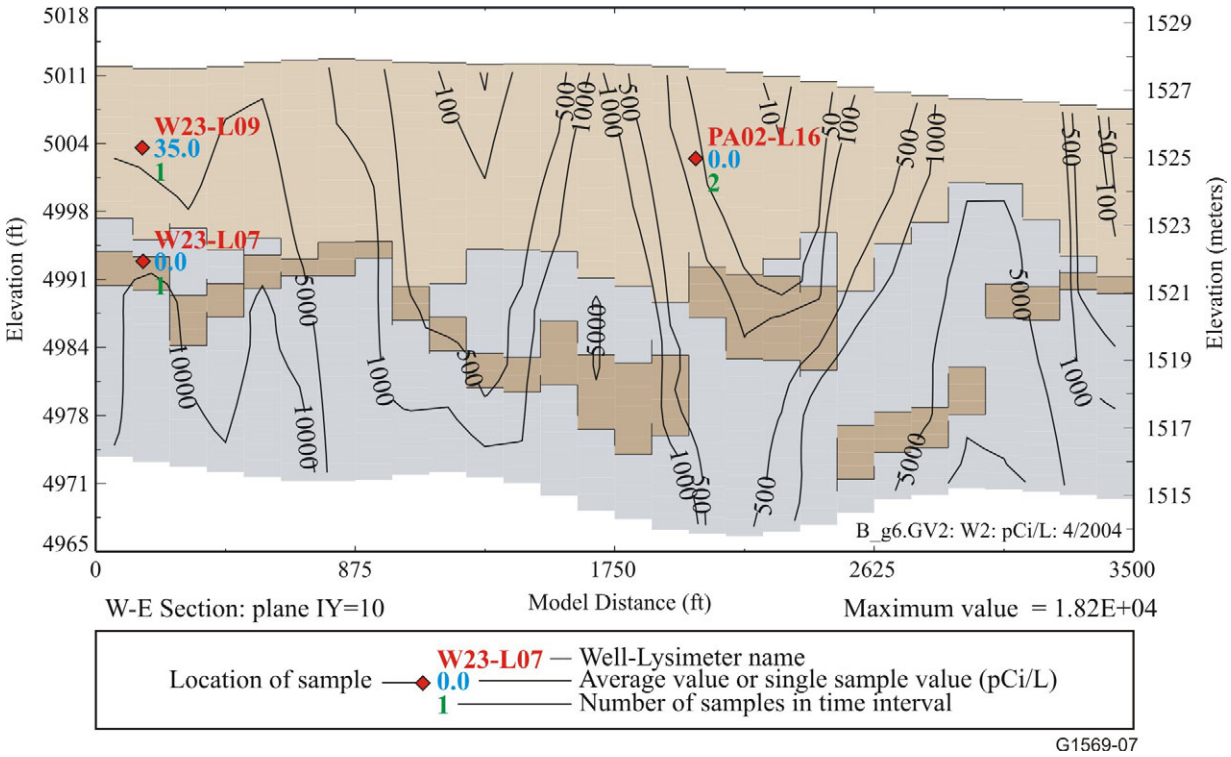

Figure 6-6. Cross section showing simulated technetium-99 aqueous concentrations in Calendar Year 2004 (see Figure 6-3 for the location of the cross section).

6.1.1.3 Nitrate—Elevated nitrate concentrations were seen at two locations, Wells PA02 and W25, in the 0- to 10.7-m (0- to 35-ft) zone (see Figure 6-7). The vertical concentration scale is different for the two locations in order to show detail, although both show the simulated concentration to be higher than the observed concentration. In contrast to the U-238 simulation results, even though the gridblock containing Well PA02 does not receive contaminant mass from the source-release model assigned to it, sufficient mass is assigned to the nearby Pad A waste stream blocks to result in appreciable nitrate appearing in the simulation results at this location. These locations were chosen because they show elevated nitrate concentrations; therefore, the model results at all other locations would also show overprediction, leading toward the conclusion that nitrate simulation results are conservative with respect to maximizing groundwater-pathway concentrations.

6.1.2 Vadose Zone: 10.7 to 76.2 m (35 to 250 ft)

Similar to the shallow vadose zone in the 0- to 10.7-m (0- to 35-ft) interval, simulated time histories are compared in this section for those monitoring locations from the 10.7- to 76.2-m (35- to 250-ft) interval that have elevated—even if only slightly—U-238, Tc-99, and nitrate concentrations.

6.1.2.1 Uranium-238. Lysimeters showing slightly elevated U-238 concentrations above background are I1S-DL09, I4S-DL15, D06-DL01, DO6-DL02 and TW1-DL04. For the Well D06 location, only the uppermost lysimeter (i.e., Lysimeter DL02) is shown in Figure 6-8. Intervals of 10.7 to 42.7 m (35 to 140 ft) and 42.7 to 76.2 m (140 to 250 ft) are combined for this discussion because so few locations are showing elevated concentrations in the deeper interval.

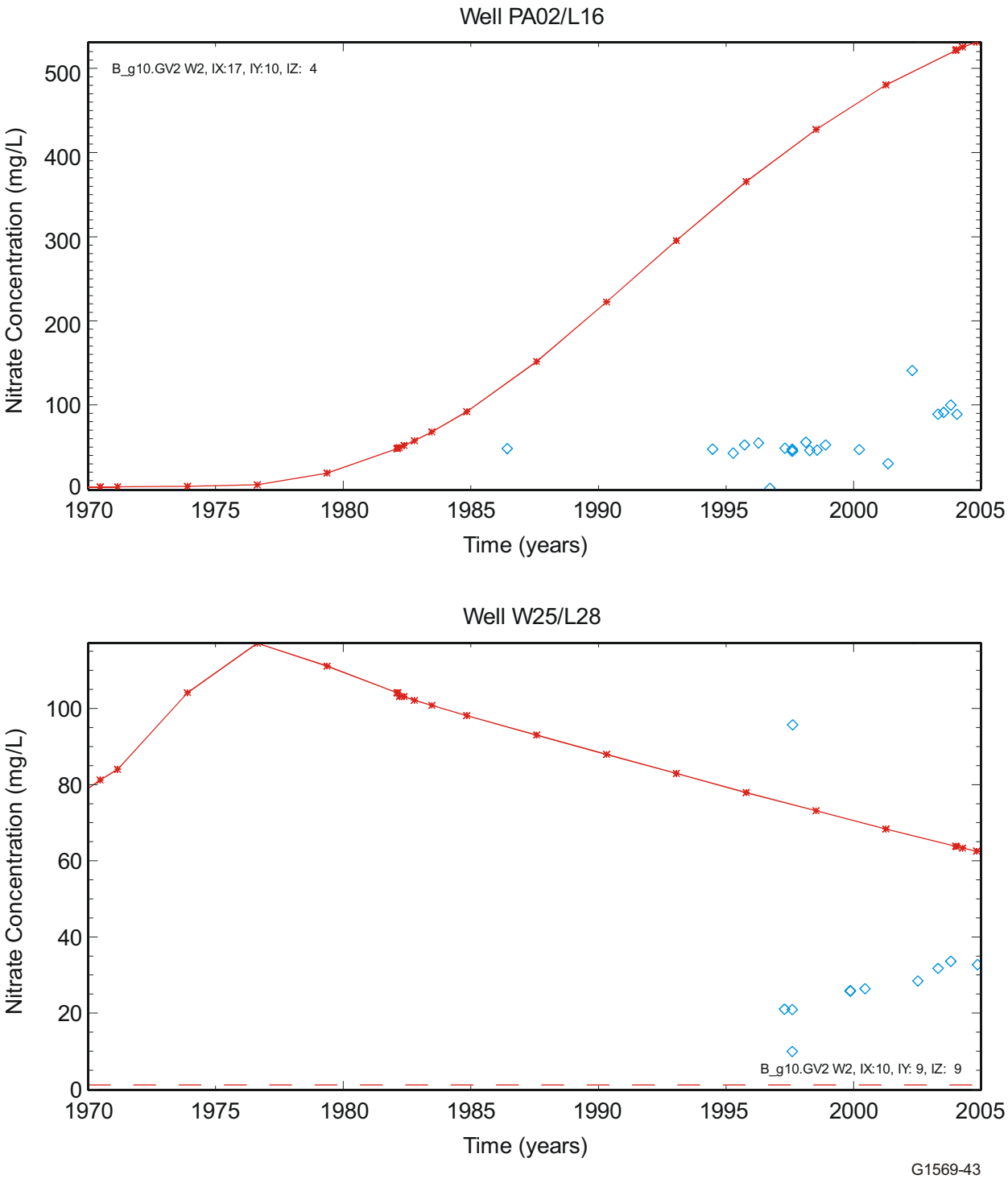

Figure 6-7. Time-history comparison of simulated (red line) and observed (blue diamonds) concentrations for nitrate in Lysimeters PA02-L16 and W25-L08. Background concentration is indicated by the dashed line.

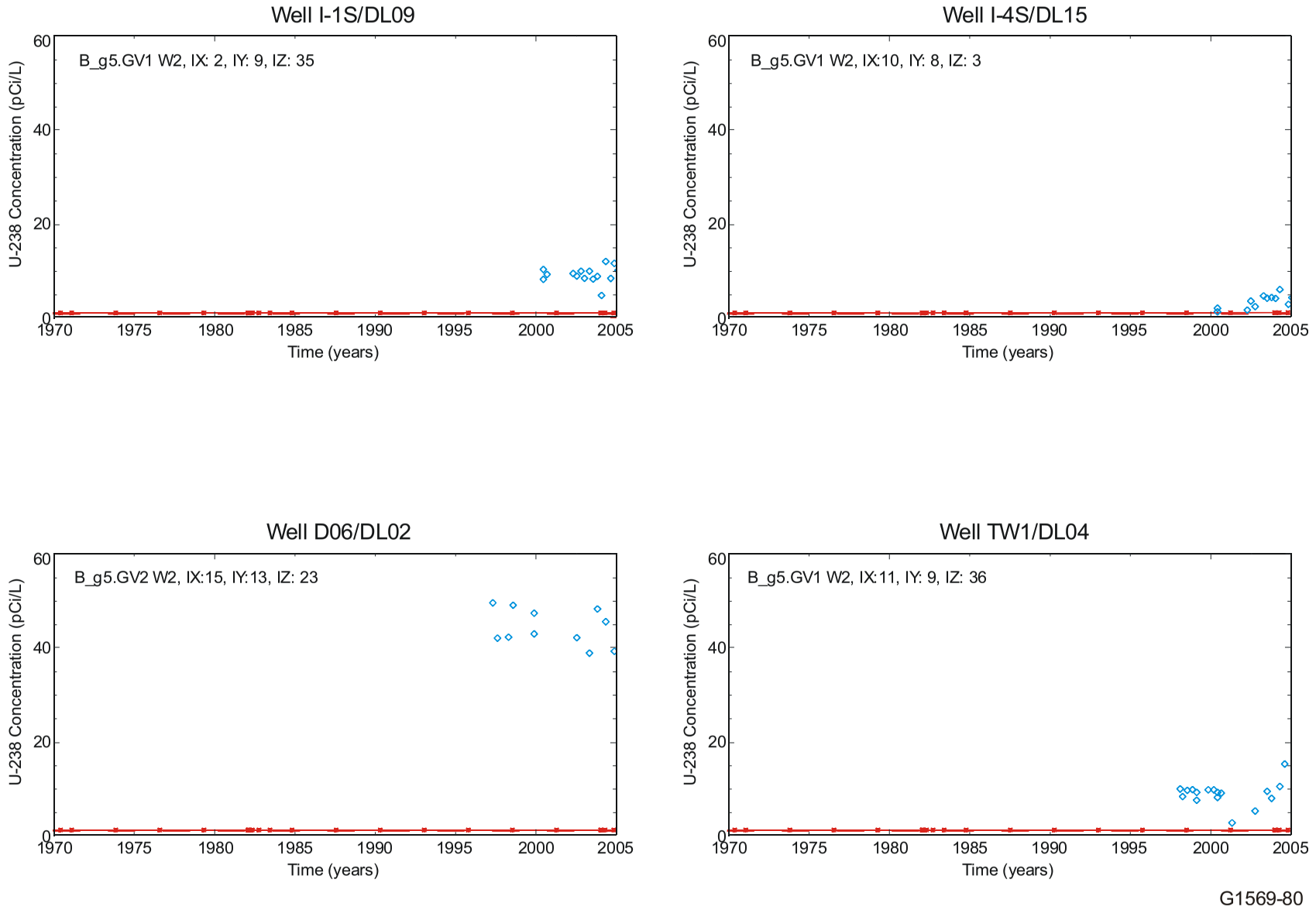

Figure 6-8. Time history-comparison of simulated (red line) and observed (blue diamonds) concentrations for uranium-238 in the lysimeters in the 10.7- to 76.2-m (35- to 250-ft) depth interval. Background concentration is indicated by the dashed line.

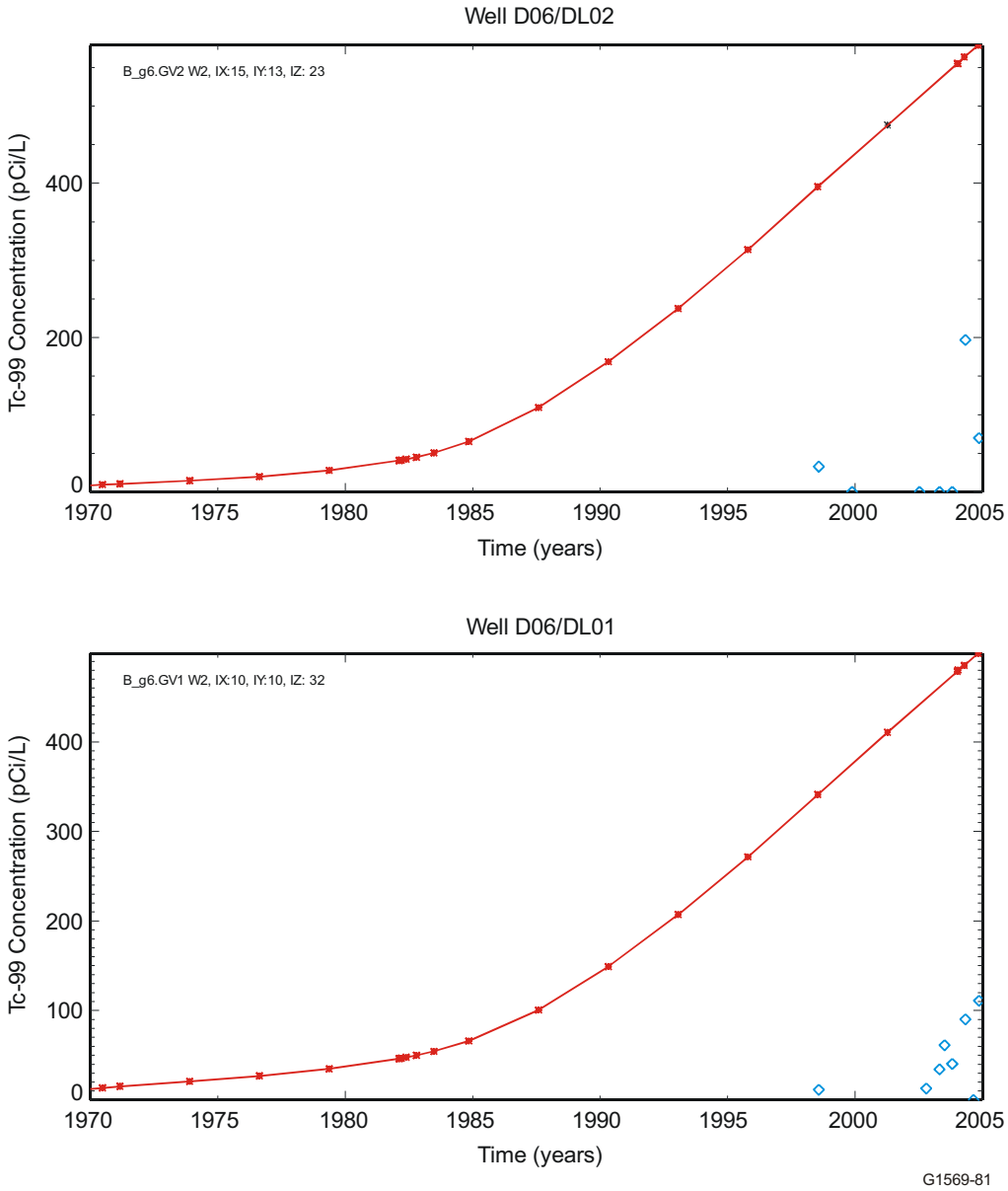

Figure 6-9. Time-history comparison of simulated (red line) and observed (blue diamonds) concentrations for technetium-99 in the lysimeters in the 10.7- to 76.2-m (35- to 250-ft) depth interval.

Although simulated concentrations are nonzero, they are very low and essentially plot just at background. Simulations represent averaged concentrations over larger gridblock volumes at this depth—76.2 m (250 ft) on a side—and again cannot be expected to exactly mimic observations at a specific point. Also note that the plots show only locations with elevated concentrations. The other monitoring locations (i.e., the majority) all show nondetects.

6.1.2.2 Tc-99. Elevated concentrations of Tc-99 in the 10.7- to 76.2-m (35- to 250-ft) interval were observed at Wells D06 in Lysimeters DL01 and DL02. Simulated Tc-99 concentrations for gridblocks containing these lysimeters are shown in Figure 6-9. These results are plotted with a linear vertical axis because the concentrations are not as overpredicted at this location as they were for the shallower Well W23 location shown previously.

6.1.2.3 Nitrate. Elevated concentrations of nitrate in the 10.7- to 76.2-m (35- to 250-ft) interval were observed at Wells I-2S and I-4S. These simulation results are shown in Figure 6-10. Lysimeter I-2S-DL11 shows very high monitoring results for nitrate; therefore, it is not surprising that the model underpredicts in comparison. Lysimeter I-4S-DL15 has lower monitoring results; the model results overpredict for this location.

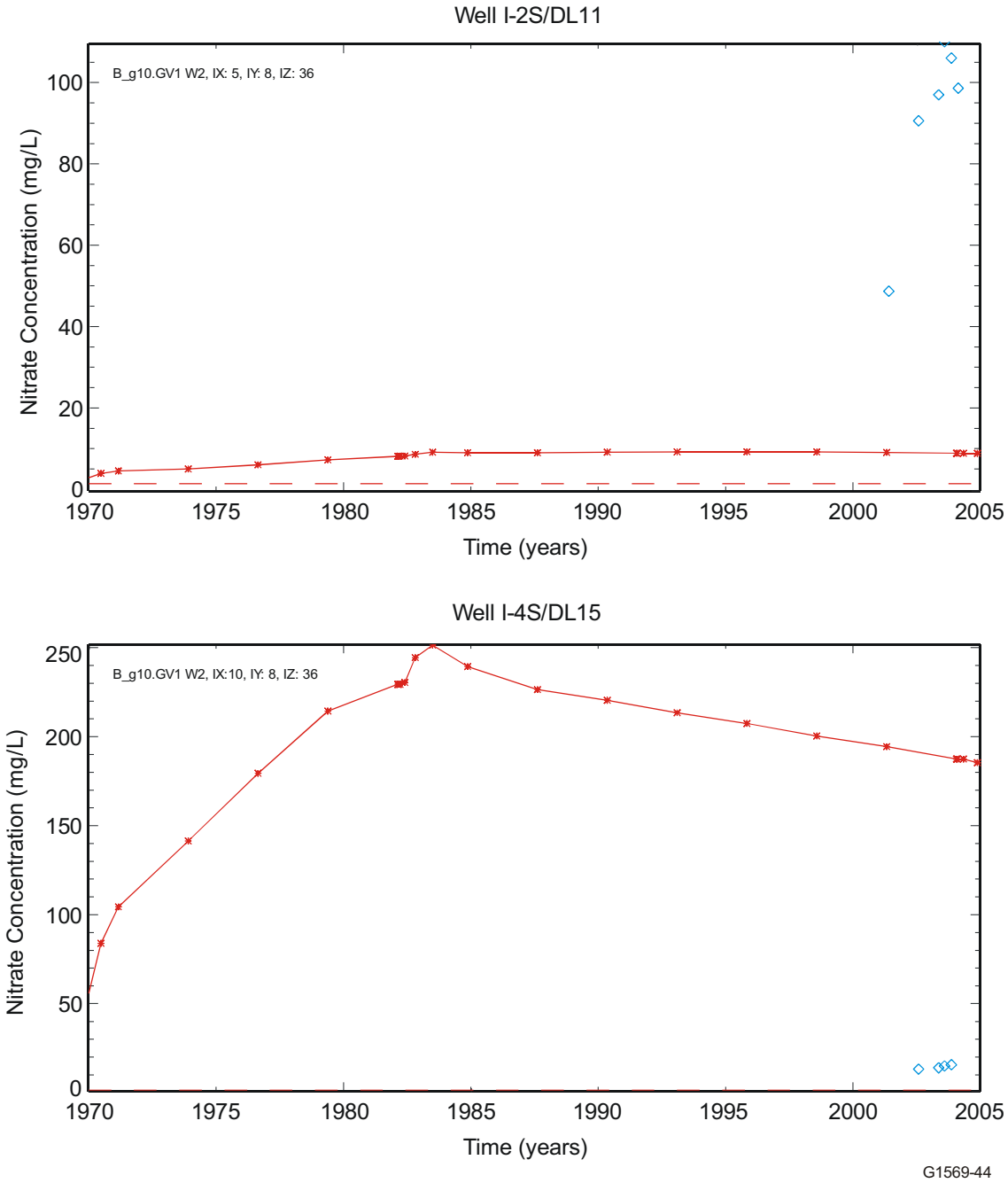

Figure 6-10. Time-history comparison of simulated (red line) and observed (blue diamonds) concentrations for nitrate in the lysimeters in the 10.7- to 76.2-m (35-to 250-ft) depth interval. Background concentration is indicated by the dashed line.

6.1.3 Aquifer

This subsection first compares simulated and observed nitrate and chromium concentrations. These two contaminants are chosen for consistency to allow comparison to ABRA modeling results and because they offer insight into how the model results compare to monitoring data. Both contaminants are conservative in that they do not sorb, and thus, avoid the complication of assigning a K_d. Lastly, time histories for simulated aquifer concentrations for all contaminants in the RI/FS model that have detections from aquifer monitoring are compared to the observations.

6.1.3.1 Comparison of Simulated and Observed Nitrate Concentrations. This subsection shows comparisons of simulated results and monitoring results for nitrate as elemental nitrogen. Time histories, contour plots, and vertical profiles through the aquifer domain are presented to show spatial resolution.

Calibration to the observed aquifer nitrate concentrations was not attempted for these simulations. Rather, simulations for both the vadose zone and the aquifer were developed based on best-available information. Then simulations were run once in a forward mode.

Nitrate is a ubiquitous chemical in groundwater. Background concentrations must be considered when making comparisons, even though it is assumed for RI/FS modeling that contaminant concentrations in the vicinity of the SDA are not influenced by upgradient sources. A background concentration of 1.0 mg/L was added to simulated values in the time-history plots shown in Figure 6-11. This background concentration appears appropriate for the local RWMC area and is within the range of background concentrations typical for the INL Site (i.e., 0.4 to 5.0 mg/L) as presented in Section 4 of the draft RI/BRA document. The time-history plots are all shown with a consistent time axis and a consistent concentration axis, except for Well M17S, which has one-order-of-magnitude-larger concentration axis to show the simulated results. Simulation results representing all wells, except Well M4D, are taken from the second gridblock down in the aquifer model. Well M4D is unique in that it is screened much deeper; therefore, simulated concentrations from deeper in the model are used. The second gridblock extends from 8 to 16 m (26 to 52 ft) in the aquifer domain and is similar to most of the screened intervals in the monitoring wells (see Figure 5-33). As such, simulated concentrations represent concentrations at a depth of 12 m (39 ft) below the water table. In general, the simulation results show slightly lower predicted concentrations in the aquifer than those in the ABRA model due to a combination of reduced inventory and changes in transport through the vadose zone. Figure 6-11 illustrates that nitrate is sometimes overpredicted and sometimes shows no contribution from SDA sources when compared to monitoring data. Also evident in the monitoring data is that the mean local background estimate has some degree of variability around it.

A contour plot of the simulated nitrate concentrations in Calendar Year 2004 is shown in Figures 6-12 and 6-13 for the refined and base aquifer-simulation domains, respectively. Again, concentrations are taken from the second gridblock down from the aquifer model. The estimated local background of 1.0 mg/L is not added to the simulation results in Figures 6-12 and 6-13. Simulated results show that nitrate is predicted to move east-southeast within the area of the refined domain due to topography influences in the vadose zone and slightly south-southeastern water velocities under the eastern portion of the SDA and the Transuranic Storage Area. In the larger base domain, control of the regional gradient is exerted and the simulated plume moves south-southwest.

The predicted movement of nitrate east-southeast within the aquifer model-refined domain can be seen more easily in Figure 6-14, where time histories from Figure 6-11 are portrayed in spatial relation to their well locations. Elevated nitrate concentrations are predicted by current time for Wells M17S, USGS-119, USGS-90, and M15S, which are all beneath the SDA or south-southeast. Well M6S would

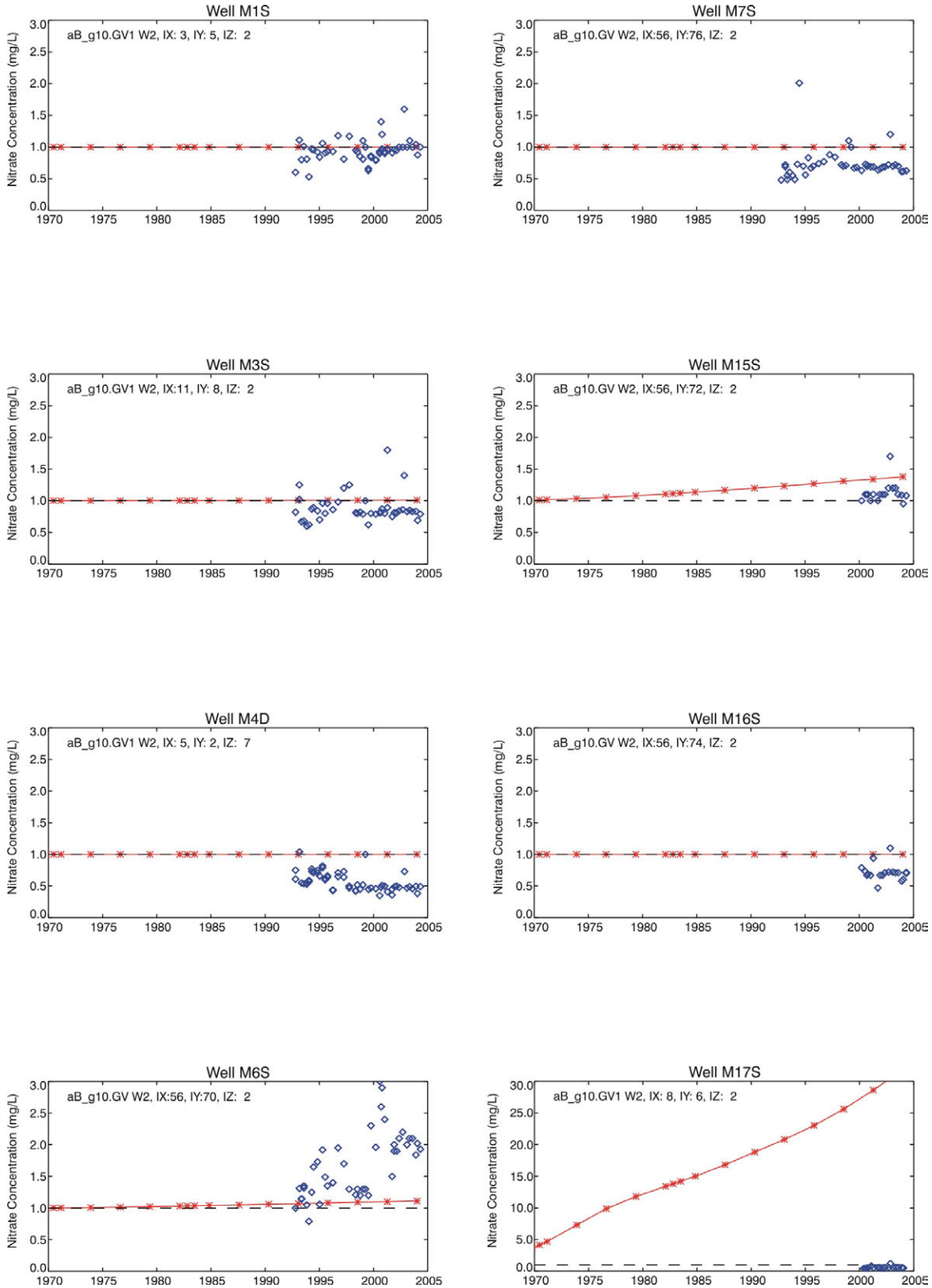

Figure 6-11. Comparison of simulated (red line) and observed (blue diamonds) nitrate (as N) concentration time histories for aquifer-monitoring wells in the vicinity of the Subsurface Disposal Area. Background concentration is indicated by the dashed line.

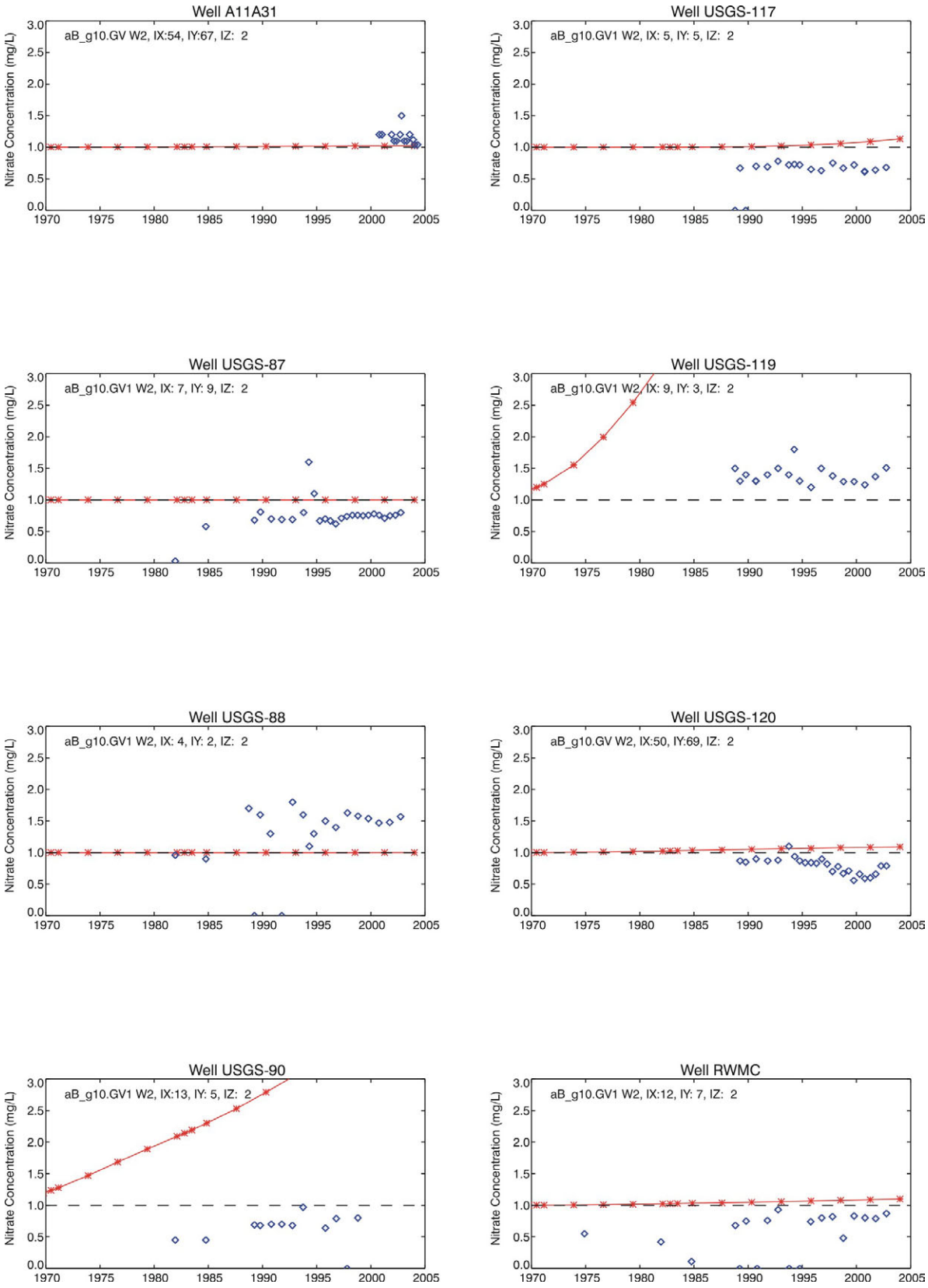

Figure 6-11. (continued).

have a higher predicted concentration, but it is outside the refined area; therefore, the predicted concentration is subject to averaging over a much larger gridblock volume, which dilutes the simulated concentration. In terms of monitoring data, some patterns can be interpreted when compared to the local background estimate of 1.0 mg/L. For purposes of comparison, monitoring results are grouped into four classes with an indication found in the upper right corner of each time-history plot. An "L" indicates the monitoring data were mostly below the background, an "M" indicates the monitoring data mostly match the background, and an "H" indicates the monitoring data are mostly higher than the background. Following this categorization, Wells USGS-87, M3S, M7S, M16S, USGS-90, M17S, USGS-117, M4D, and USGS-120 all show concentrations mostly below background. Wells M1S and M15S match the local background. Wells USGS-119 and USGS-88 are elevated compared to the local background and Well M6S has the highest concentrations above the local background estimate. Grouped in this fashion, monitoring data also show a tendency for nitrate concentrations to be elevated in several wells south of the SDA, with one group including Wells USGS-119, M15S, and M6S, which are in the direction of predicted local transport to the southeast.

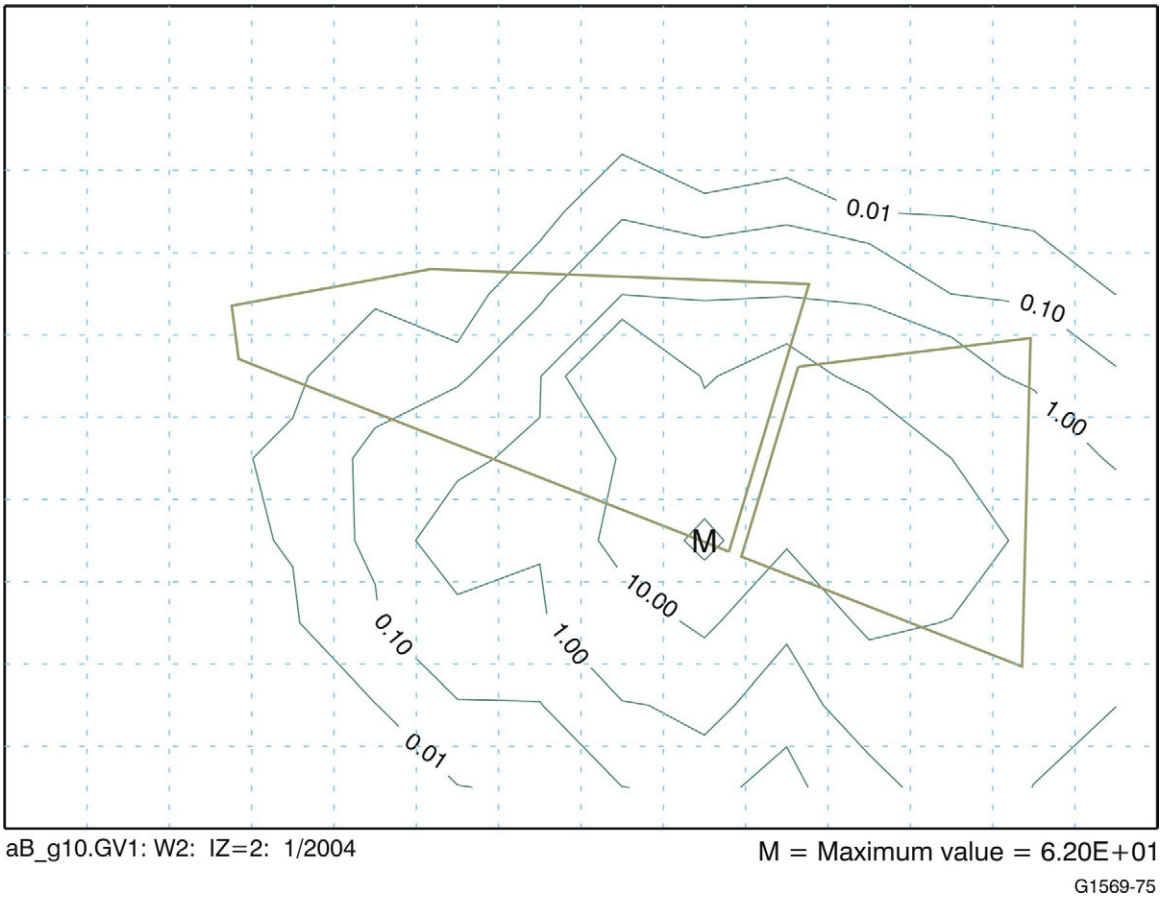

Figure 6-12. Simulated aquifer nitrate concentrations (mg/L) for the year 2004 for the refined aquifer domain. The results do not include any additional contribution from local background concentrations.

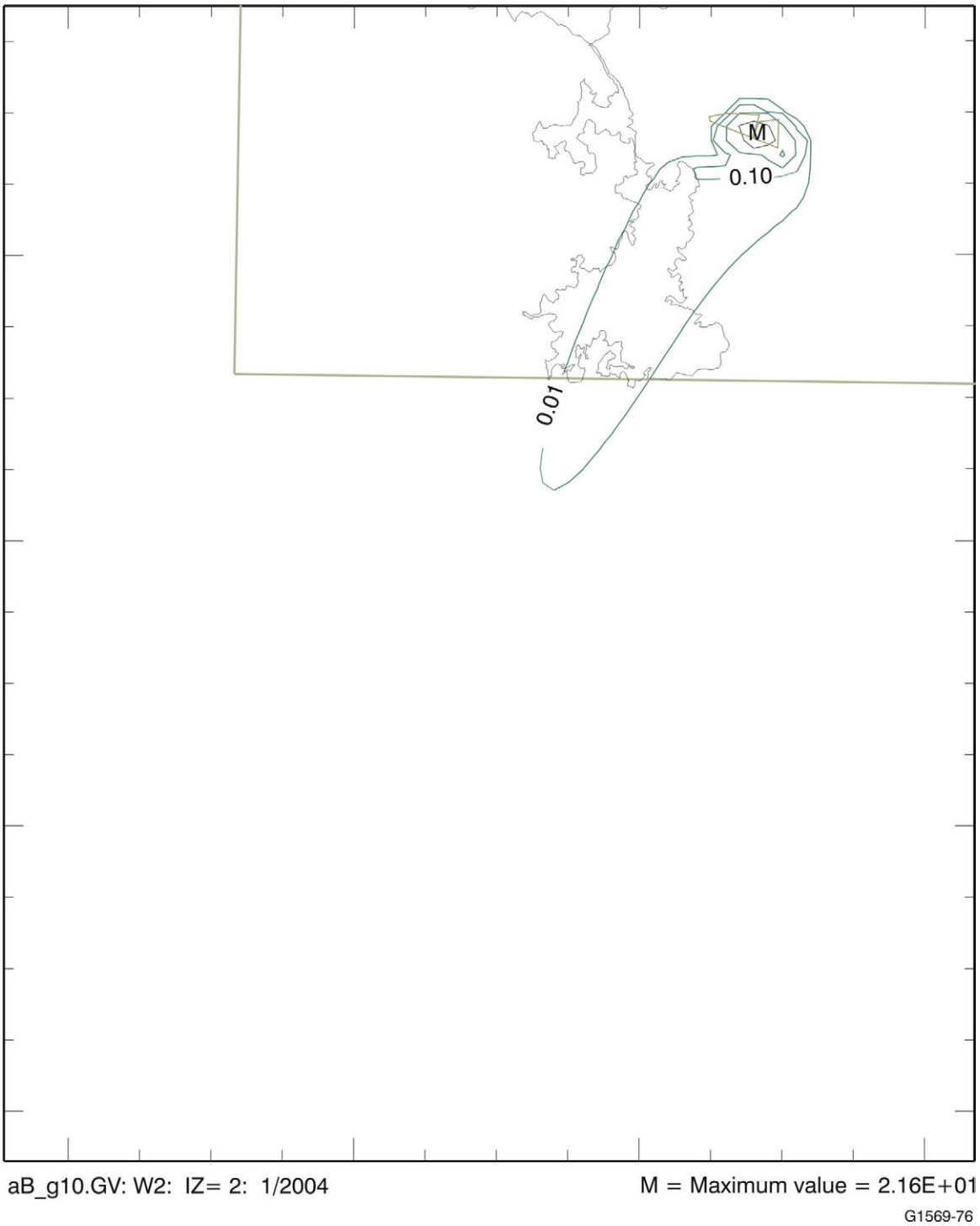

Figure 6-13. Simulated aquifer nitrate concentrations (mg/L) for the year 2004 for the base aquifer domain. The results do not include any additional contribution from local background concentrations.

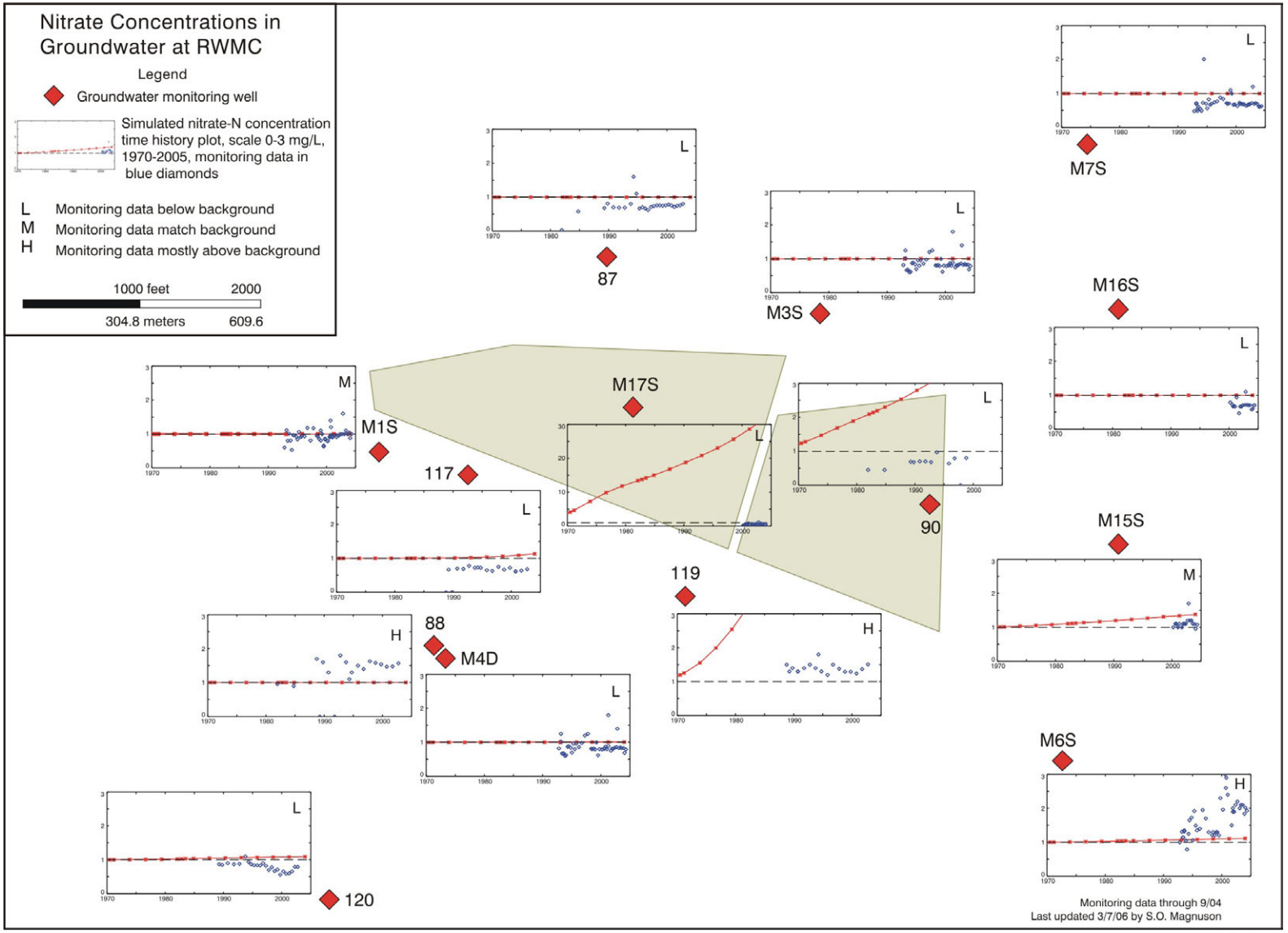

Figure 6-14. Simulated and observed nitrate concentrations superimposed onto monitoring locations in the vicinity of the Radioactive Waste Management Complex. Background concentration is indicated by dashed line.

Most of the monitoring data are consistent with the conceptual model and numerical implementation. The aquifer flow system is dominated by a low-permeability region south and southwest of the SDA that directs flow eastward around the low-permeability system. In comparing simulation results to monitoring results, concentrations are overpredicted in Well M17S (inside the SDA), Well USGS-119 (immediately south of the SDA), and Well USGS-90 (east of the SDA). Predicted concentrations slightly overpredict observed concentrations at Well M15S (east of the Transuranic Storage Area).

Concentrations are underpredicted at Well M6S (southeast of the SDA). The simulation results at the grid location corresponding to Well M6S are subject to additional dilution due to being outside the refined area. Without this dilution, the agreement would be better. The majority of other locations outside this predicted contaminant plume essentially shows no simulated impact above local background concentration. Obviously, the system is more complex than has been represented in the model. However, the model does provide a foundation for explaining most of the observed behavior and, thus, meets a goal of general representativeness.

Vertical profiles of simulated nitrate concentrations at the gridblock location with the maximum simulated concentration in Calendar Year 2004 (Figure 6-12) are shown in Figure 6-15 for four different dates. These plots do not have the background concentration added to the simulation results. This same location remains the location of maximum concentration until Calendar Year 2120, when it shifts southward with the center of mass. Note that the horizontal-concentration scale changes in the profile for Calendar Year 2997. Contours of the simulated concentration for the same times from the corresponding north-south cross section in the refined aquifer domain are shown in Figure 6-16. Only Calendar Years 2004, 2066, and 2110 are shown, because the simulated concentration for Calendar Year 2997 is below 1 mg/L.

Understanding the dynamic behavior of simulated profiles requires knowing (1) the contaminant-loading history from the vadose zone simulation at this location, (2) that water flux from the vadose zone is relatively constant, and (3) that the low-permeability region in the aquifer results in slow horizontal velocities, which increases the effect of contaminant flux coming into the model from the vadose zone. A one-to-one correspondence from the bottom of the vadose zone to the top of the refined domain in the aquifer and nitrate loading from the vadose zone model for the gridblock location profiled in Figure 6-15 is shown in Figure 6-17. During the period up to approximately Calendar Year 2050, contaminant flux to the aquifer is increasing. A profile from this period (i.e., Calendar Year 2004) shows consistently decreasing simulated concentrations with depth in the aquifer. Shortly after this period, nitrate flux from the vadose zone begins to decrease while water flux stays the same. This begins to result in lower concentrations at the surface (Calendar Year 2066), possibly indicating that a slight downward gradient has developed in the aquifer simulation within the low-permeability region. By Calendar Year 2110, this reversal in the concentration gradient has almost penetrated to the bottom of the simulation domain. At a much later time (i.e., Calendar Year 2997), the concentration gradient is reversed, with the highest concentration at the bottom of the domain, although concentrations at this later time are much lower.

This simulation behavior of the concentration not always being greatest at the uppermost gridblock has implications when extracting concentrations from the model for risk assessment. It would not necessarily always be conservative to use concentrations from the uppermost gridblock in the aquifer domain. In this baseline risk assessment, concentrations are taken from the second gridblock down, as discussed in Section 6.2. Section 6.1.1.3.3 shows similar vertical profiles for other contaminants to further illustrate this point.

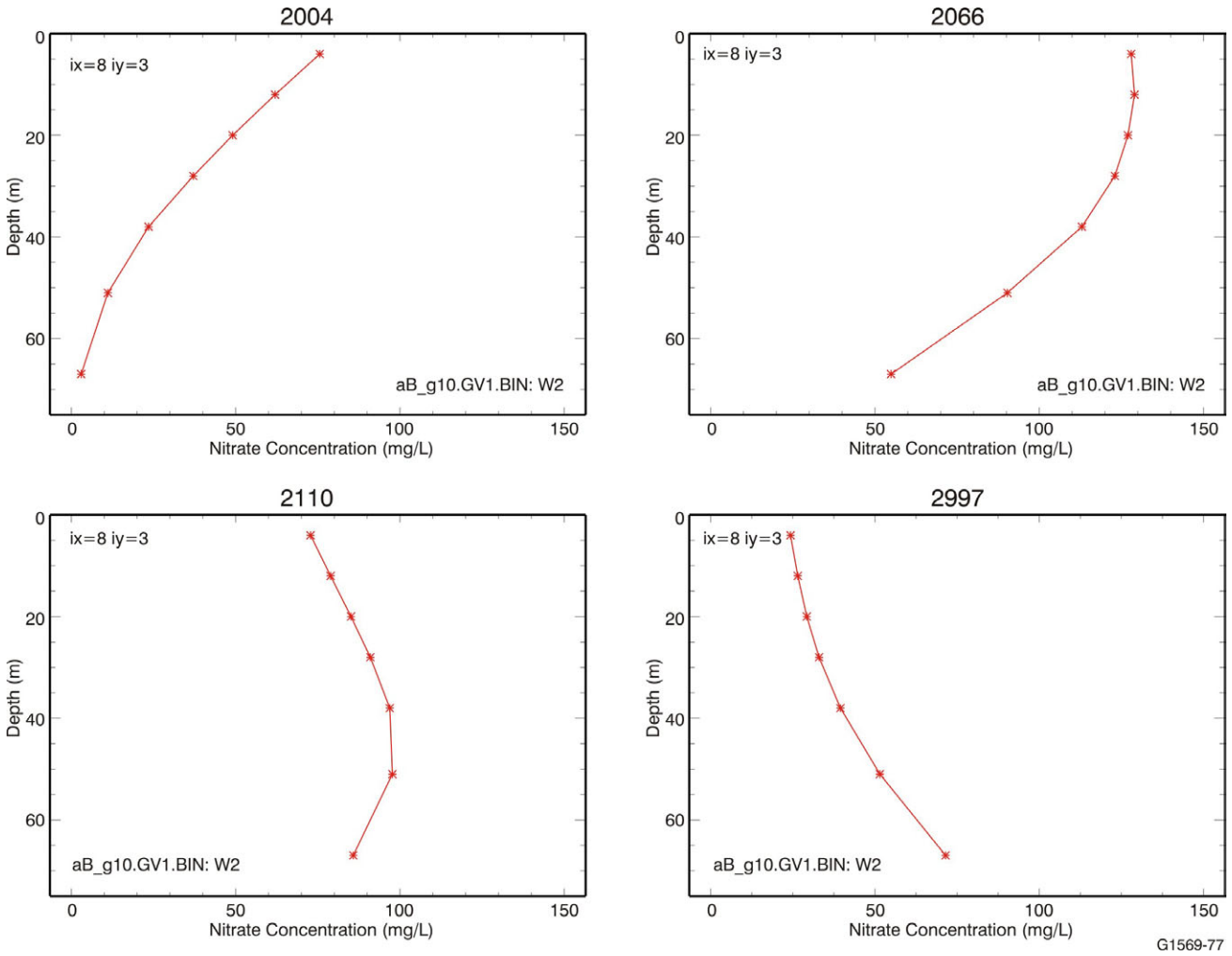

Figure 6-15. Simulated aquifer nitrate concentration profiles beneath the Subsurface Disposal Area. The year is shown at the top of each plot.

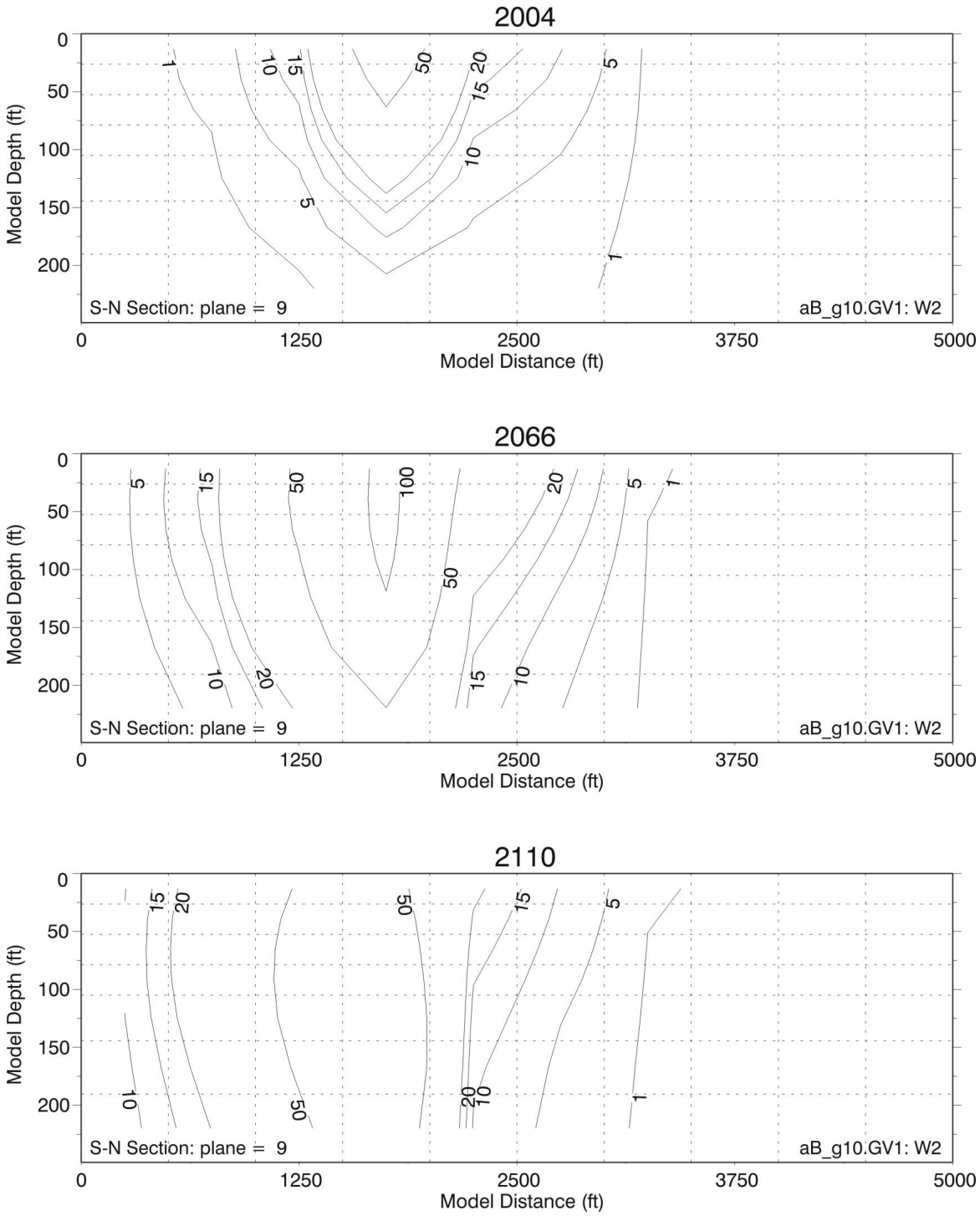

Figure 6-16. Simulated aquifer nitrate concentrations (mg/L) for north-south cross sections through the location of maximum simulated concentration at times corresponding to profiles shown in Figure 6-15.

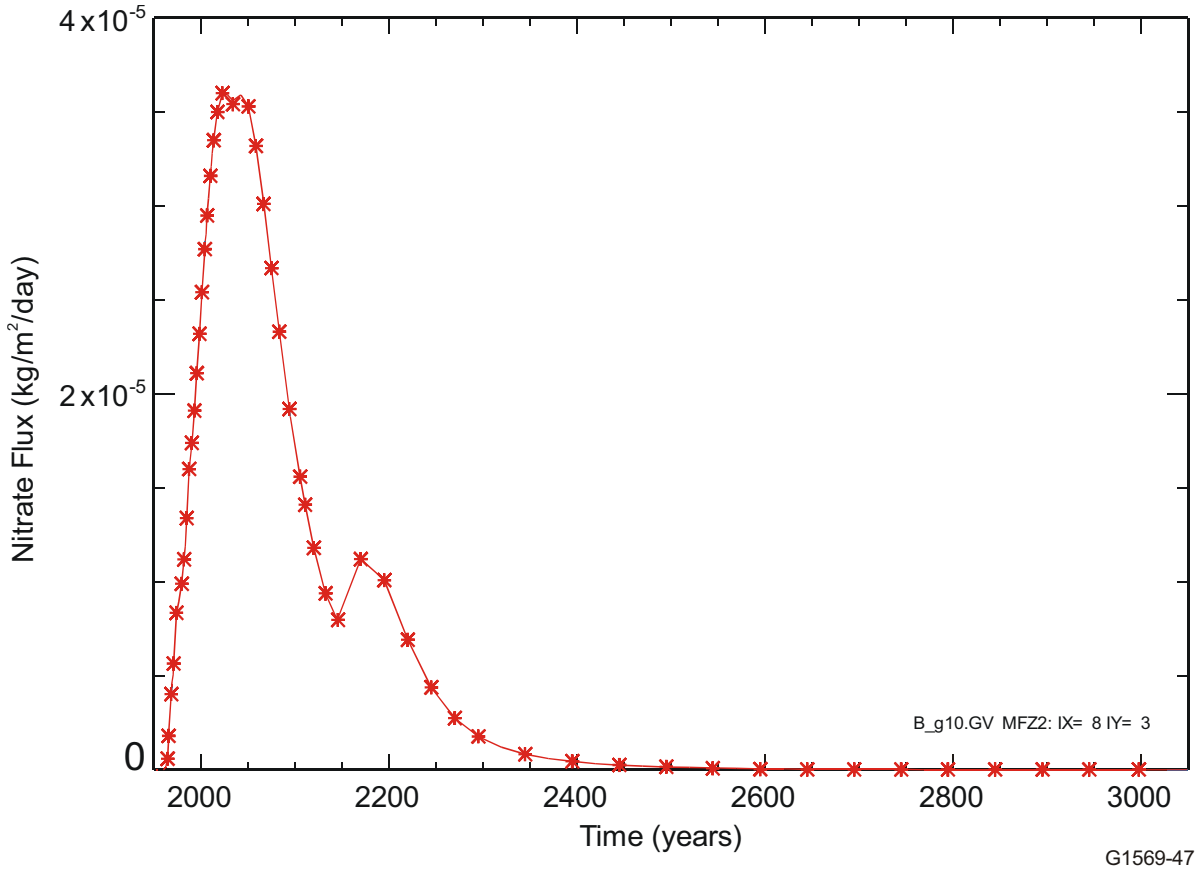

Figure 6-17. Time history of the simulated nitrate flux from the vadose zone simulation at the grid location profiled in Figure 6-15.

6.1.3.2 Comparison of Simulated and Observed Chromium Concentrations. Chromium is another contaminant buried in the SDA for which transport was simulated. In these transport simulations, chromium was assumed to remain in the mobile hexavalent state. Though chromium is not considered a COPC in the draft RI/BRA, subsurface model predictions for chromium are compared to measured values because sufficient monitoring data are available to support the comparison. Figure 6-18 illustrates time histories of simulated chromium concentrations compared to observed aquifer concentrations. The monitored concentrations are inferred to represent hexavalent chromium also. Similar to the time-history plots for nitrate concentrations, the simulated chromium concentrations are added onto the upper end of the aquifer background concentration range of 1-22 µg/L for the Snake River Plain aquifer (see Section 4 of the draft RI/BRA). Only simulated chromium concentrations for Wells M17S and USGS-119 begin to be discernable above background for the 1970 through Fiscal Year 2004 timeframe presented in Figure 6-18. The maximum simulated chromium concentration anywhere in the aquifer through Fiscal Year 2004 is 30 µg/L. This concentration is approximately an order of magnitude greater than the maximum simulated chromium concentration through the same period for the ABRA model. Both the ABRA and RI/FS models underpredict observed values.

Field data for chromium show considerable variability, similar to nitrate. Locations showing the most consistent elevated concentrations are Wells M1S, M15S, and M6S. Two of these are in the direction of interpreted and simulated flow to the east-southeast in the locally refined portion of the aquifer domain.

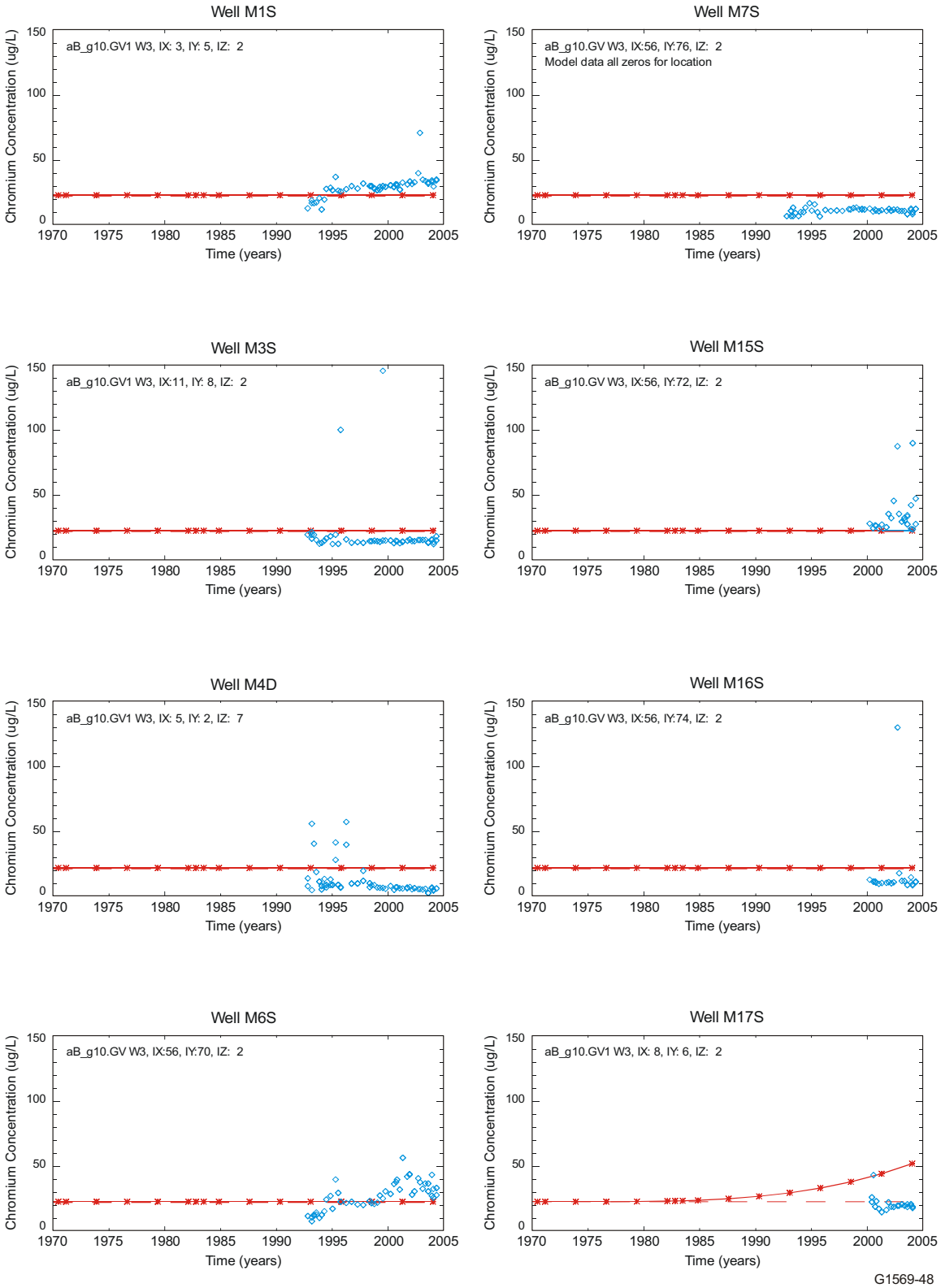

Figure 6-18. Comparison of simulated (red line) and observed (blue diamonds) chromium concentration time histories for aquifer-monitoring wells in the vicinity of the Subsurface Disposal Area. Background concentration is indicated by the dashed line.

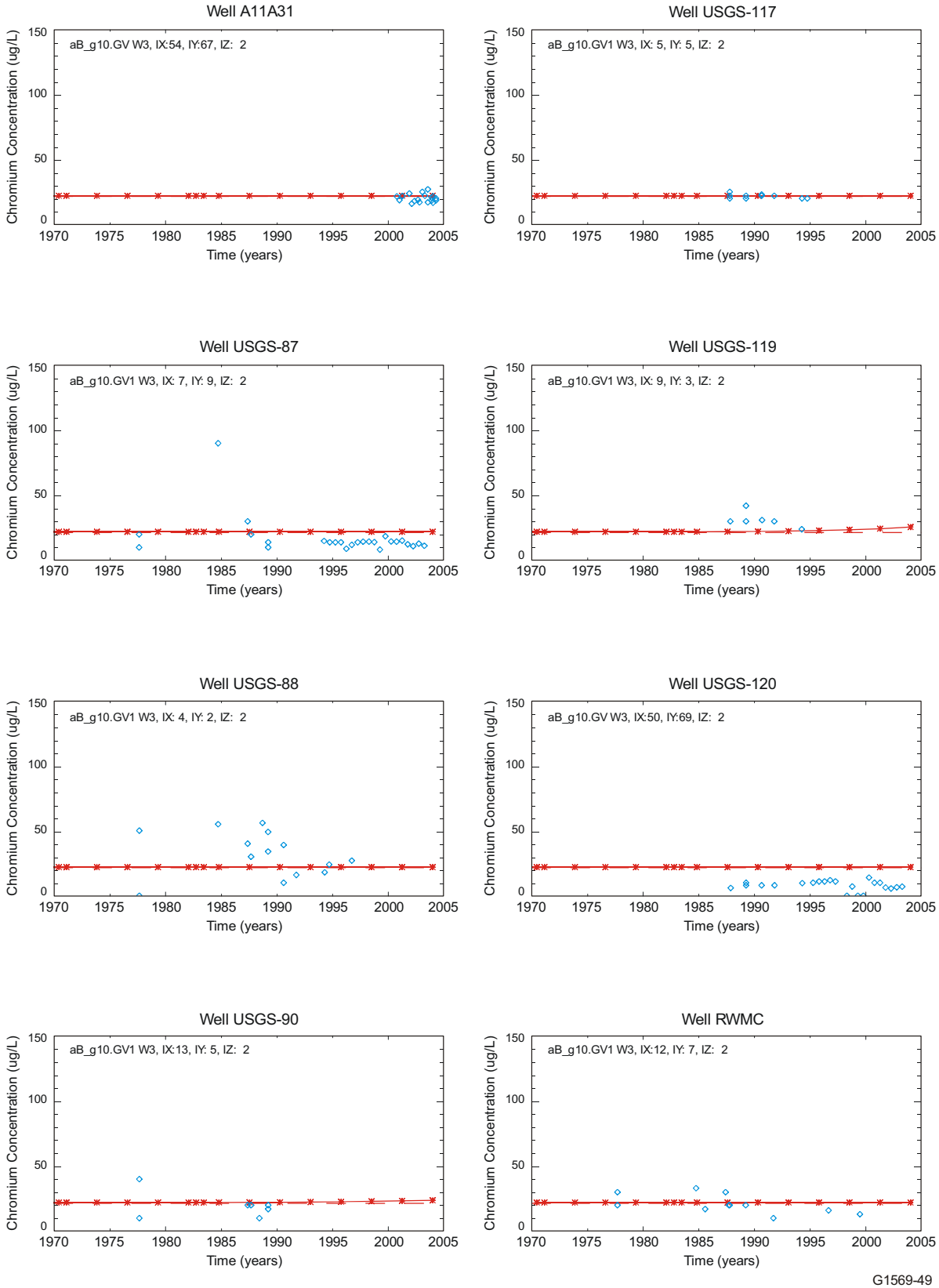

Figure 6-18. (continued).

The maximum simulated chromium concentration anywhere in the aquifer through Fiscal Year 2004 is 34 µg/L (see Figure 6-19). This is approximately an order of magnitude greater than the maximum simulated chromium concentration through the same period for the ABRA model and reflects an improvement when compared to field monitoring results (see Section 4 of the draft RI/BRA). Simulated chromium concentrations, although slightly underpredicted, are approaching the same order of magnitude as the observed chromium concentrations in the aquifer just south of the SDA. Note that it is uncertain to what extent impacts from SDA waste or from upgradient facilities have on these observed concentrations.

Figure 6-19. Simulated aquifer chromium concentrations (ug/L) for Calendar Year 2004 for the refined aquifer domain. Background concentrations are not added to simulation results.

6.1.3.3 Comparisons of Simulated and Observed Concentrations for Dissolved-Phase Radionuclide Constituents. This subsection presents comparisons of time histories of simulated results from the base-case simulation for those dissolved-phase radionuclides that have detections in the aquifer from monitoring. These contaminants are I-129, Tc-99, Am-241, Np-237, Pu-238, and Pu-239. Results are presented graphically as time-history comparisons to field-monitoring results at grid locations representing SDA aquifer-monitoring wells (Figures 6-20 through 6-25). In contrast to results presented previously for nitrate and chromium, contaminants in these figures are anthropogenic and have no background concentrations to add to simulation results, except for I-129 with a local background of 0.05 pCi/L. This latter background is indistinguishable in Figure 6-20. Monitoring results for radionuclide COPCs that represent 3σ detections, or greater, are included as blue diamonds on the time-history plots along with a whisker-style indication of their associated 1σ uncertainties. In cases where analyses were performed but no COPCs were detected, nondetects are plotted in green at the extreme lower-bound inventory of the plot. Simulation results are portrayed as a continuous line with black asterisks. Simulation results representing all wells, except Well M4D, are taken from the second gridblock down in the aquifer model. Well M4D is unique because it is screened much deeper; therefore, simulated

concentrations from deeper in the model are used. The second gridblock extends from 8 to 16 m (26 to 52 ft) in the aquifer domain and is similar to most of the screened intervals in the monitoring wells. As such, simulated concentrations represent concentrations at a depth of 12 m (39 ft) below the water table.

Results in Figures 6-20 through 6-25 highlight the erratic nature of detections compared to the majority of nondetect results, and those results lend credence to the assumption that these detections are not representative of transport and simulation results need not mimic them. These sporadic detections include low-level actinide concentrations that are just at instrument detection limits and may be false-positives.

Table 6-1 lists the maximum simulated concentrations from anywhere in the aquifer through Calendar Year 2004 for all human health COPCs, their long-lived decay-chain progeny, and chromium. No background concentrations are added to any of the simulated results. All simulated peak values listed in Table 6-1 occur during Calendar Year 2004, indicating that concentrations were still increasing at that time. For comparison, corresponding maximum simulated concentrations through 2001 for the ABRA model and through 1995 from the IRA model are given in the third and fourth columns of Table 6-1. Aquifer background concentrations from Section 4 of the draft RI/BRA are shown in the fifth column of Table 6-1 for comparison to simulation results. The last two columns present the range of observed values taken from the nature and extent discussion in Section 4 of the draft RI/BRA, along with comments concerning some of those values. Observed values from earlier than 1987 are not presented in Table 6-1. Numerous COPCs do not have corresponding analyses, as indicated in Table 6-1.

Changes in simulated values between the RI/FS model and the ABRA model result from numerous causes. The simulated C-14 concentration drops two orders of magnitude primarily due to allowing C-14 to partition into the gaseous phase and diffuse to the atmosphere. This vapor-phase simulation is discussed in Section 5.5. Simulated concentrations for Np-237 and the uranium isotopes have decreased due to an increase in their assigned distribution coefficients. Simulated concentrations for Pu-239 and Pu-240 increased due to increased mobility above the B-C interbed. Plutonium-238 was not treated this way, but shows a slightly increased concentration nonetheless, most likely due to either changes in inventory, changes in water travel time resulting from the topography, or both. Simulated concentrations for the fission products (i.e., Tc-99 and I-129) and activation products (i.e., C-14 and Cl-36) all decreased due to changes in inventory and source-release parameters. All other COPCs have slight changes that are most likely due to inventory changes or changes in assigned parameters for release mechanisms.

In comparing simulated results from the RI/FS model to the range of observed 3σ detections or the background concentrations, several patterns emerge. Simulated aquifer concentrations for fission and activation products are still overpredicted to varying degrees compared to observed monitoring results, but not as much as they were for the ABRA. This overprediction is thought to be more likely caused by inadequacies in the source-release model than in the subsurface flow and transport model. Monitoring results for U-234, U-235, and U-238 are similar to reported background values. Simulated uranium isotope values are much less than observed values or background values, consistent with the conclusion of no observable impact in aquifer monitoring to date. All other contaminants are predicted to be either not in the aquifer yet or to be present at concentrations below detectable levels. If it is assumed that background concentrations for anthropogenic radioisotopes are zero for those contaminants not explicitly identified in Knobel, Orr, and Cecil (1992), then model results are in agreement with nondetections for this last group of contaminants. This statement disregards sporadic detections of plutonium isotopes and Am-241 as anomalies. At a minimum, for this latter set of contaminants, model results are not in conflict with observed results. Inorganic contaminants (i.e., nitrate and chromium) are both overpredicted when compared to the majority of observed values.

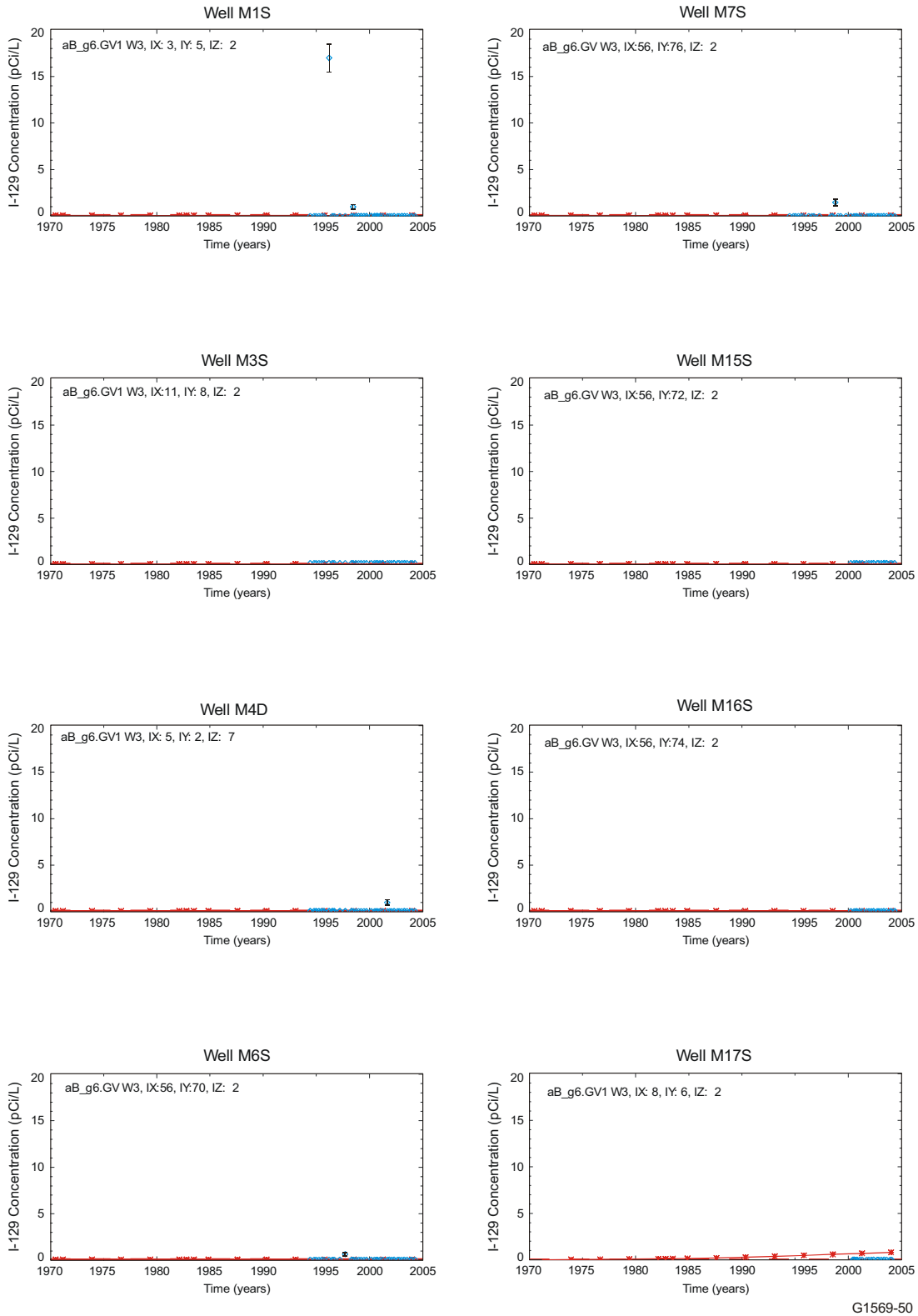

Figure 6-20. Comparison of simulated (red line) and observed (blue diamonds) iodine-129 concentration time histories for aquifer-monitoring wells in the vicinity of the Subsurface Disposal Area. Background concentration is indicated by the dashed line.

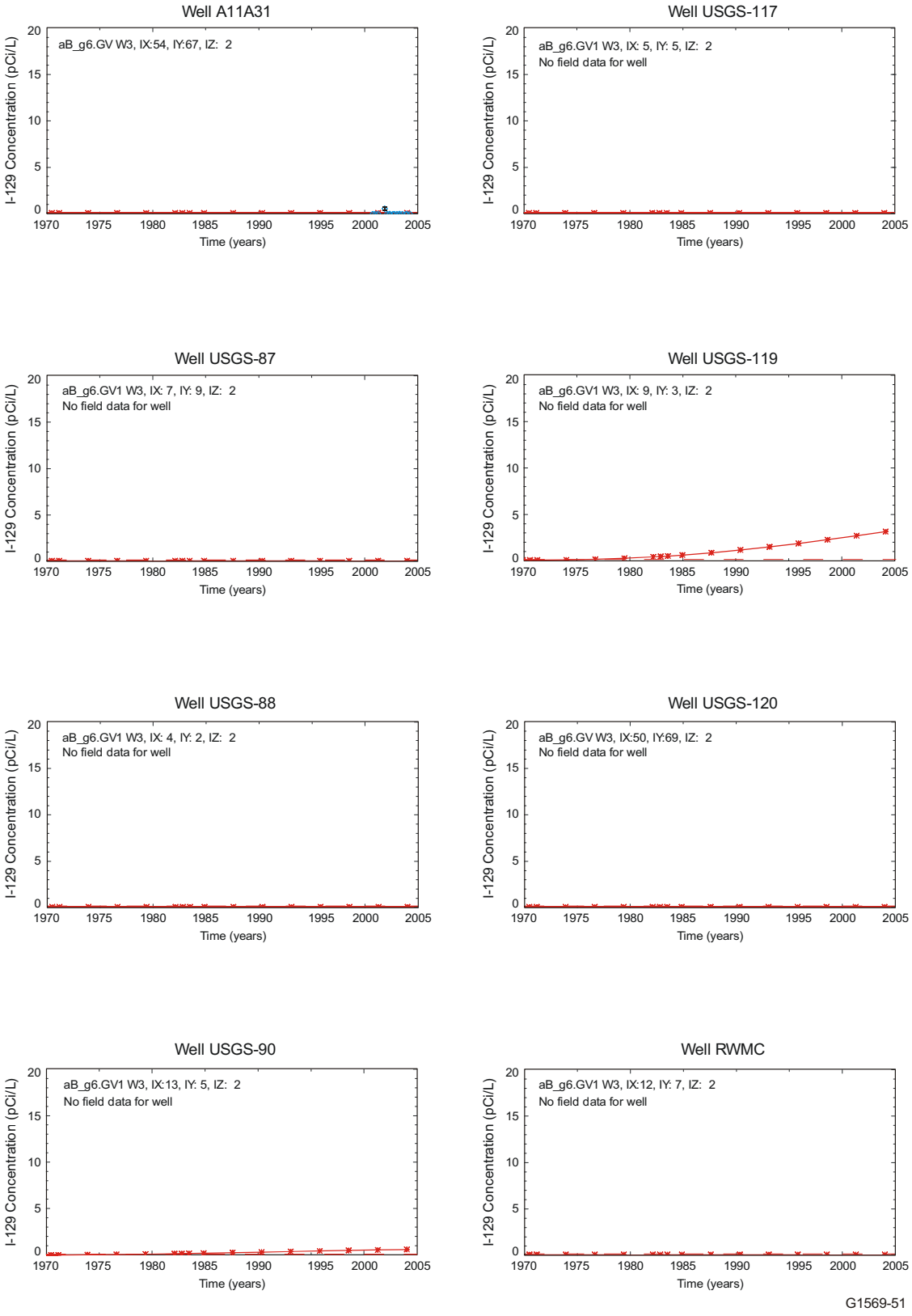

Figure 6-20. (continued).

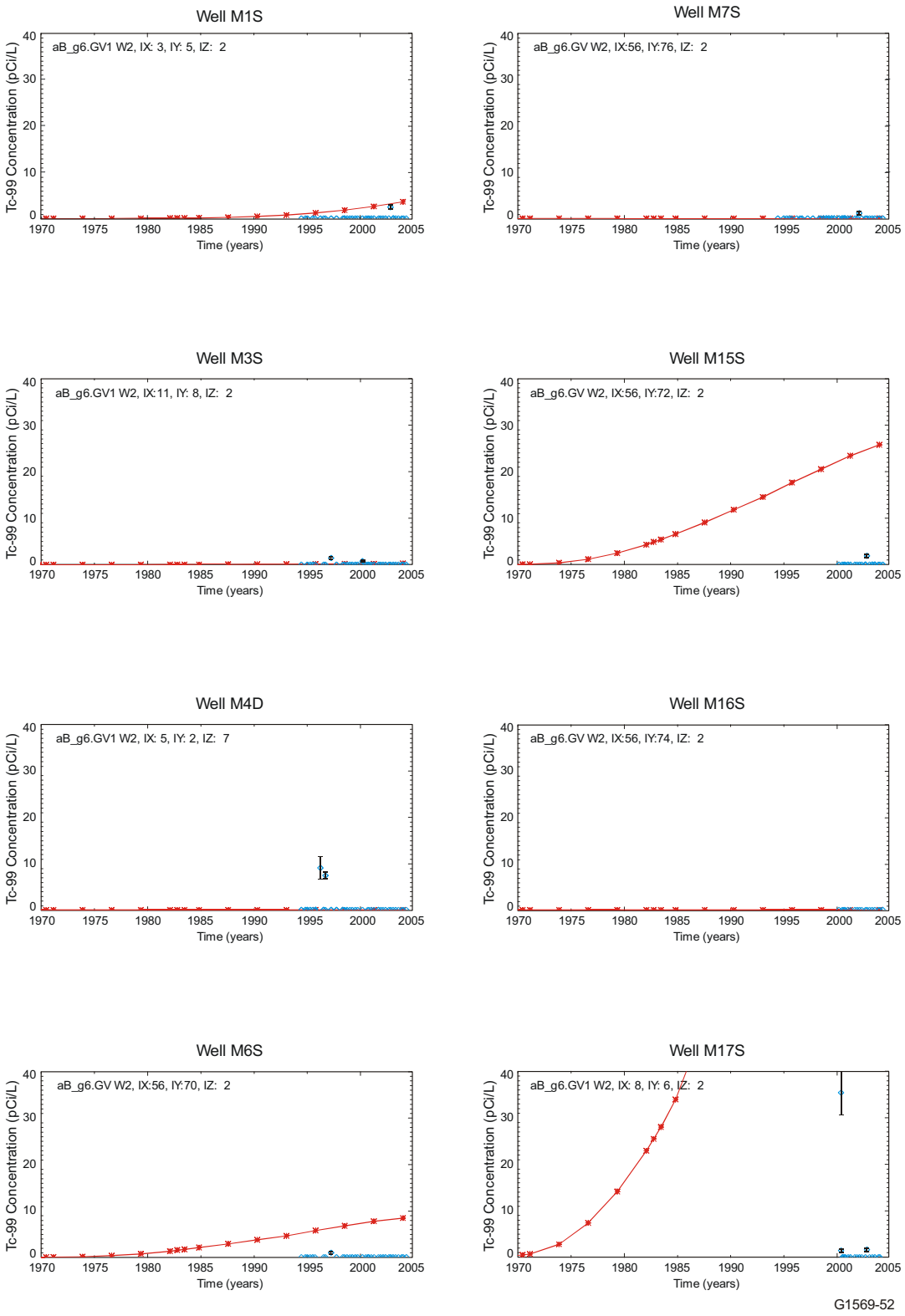

Figure 6-21. Comparison of simulated (red line) and observed (blue diamonds) technetium-99 concentration time histories for aquifer-monitoring wells in the vicinity of the Subsurface Disposal Area.

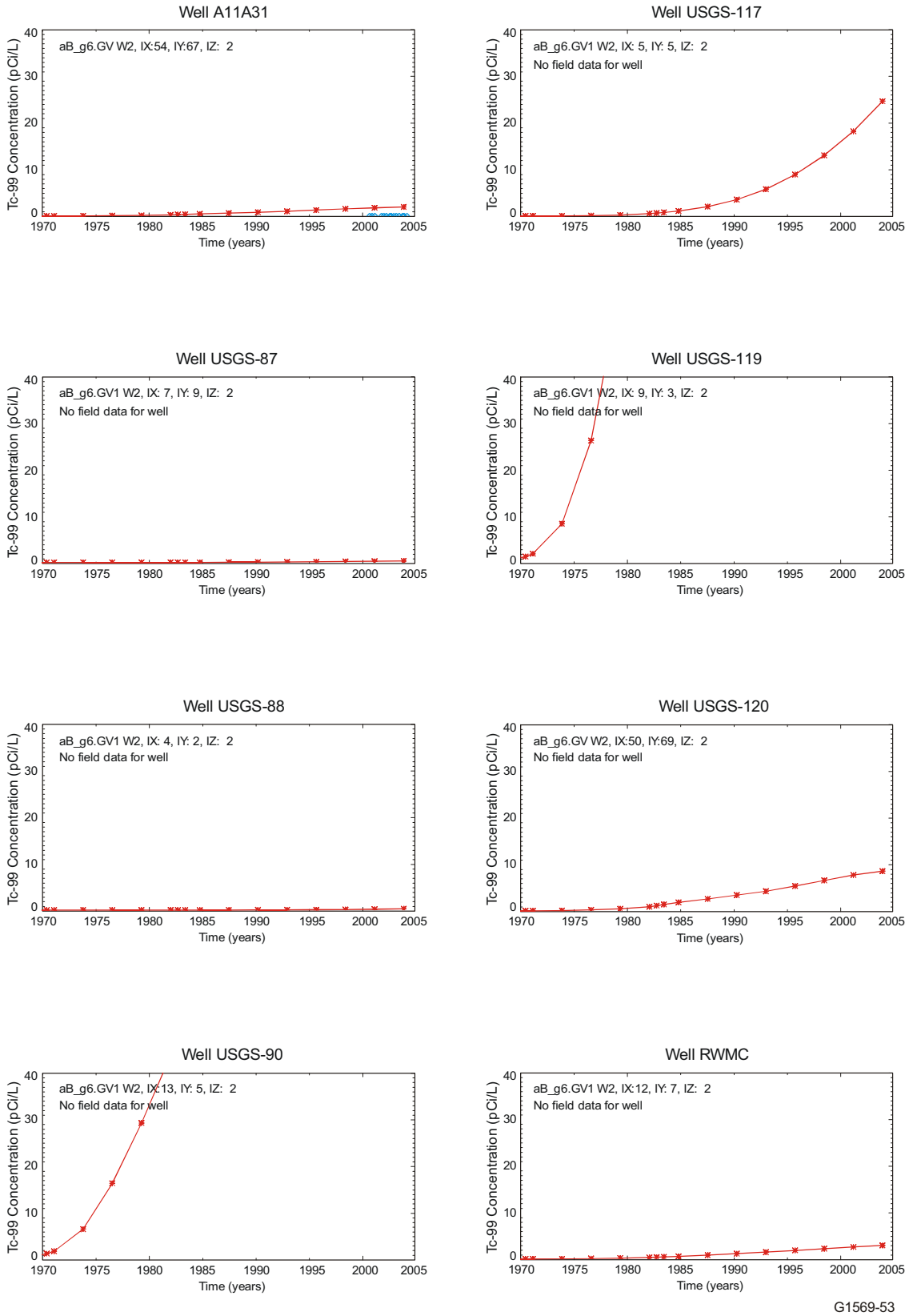

Figure 6-21. (continued).

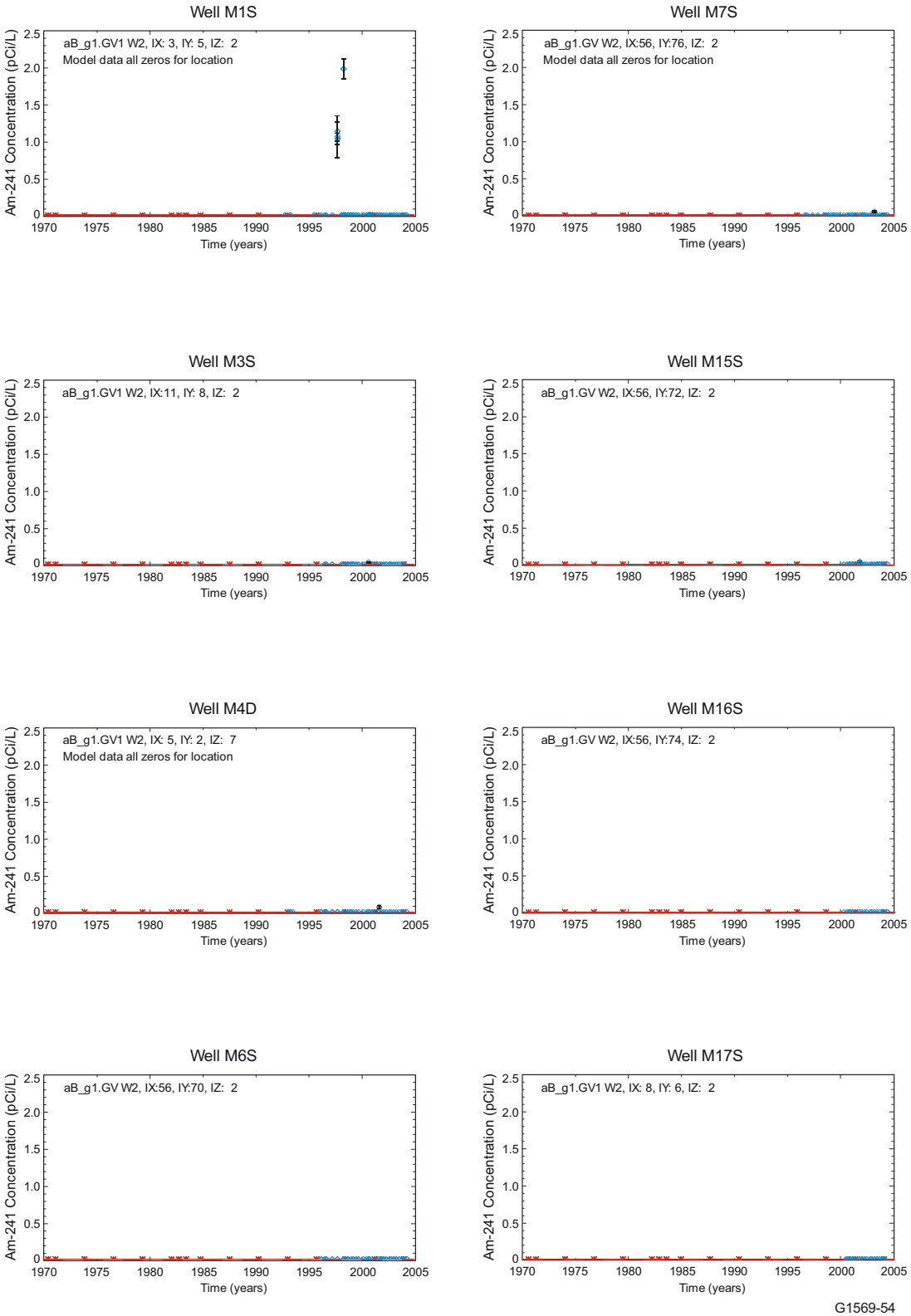

Figure 6-22. Comparison of simulated (red line) and observed (blue diamonds) americium-241 concentration time histories for aquifer-monitoring wells in the vicinity of the Subsurface Disposal Area.

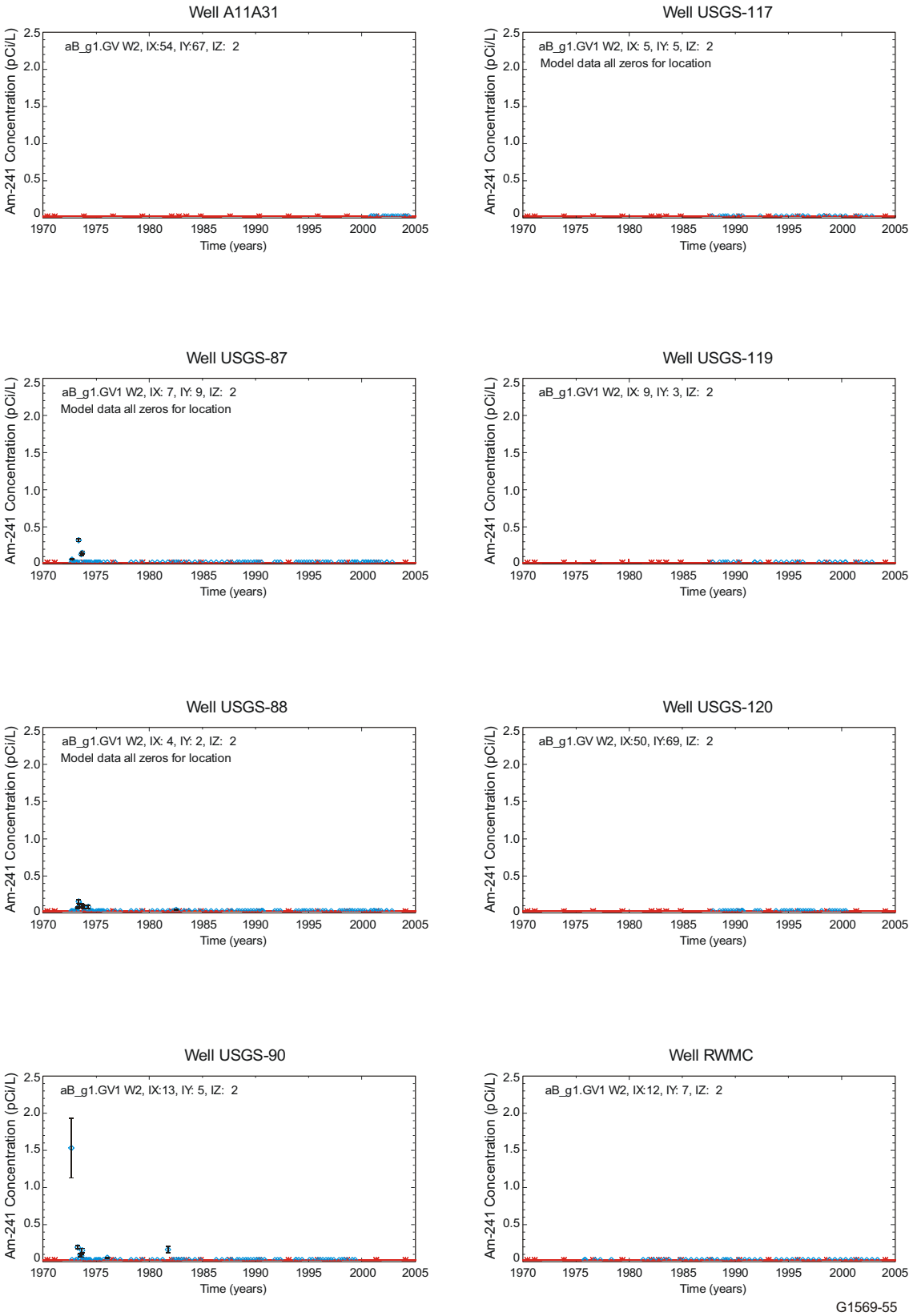

Figure 6-22. (continued).

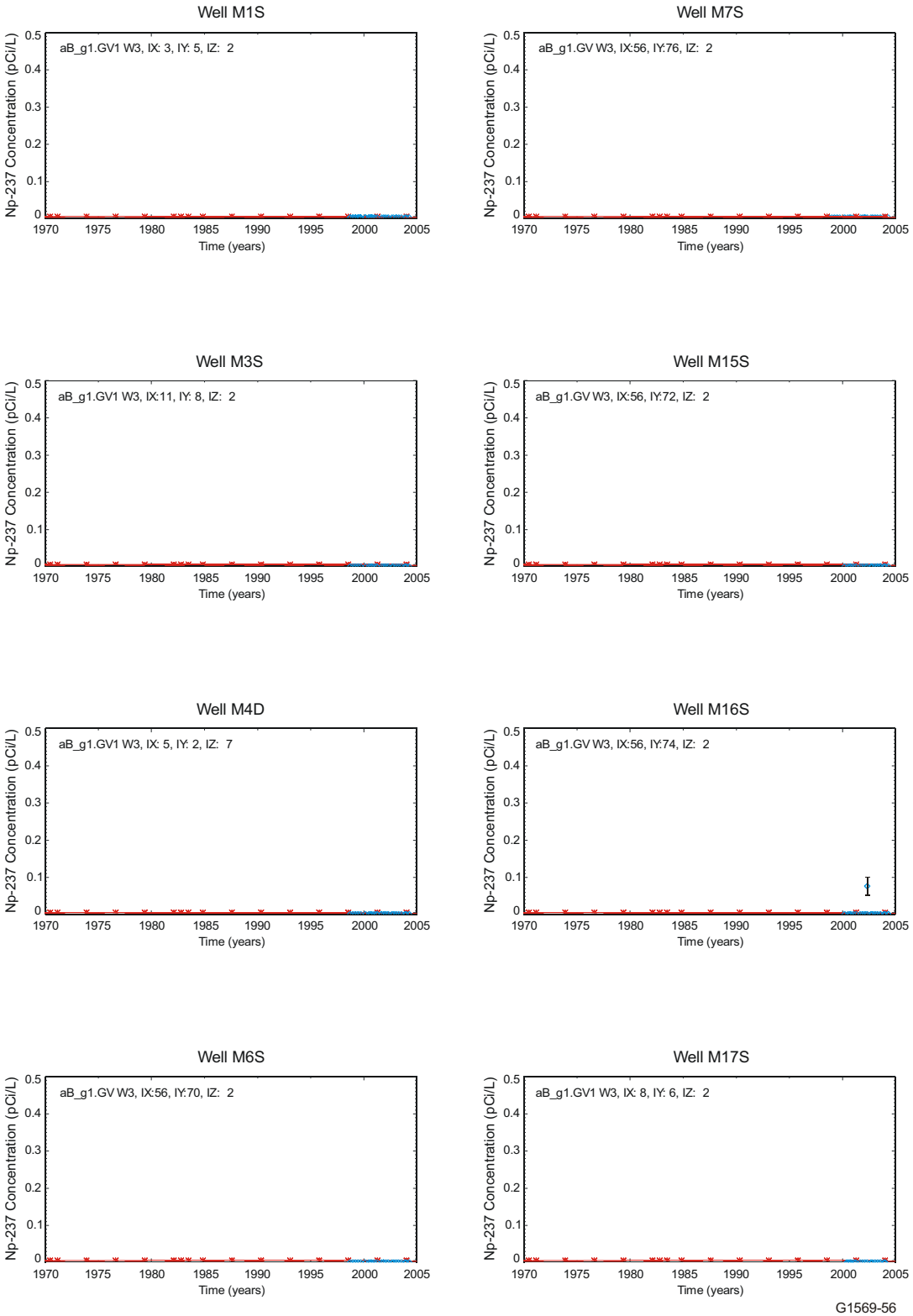

Figure 6-23. Comparison of simulated (red line) and observed (blue diamonds) neptunium-237 concentration time histories for aquifer-monitoring wells in the vicinity of the Subsurface Disposal Area.

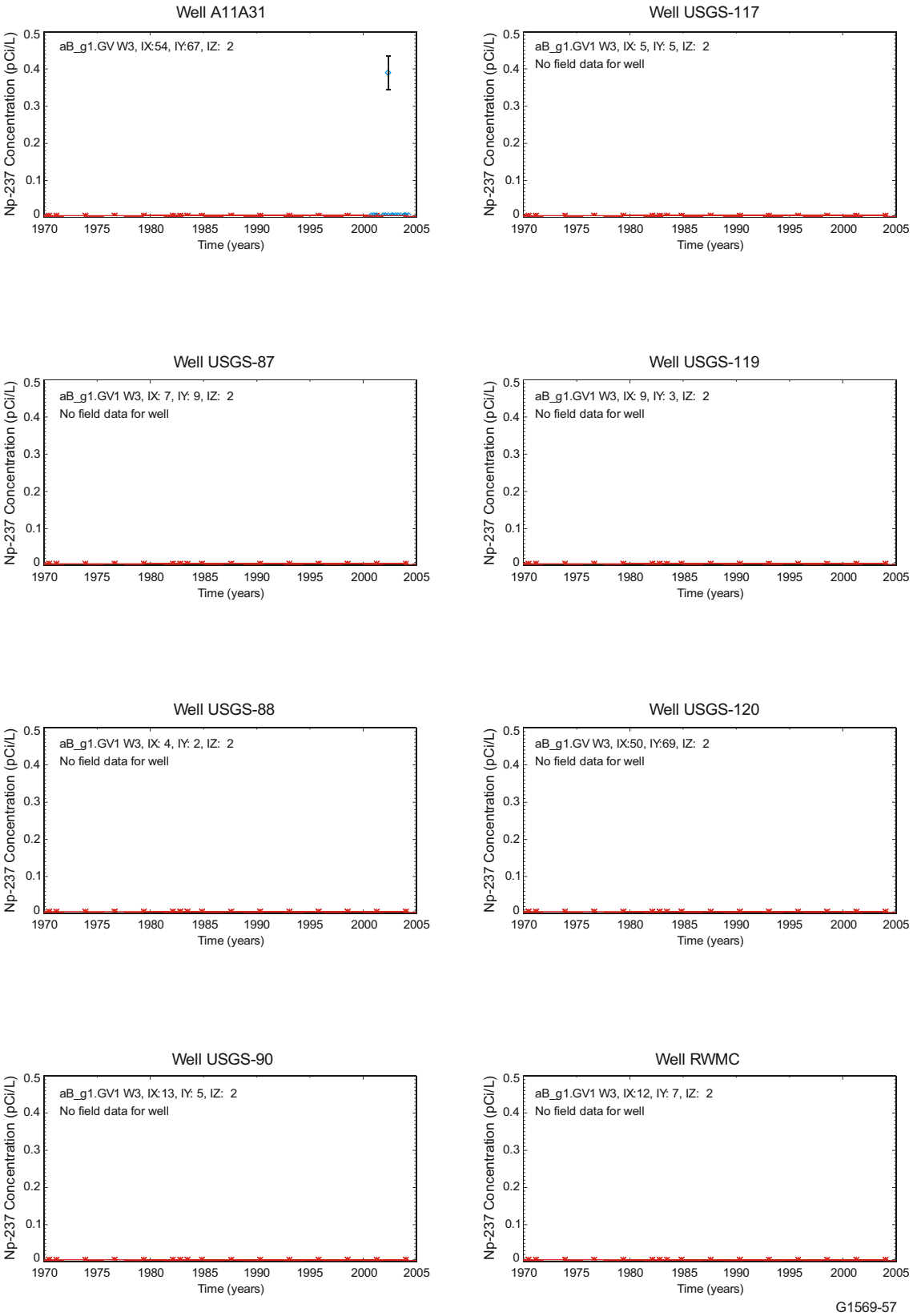

Figure 6-23. (continued).

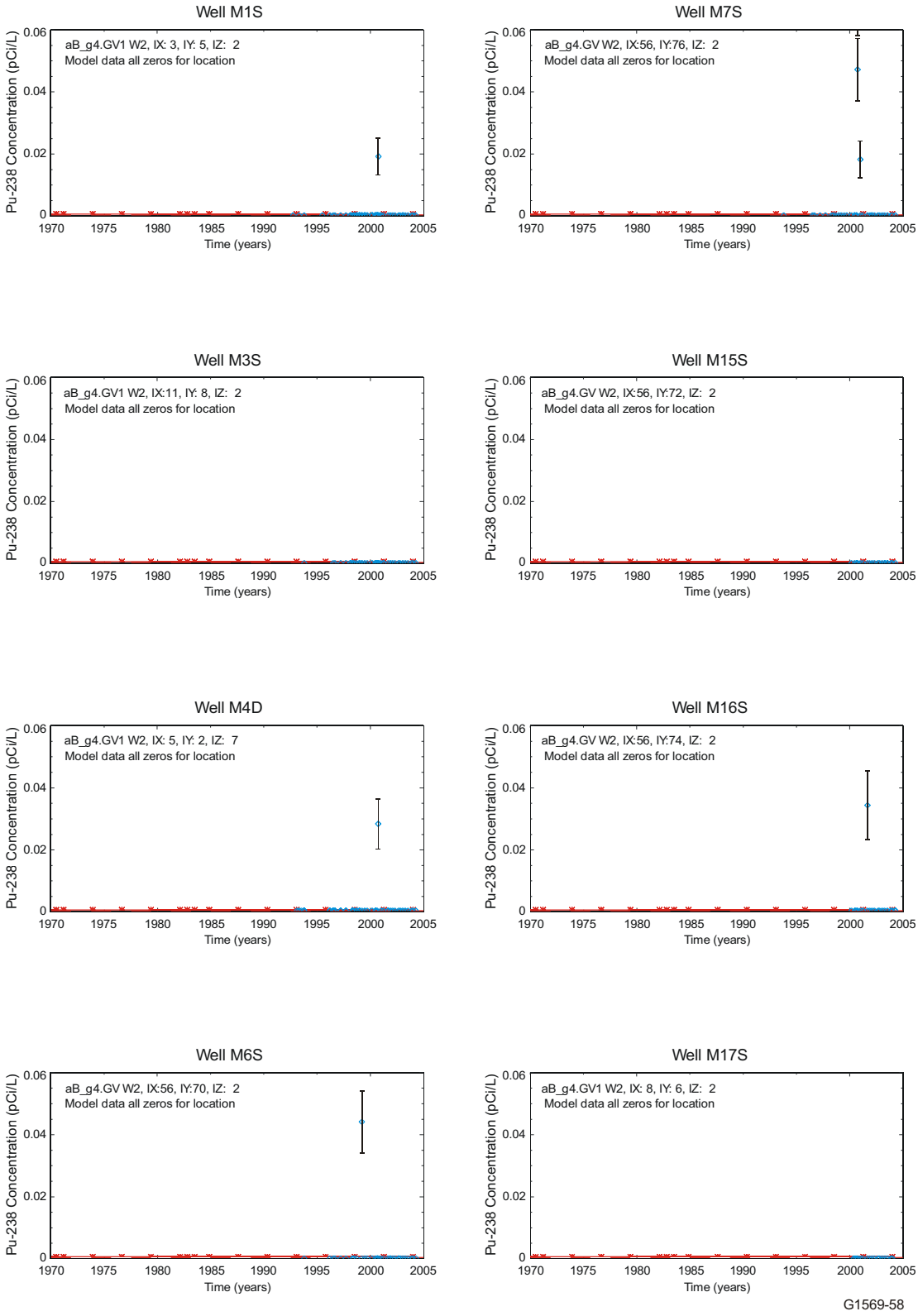

Figure 6-24. Comparison of simulated (red line) and observed (blue diamonds) plutonium-238 concentration time histories for aquifer-monitoring wells in the vicinity of the Subsurface Disposal Area.

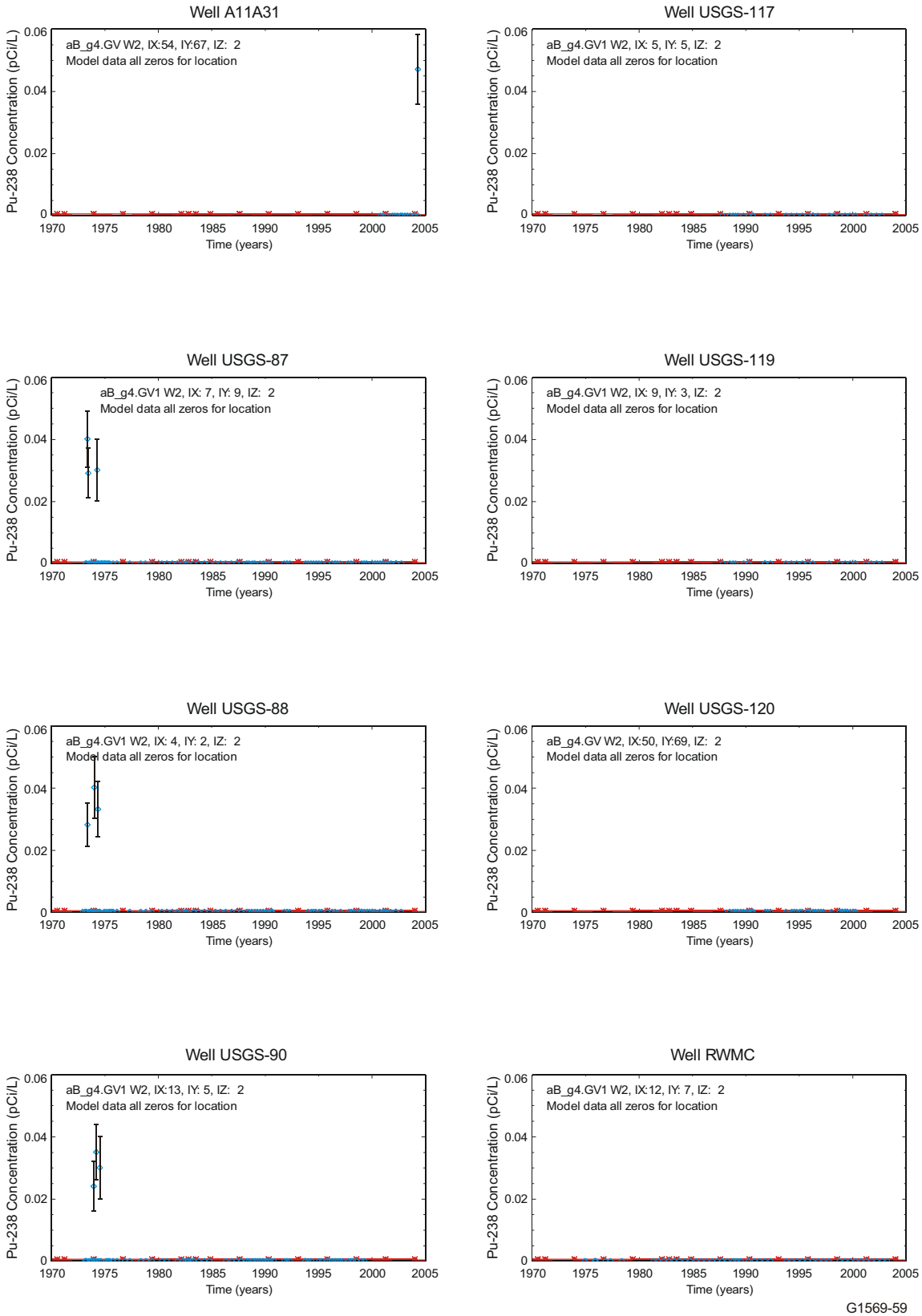

Figure 6-24. (continued).

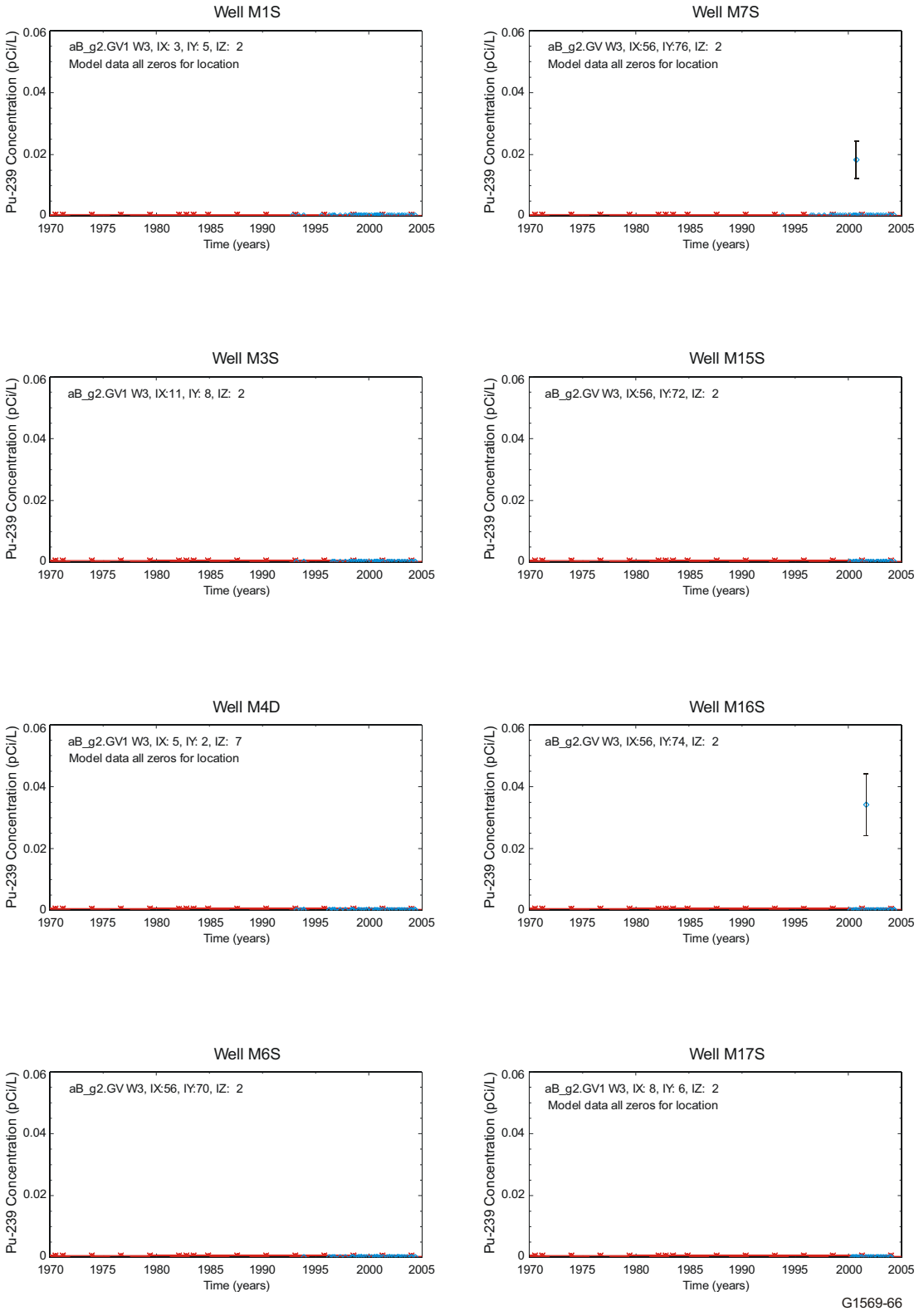

Figure 6-25. Comparison of simulated (red line) and observed (blue diamonds) plutonium-239 concentration time histories for aquifer-monitoring wells in the vicinity of the Subsurface Disposal Area.

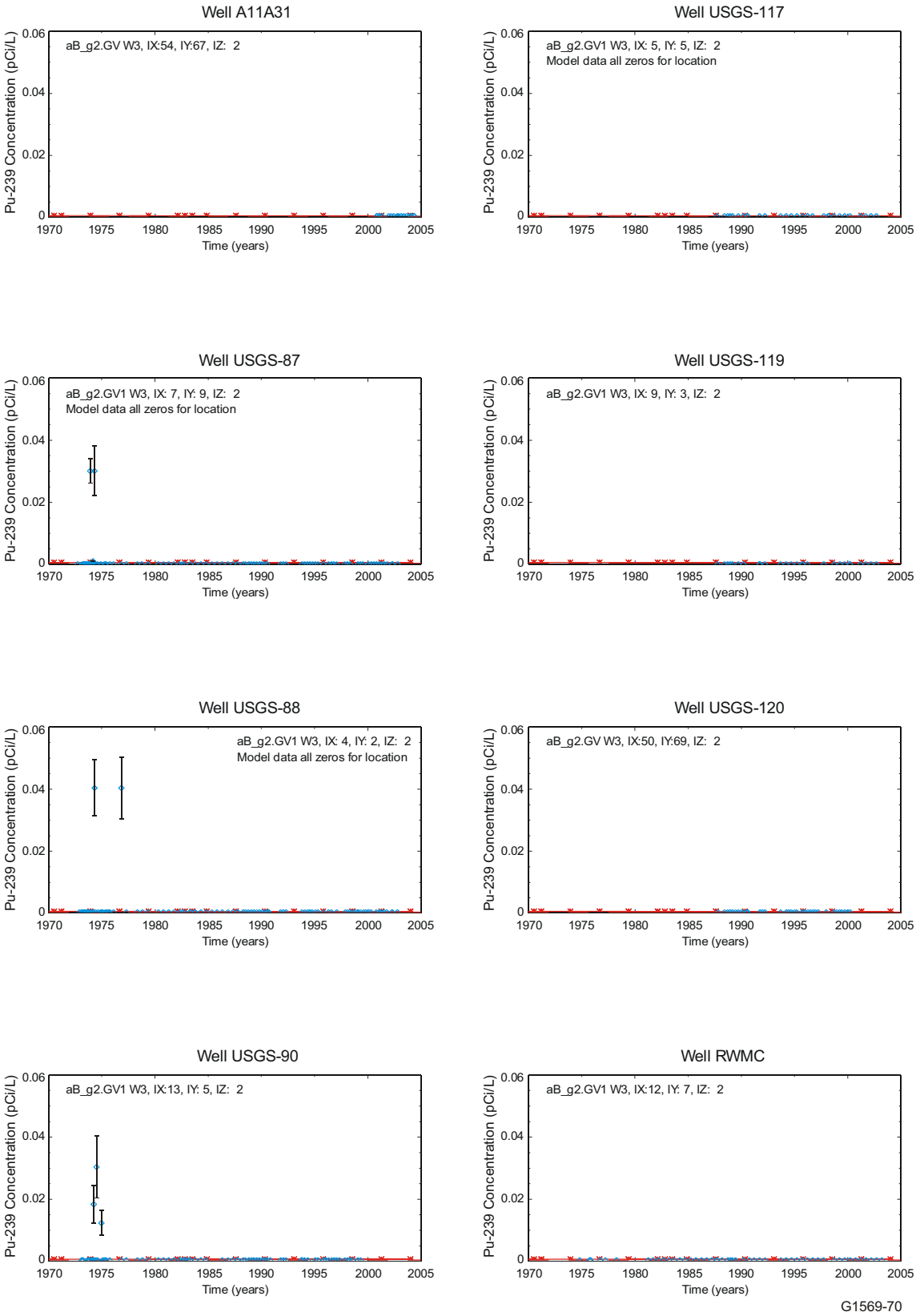

Figure 6-25. (continued).

Table 6-1. Comparison of aquifer model concentrations and observed concentrations with no adjustments for background concentrations.

Contaminant[a]	RI/FS Model Concentration[b] (pCi/L)	ABRA Model Concentration[c] (pCi/L)	IRA Model Concentration[d] (pCi/L)	Aquifer Background Concentration[e] (pCi/L)	Range of Detections[f] (pCi/L)[g]	Comments on Detections[g]
Ac-227	2E-11	5E-07	6E-08	NE	No analyses[h]	None
Am-241	7E-17	9E-17	1E-06	0	0.026–1.97	None
Am-243	3E-19	7E-24	2E-11	NE	No analyses	None
C-14	8E+01	3E+03	5 E+00	NE	1.8–42.1	Analysis began in 1994
Cl-l36	4E+00	3E+02	1E+00	NE	All nondetects	Analyses for Cl-36 began in the year 2001; Cl-36 analyses are done semiannually
I-129	1E+01	5E+01	4E+00	0	0.59–17.0	None
Nb-94	—	1E-23	1E-14	NE	No analyses	None
Np-237	1E-10	4E-04	8E-04	NE	0.08–0.38	None
Pa-231	1E-10	7E-06	1E-06	NE	No analyses	None
Pb-210	1E-17	3E-10	4E-08	NE	No analyses	None
Pu-238	4E-26	0	1E-12	0	0.018–0.37	NA
Pu-239	3E-17	5E-28	2E-11	0	0.034–4.3	None
Pu-240	3E-17	3E-30	7E-12	0	0.034–4.3	None
Ra-226	3E-17	4E-09	1E-08	0.01–0.37	4.0–12.7	Reported through gamma analysis when detected above laboratory instrument and sample matrix background
Ra-228	7E-19	—[i]	8E-12	0–2.7	No analyses	Reported through gamma analysis when daughter products are detected above laboratory instrument and sample matrix background
Tc-99	5E+03	4E+04	5E+01	NE	0.97–35.4	None
Th-229	4E-11	1E-06	4E-08	NE	No analyses	None
Th-230	2E-14	3E-06	8E-7	NE	No analyses	None
Th-232	2E-18	6E-13	1E-11	NE	No analyses	None
U-233	8E-08	4E-03	3E-04	NA	No analyses	NA
U-234	4E-10	1E-01	5E-02	1.92	2.0–4.3	None
U-235	2E-10	2E-02	3E-03	0.15	0.18–3.0	None
U-236	9E-09	4E-03	2E-03	NA	No analyses	None
U-238	9E-10	3E-01	4E-02	0.90	1.7–2.1	None

Table 6-1. (continued).

Contaminant[a]	RI/FS Model Concentration[b] (pCi/L)	ABRA Model Concentration[c] (pCi/L)	IRA Model Concentration[d] (pCi/L)	Aquifer Background Concentration[e] (pCi/L)	Range of Detections[f] (pCi/L)[g]	Comments on Detections[g]
Nitrate (as nitrogen-N)	6E+01 mg/L	1E+02 mg/L	1.4E+01 mg/L	0.4–5.0 mg/L	0.28–3.4 mg/L	None
Chromium (total)	3E+01 µg/L	1E+00 µg/L	1E-01µg/L	1–22 µg/L	4.6–99.6 µg/L	Most other high chromium values were approximately 40 to 60 pCi/L
Carbon tetrachloride	1E+02 µg/L	—[i]	8E+00 µg/L	0 µg/L	0–8 µg/L[f]	None
Methylene chloride	1E+01 µg/L	—[i]	1E-01 µg/L	0 µg/L	0–6 µg/L	Single detection of 6 µg/L was not believed to be a valid result
Tetrachloroethylene	1E+01 µg/L	—[i]	6E-01 µg/L	0 µg/L	0–0.4 µg/L[f]	None
1,4-dioxane	1E+02 µg/L	—[i]	—[i]	0 µg/L	No analyses	1,4-dioxane was only recently added to the analyte list

a. Observed values from earlier than 1987 are not presented in this table.
b. Maximum simulated concentration at 12-m depth through Fiscal Year 2004.
c. Maximum simulated concentration at 12-m depth through Fiscal Year 2001.
d. Maximum simulated concentration at 12-m depth through Fiscal Year 1995.
e. Aquifer background concentrations are from Table 4-1 in the draft remedial investigation and baseline risk assessment.
f. In the Subsurface Disposal Area-vicinity wells since 1987.
g. The range of observed values is taken from the nature and extent discussion in Section 4 of the draft remedial investigation and baseline risk assessment.
h. See the respective contaminant discussions in Section 4 of the draft remedial investigation and baseline risk assessment regarding lack of analysis.
i. Not reported in the IRA or ABRA.

ABRA = Ancillary Basis for Risk Analysis (Holdren et al. 2002)
IRA = Interim Risk Assessment (Becker et al. 1998)
NA = information not available on background concentrations
NE = not established
RI/FS = remedial investigation and feasibility study

Note: 0.0 pCi/L for radionuclides signifies a nondetectable result (i.e., result is <3σ and <maximum detectable concentration) using traditional radiochemical analyses methods.

Simulated vertical profiles of C-14 and U-238 concentrations within the aquifer are shown in Figures 6-26 and 6-27 to illustrate behavior for selected contaminants. These vertical profiles are at the same horizontal location as that shown previously in Figure 6-15 for nitrate, which generally contained the maximum concentration for most times. Similar to profiles for nitrate, there are times when the maximum concentration does not occur at the uppermost gridblock for C-14. This is because contaminant flux from the vadose zone model behaved similarly for nitrate and C-14 with a pulse of contaminant followed by clean water. The simulated profile for U-238 shows that the maximum concentration always occurs in the uppermost gridblock, reflecting the long-duration, delayed contaminant flux from the vadose zone model. The overall implication for the baseline risk assessment remains the same, that it is not necessarily conservative to extract concentrations from the uppermost gridblock.

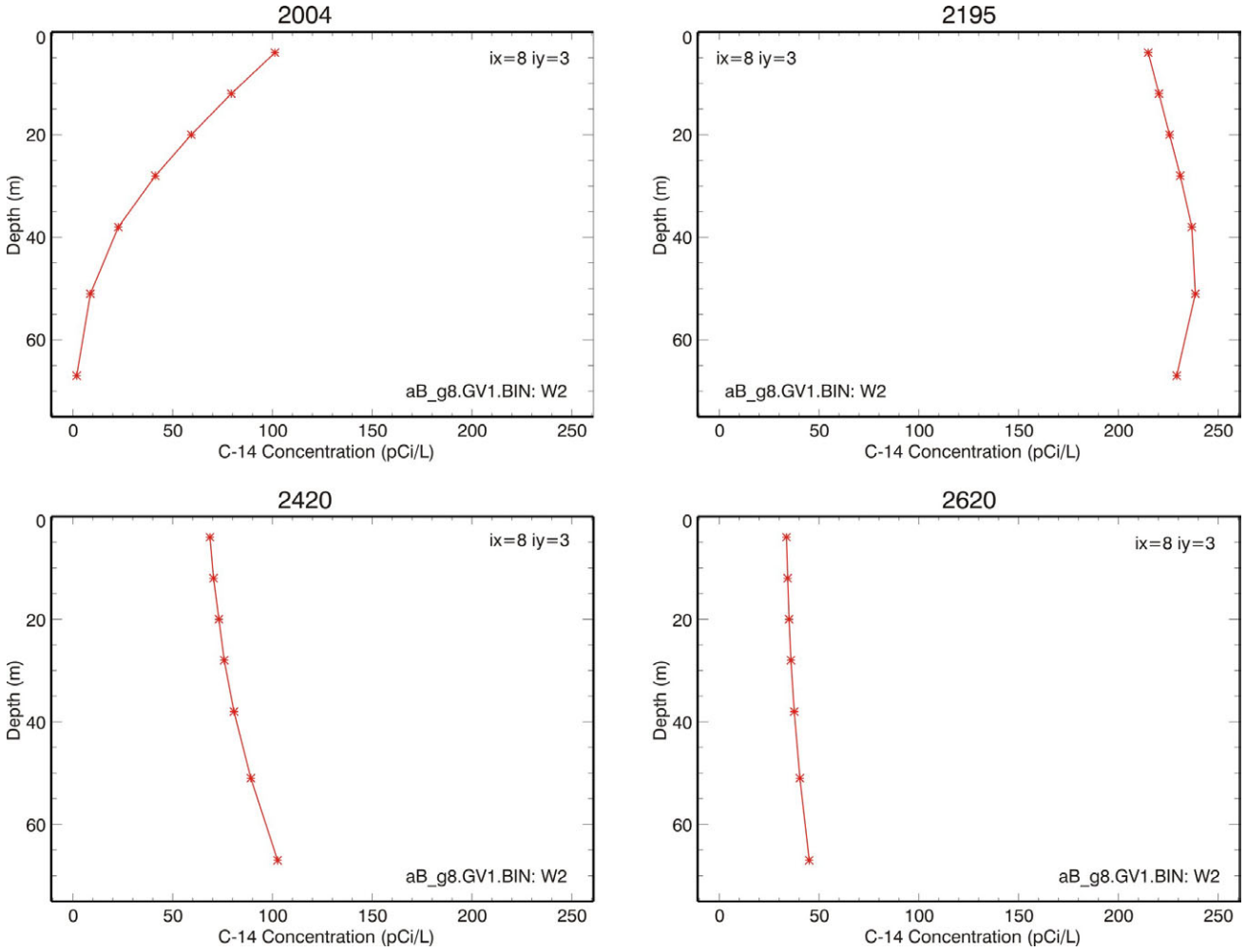

Figure 6-26. Simulated aquifer carbon-14 concentration profiles beneath the Subsurface Disposal Area. The year is shown at the top of each plot.

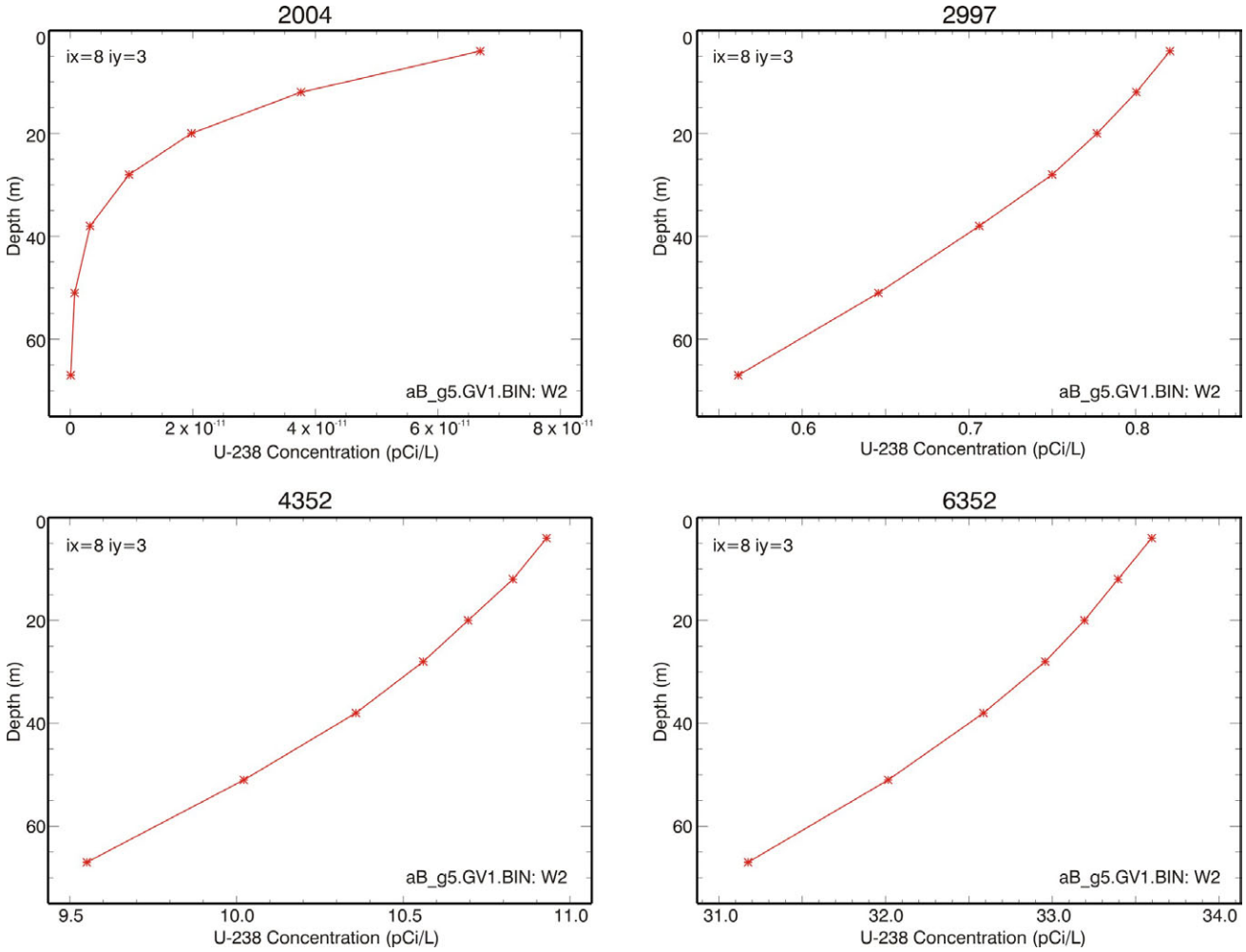

Figure 6-27. Simulated aquifer uranium-238 concentration profiles beneath the Subsurface Disposal Area. The year is shown at the top of each plot.

6.2 Receptor Locations and Extraction of Simulated Aquifer Concentrations for Risk Evaluation

Simulated aquifer COPC concentrations and hypothetical receptors are used for the risk evaluation. These simulated concentrations are taken from the results from a variety of locations. For the draft RI/BRA, the locations where receptors are allowed are defined in Holdren and Broomfield (2004) as being at the INL Site boundary during the period of institutional control, which lasts until Calendar Year 2110, and up to the RWMC fence boundary after institutional control ends. This receptor definition was implemented for purposes of extracting simulated concentrations from the TETRAD model results at the current SDA fence boundary as shown in Figure 6-28. Maximum simulated aquifer concentrations, as a function of time from those gridblocks with a centroid located outside the SDA fence, were used in calculations. Shaded blocks in the Figure 6-28 represent locations that were excluded from the risk evaluation.

The location of the gridblock with the maximum concentration changed during every simulation. Generally, but not always, the location of maximum simulated aquifer concentration occurred either within the SDA or at one of the gridblocks in immediate proximity to the SDA. For some mobile

contaminants, such as Tc-99, the maximum simulated concentration occurred in gridblocks away from the SDA to the southeast. These occurrences most likely resulted because of lateral movement of water and contaminants away from the SDA that was caused by the general slope of the B-C and C-D interbeds to the east-southeast. This lateral movement demonstrates the importance of including variable interbed topography in simulating water and contaminant transport through the vadose zone.

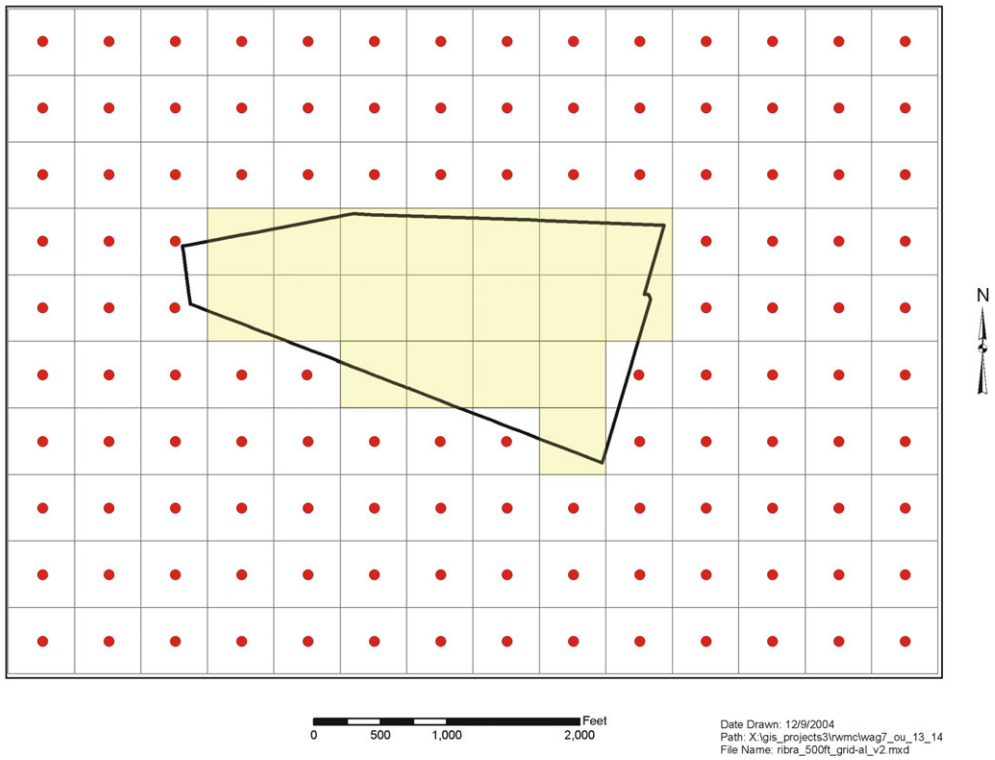

Figure 6-28. Subsurface Disposal Area fence superimposed on the first-level refined grid of the aquifer simulation for purpose of defining hypothetical receptor locations for the draft remedial investigation and baseline risk assessment. Gridblocks whose centroid (indicated by a dot) is outside the fence boundary are potential receptor locations.

Extraction of maximum simulated concentrations as a function of time from the TETRAD results was automated via a PV-Wave post-processing routine. In addition to determining maximum concentrations along the INL Site boundary and for locations outside the SDA fence, there were two other methods implemented. To provide results for comparisons to simulated concentrations and risks from the ABRA model, the maximum simulated concentration anywhere, including the excluded gridblocks inside the SDA fence boundary, were extracted. And lastly, for the low-level waste performance assessment and composite analysis, simulation results were extracted slightly differently because a 100-m buffer zone outside the SDA facility fence is defined in Department of Energy Order 435.1, resulting in a slightly different set of allowed receptor locations with more gridblocks proscribed as receptor locations.
The potential receptor locations for the low-level waste performance assessment and composite analysis are indicated in Figure 6-29 with the proscribed gridblocks shaded. Maximum concentration as a function of time was saved in files, along with gridblock locations of the maximums.

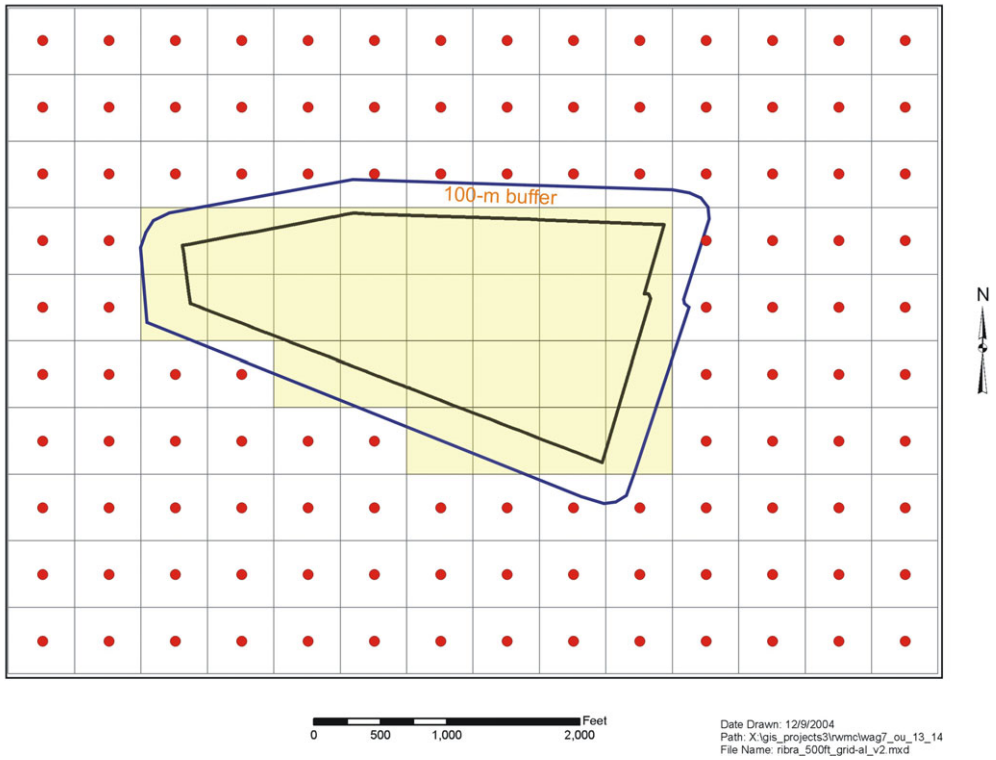

Figure 6-29. Subsurface Disposal Area fence plus a 100-m buffer superimposed on the first-level refined grid of the aquifer simulation for the purpose of defining hypothetical receptor locations for the low-level waste performance assessment and composite analysis. Gridblocks whose centroid (indicated by a dot) is outside the 100-m buffer are potential receptor locations.

In all cases, simulated concentrations are extracted from the second gridblock down from the top of the aquifer. This gridblock extends from the 8- to 16-m (26.2- to 52.5-ft) depth with a midpoint of 12 m (39.4 ft). This second gridblock approximates a well that is screened from 8 to 16 m (26.2 to 52.5 ft). As shown previously in Section 6.1, concentration profiles are not always automatically highest at the uppermost gridblock, depending on the contaminant mass loading history. Therefore, it is not automatically conservative to extract concentrations from the uppermost gridblock.

6.3 Risk and Hazard Index Isopleth Methodology

As indicated in the previous simulation, the location of maximum concentration shifted spatially over time. Risk determined from these location-varying concentrations is conservative because it is not realistic to require a receptor to get water from a well at one location during one time period, and then switch to getting water from a different well at another location for another time period. To evaluate the amount of conservatism, a different approach was used to evaluate risk for a receptor that got water from a well at one location consistently. This approach used a spatially-consistent receptor. In this method, simulated concentrations for all COPCs at each gridblock (second gridblock down again) at each time were converted to their equivalent risks and summed to get the cumulative risk. These spatially-consistent receptor risks could then either be contoured to show the horizontal extent of risk, or further interrogated to determine the maximum spatially-consistent receptor risk as a function of time. These extensive calculations were automated in a PV-Wave post-processing routine. The results of these analyses are presented in Section 6 of the draft RI/BRA.

6.4 Base-Case Sensitivity Simulations

This section discusses implementation of simulations for the RI/BRA sensitivity analyses, which were defined in Holdren and Broomfield (2004). Results, when presented, are in terms of water saturations or simulated concentrations. Results are presented for U-238, C-14, and nitrate simulations to demonstrate the impact from a variety of contaminants with sorbing and nonsorbing behavior for most of the sensitivity cases. Exceptions are presentation of Pu-239 and Pu-240 for a case with no sorption in the interbeds and Tc-99 for evaluation of impacts from increasing the fractured-basalt permeability anisotropy ratio. Technetium-99 and I-129 are not shown for most of the sensitivity cases because those results are being revised for the feasibility study. The C-14 results presented in these sensitivity simulations use the model that includes both gaseous-phase and dissolved-phase transport and the effect of vapor vacuum extraction described above in Sections 5.4 and 5.5. Both the time and concentration axes vary on the sensitivity results plots to show adequate detail in the results to discern behavior. The sensitivity results also are presented in terms of impacts to groundwater-pathway risks in Section 6 of the draft RI/BRA. These sensitivity simulations test assumptions used in the model, and as such, the simulations represent an assessment of conceptual uncertainty.

6.4.1 Upper-bound Inventories

A simulation suite was performed where upper-bound inventories were used instead of best estimates. The only difference in the subsurface flow and transport models was that a different source term was supplied. The entire suite of potential contaminants was simulated. Figure 6-30 shows a comparison of the concentration of U-238, C-14, and nitrate between the base case and the upper-bound inventory simulation. In each case, simulated concentrations are larger, although it takes longer for this to be evident for U-238, which undergoes sorption, thus, the longer time portrayed on the horizontal axis. Note that the concentrations shown in this sensitivity section are for the maximum simulated concentration anywhere in the aquifer, including beneath the SDA, for all simulated times. This is in contrast to risks presented in Section 6 of the draft RI/BRA, which are based on maximum simulated concentration anywhere outside the SDA fence after institutional control ends in Calendar Year 2110.

6.4.2 No B-C Interbed

The method used to define interbed upper surfaces and interbed thicknesses resulted from a consistent statistical approach that was based on all lithologic data available. To incorporate spatial variability, geostatistical analysis and interpolation methods were implemented and robustly tested by Leecaster (2002) and updated in Leecaster (2004). As with the ABRA model, the RI/FS model used kriging results without imposing any bias into them. In the IRA model, kriging results were modified to enforce gaps in the interbeds in gridblock locations containing wells that showed an interbed was missing at that location.

To bound the effect of including gaps, a simulation suite was performed where the entire B-C interbed was treated as though it were missing. The gridblocks that were assigned B-C interbed properties for the RI/FS model were assigned properties of fractured basalt instead. This allowed the mobile fraction of Pu-239 and Pu-240 to continue migrating down to the C-D interbed before being affected by the higher distribution coefficient. Upper-boundary conditions for water infiltration rates and contaminant source-term results were unchanged from the RI/FS model. The entire suite of potential contaminants was simulated, except for VOCs (Group 11). As a result of not simulating VOCs, C-14 simulation results for this case do not include the effect of VVET operation. Figure 6-31 shows a comparison of concentration of U-238, C-14, and nitrate between the RI/FS model and the sensitivity simulation without the B-C interbed. As expected, in each case, the simulated concentrations for the sensitivity case show an earlier breakthrough due to absence of the B-C interbed, with the largest

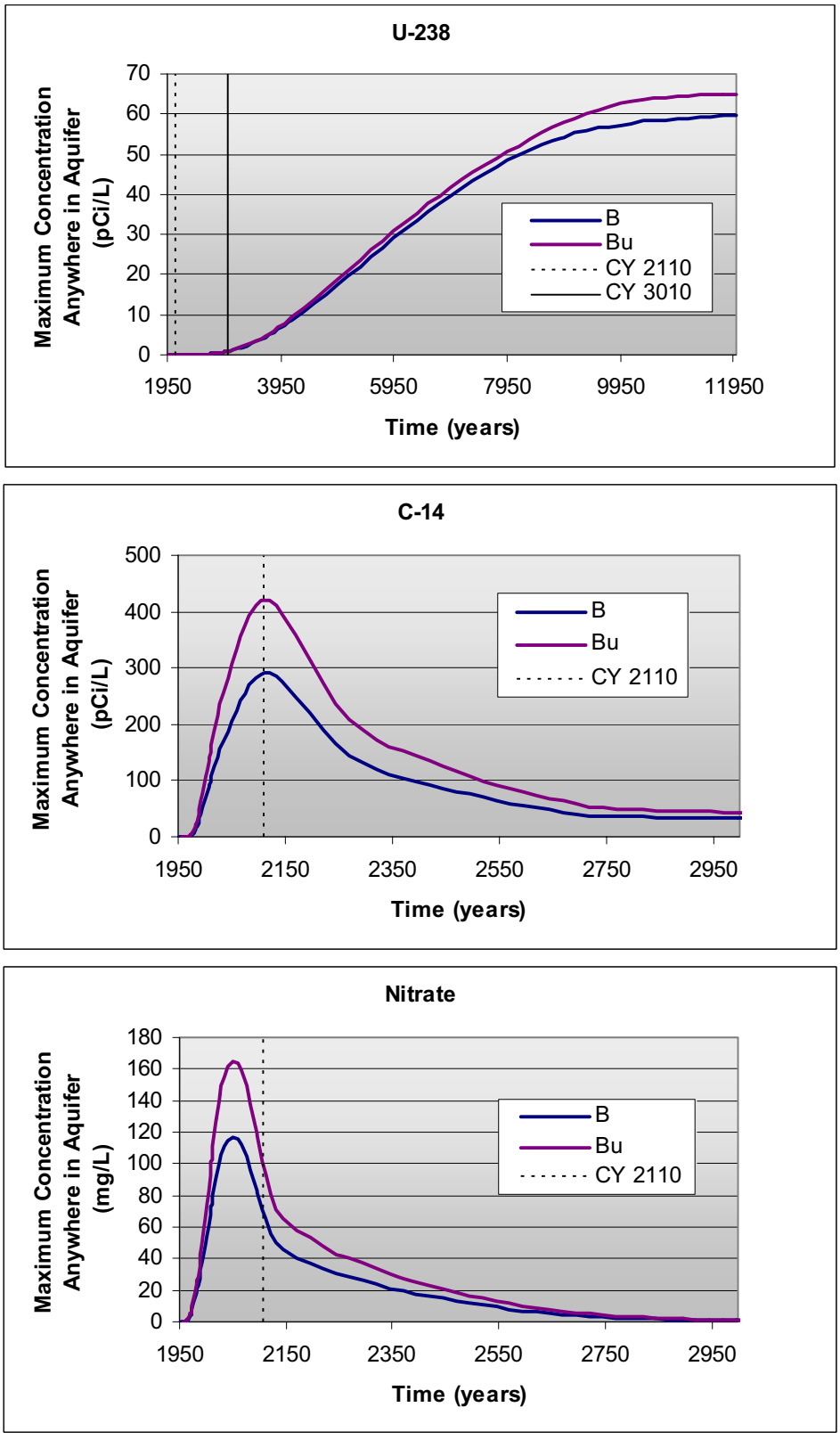

Figure 6-30. Comparison of the base (B) and the upper-bound inventory (Bu) maximum simulated concentration anywhere in the aquifer for uranium-238, carbon-14, and nitrate.

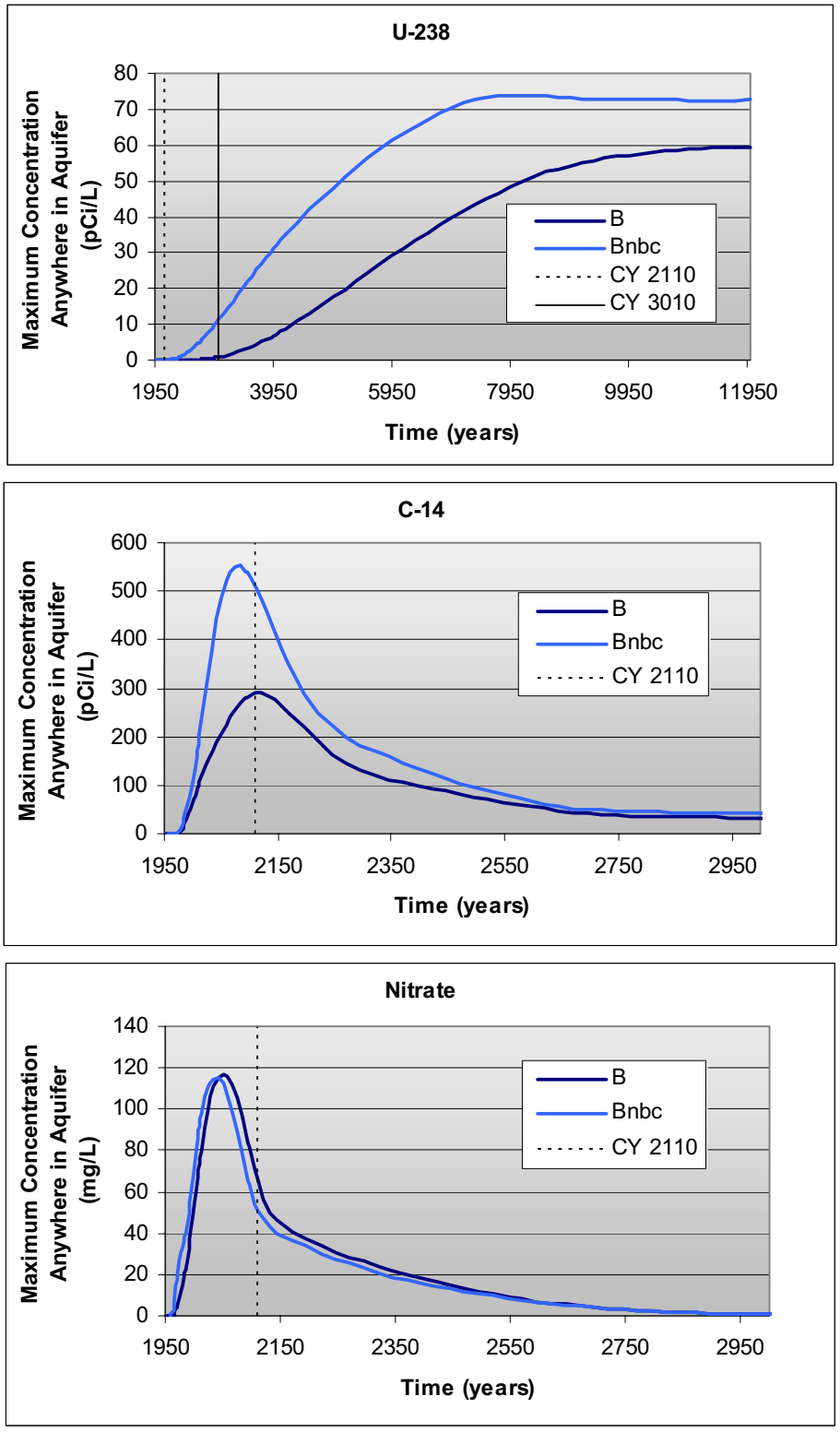

Figure 6-31. Comparison of the base (B) and the no B-C interbed (Bnbc) maximum simulated concentration anywhere in the aquifer for uranium-238, carbon-14, and nitrate. The carbon-14 results do not include the effect of vapor vacuum extraction operations.

change in results for U-238, where lack of sorption in the B-C interbed exaggerates impact. Magnitudes of peaks do not change substantially with U-238 and C-14 both increasing. The nitrate peak concentration decreases slightly, possibly due to interactions between where nitrate is released into the vadose zone model and the locations where nitrate would otherwise have been redirected when transiting the B-C interbed.

6.4.3 High Infiltration Inside the Subsurface Disposal Area

Water infiltration rates are assigned at the upper boundary of the vadose zone simulation domain. These amounts of water also are input into the source-term model and impact contaminant release. Uncertainty in assigned infiltration rates is acknowledged. To bound the effect of the infiltration rate being greater than was assigned, a sensitivity simulation was performed whereby the infiltration rate everywhere inside the SDA boundary was assigned a value of 23 cm/year (9 in./year), both in the source-release model and in the vadose zone flow and transport model, beginning in 1952. The water infiltration rate outside the SDA boundary remained at the background estimate of 1.0 cm/year (0.4 in./year). The 23-cm/year (9-in./year) infiltration rate is the same as the total annual average precipitation on the INL Site and represents a conservative upper-bound inventory on the possible net infiltration into the subsurface. The entire suite of potential contaminants was simulated.

Figure 6-32 shows a comparison of U-238, C-14, and nitrate concentrations between the base case and the sensitivity simulation with a high-infiltration rate inside the SDA. As expected, in each case, the simulated concentrations for the sensitivity case show higher concentrations and reach peak values sooner than the base-case simulated concentrations. Conceptually, water that contacts waste results in higher concentrations uniformly in the groundwater pathway. Results of this sensitivity case demonstrate this aspect of the conceptual model.

In addition to the effect on groundwater-pathway concentration results, this sensitivity simulation lends itself to assessing the impacts on simulated interbed saturations. Figure 6-33 illustrates the resulting maximum simulated water saturations in the B-C and C-D interbeds for the high-infiltration case. Water saturations in Figure 6-33 can be compared to those for the base case, which are shown previously in Section 5.1, Figure 5-4. The extent of high saturation areas above 0.9 is considerably larger, especially in the B-C interbed. Better agreement with locations that had shown perched water in the western half of the SDA is shown. These locations are shown in the base-case results presented in Section 6.1.

6.4.4 Pit 4 Inventory Not Removed and No Beryllium Block Grouting

The base-case model included removal of a portion of the Pit 4 inventory, based on the assumption that the Accelerated Retrieval Project was completed. Likewise, grouting of beryllium blocks also was included. This sensitivity study considered a case where neither of these actions occurred. The entire suite of potential contaminants was simulated.

Figure 6-34 shows a comparison of U-238 and C-14 concentrations between the base case and sensitivity simulation with the Pit 4 inventory not reduced and without beryllium block grouting. Nitrate is not shown because there was no change to the source-release modeling for this sensitivity case. Simulated U-238 concentrations for the sensitivity case are essentially the same because, although there is a larger inventory available for release in the sensitivity case, the solubility limit for U-238 keeps the source-release term almost equivalent between the two cases. The simulated C-14 concentration is slightly higher for the sensitivity case because there is a greater release from the source model due to a larger inventory.

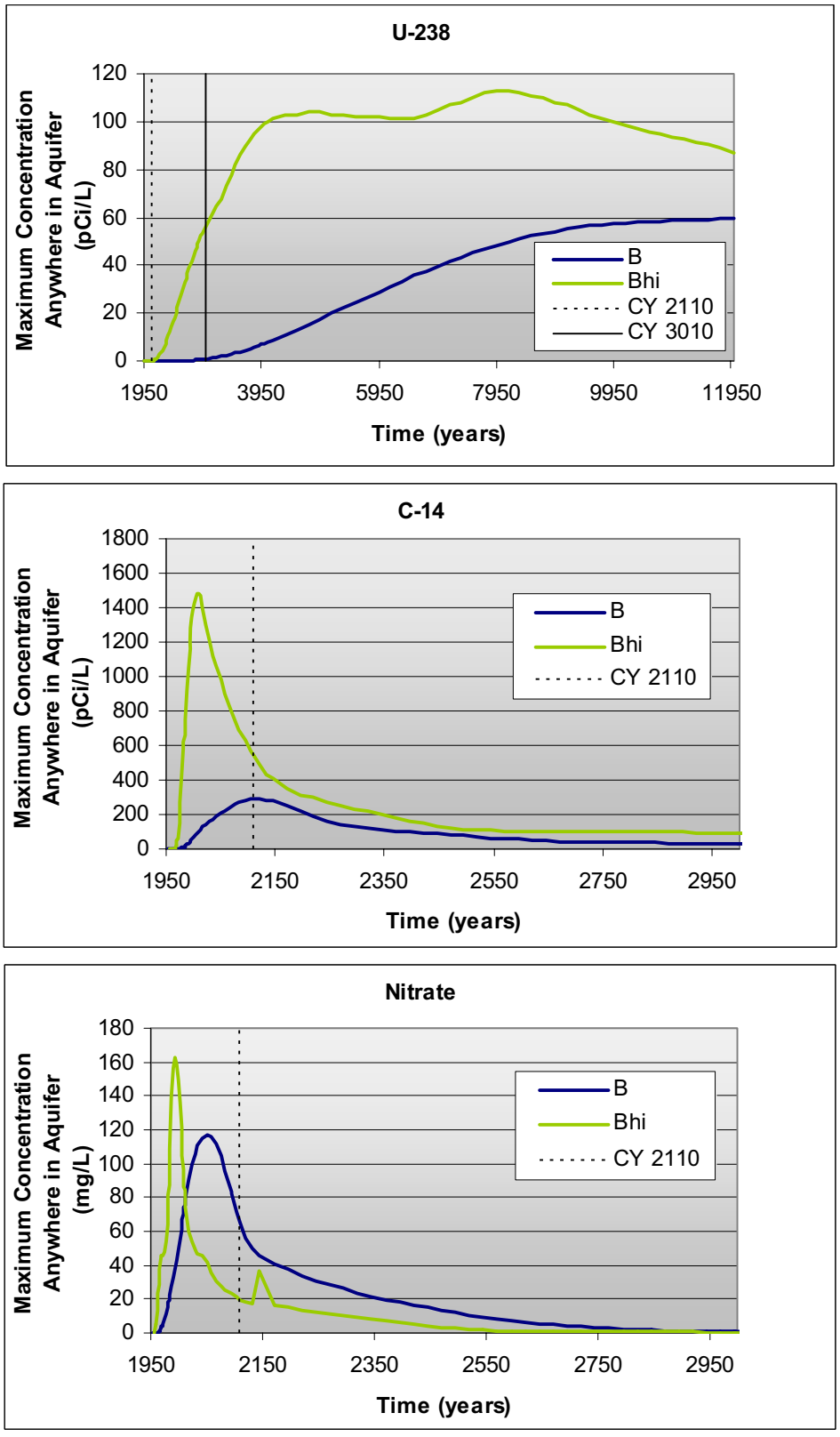

Figure 6-32. Comparison of the base (B) and high infiltration inside the Subsurface Disposal Area (Bhi) maximum simulated concentration anywhere in the aquifer for uranium-238, carbon-14, and nitrate.

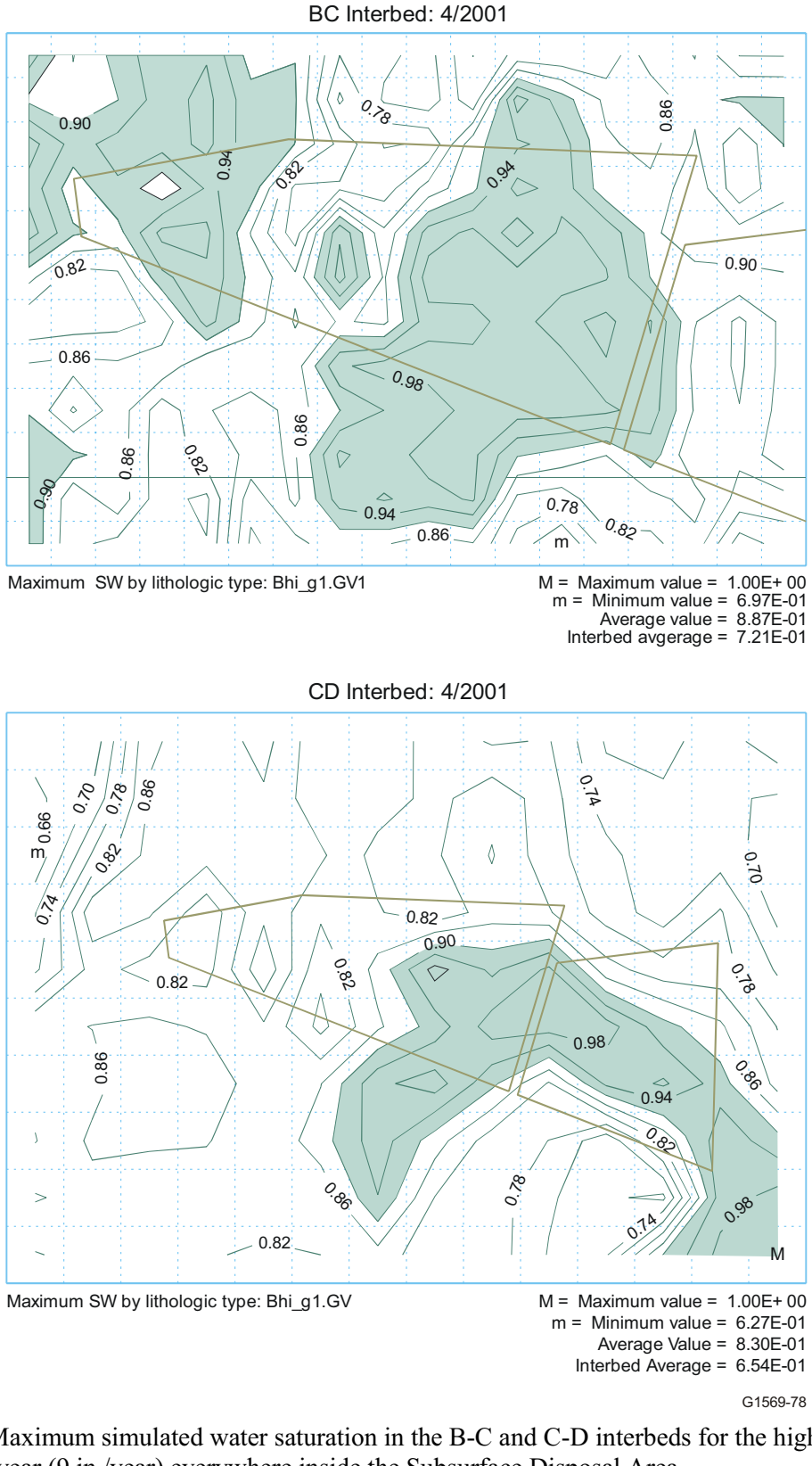

Figure 6-33. Maximum simulated water saturation in the B-C and C-D interbeds for the high-infiltration rate of 23 cm/year (9 in./year) everywhere inside the Subsurface Disposal Area.

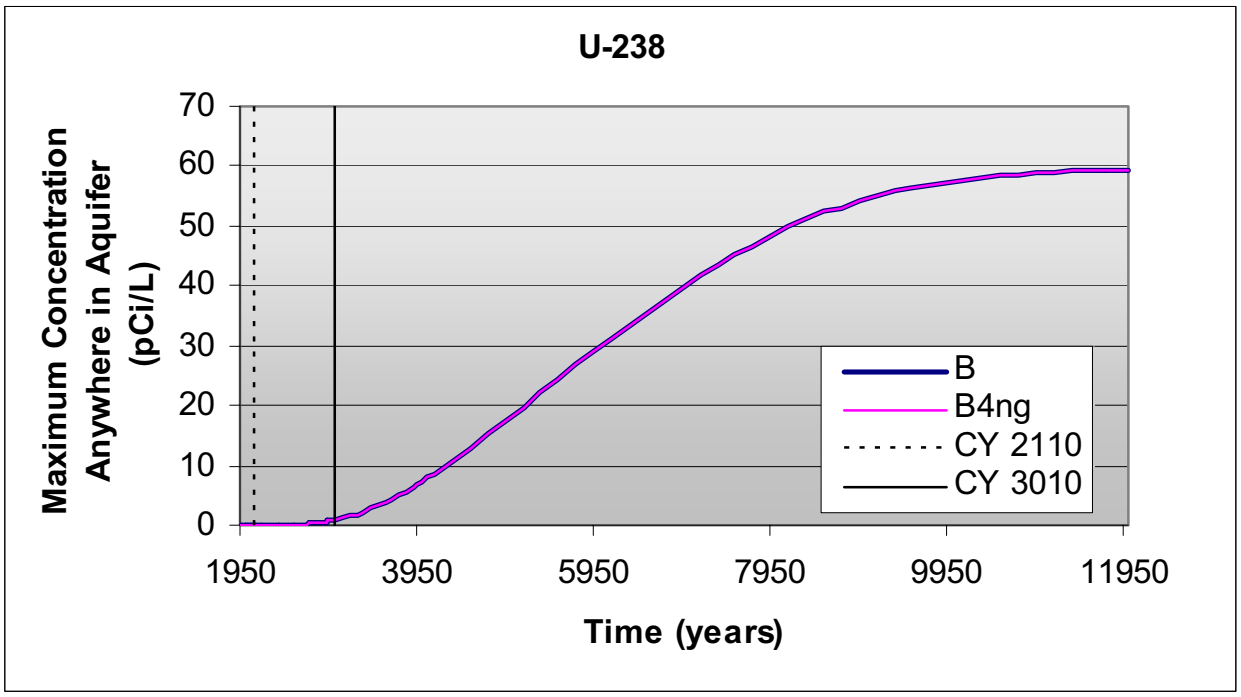

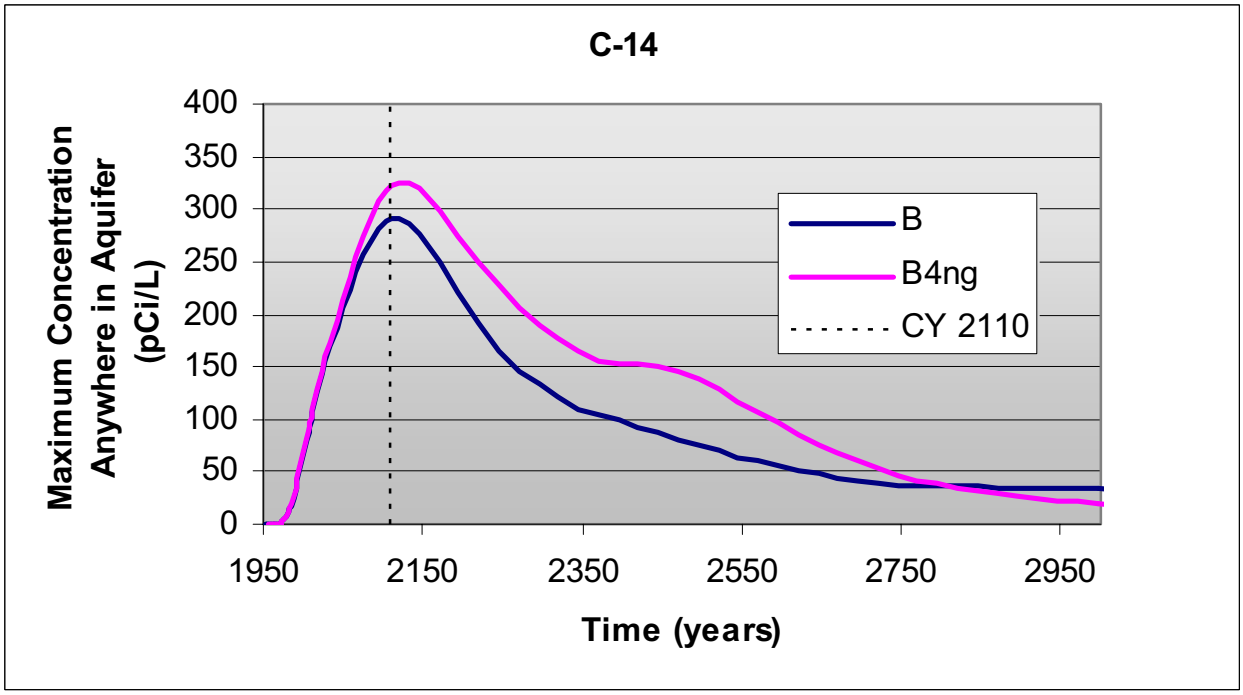

Figure 6-34. Comparison of the base (B) and Pit 4 inventory not removed and no beryllium block grouting (B4ng) maximum simulated concentration anywhere in the aquifer for uranium-238 and carbon-14. Nitrate is not shown because there was no change to the source-release modeling for this case.

6.4.5 Low Background Infiltration

The infiltration rate outside the SDA was assigned a value of 1.0 cm/year (0.4 in./year) for the RI/FS model. In this sensitivity case, a background infiltration rate that is an order of magnitude lower

was assigned to test the impact on simulated groundwater-pathway concentrations. This lower rate was assigned because ongoing investigations may lead to the conclusion that the 1.0 cm/year (0.4 in./year) background infiltration rate is too high. The lower background infiltration rate was used for initial conditions for this sensitivity simulation and was continued for infiltration outside the SDA beginning in 1952. The entire suite of potential contaminants was simulated.

Figure 6-35 shows a comparison of U-238, C-14, and nitrate concentrations between the base case and the sensitivity simulation with a lower background infiltration rate outside the SDA. For each of these three contaminants, simulated concentrations arrived slower in the sensitivity case, showing the effect of slower velocities in the vadose zone that result from less water overall in simulations. Peak concentrations for U-238 and nitrate increased, likely due to less dilution with less water overall coming into the aquifer from the vadose zone domain. However, the C-14 concentrations decreased, with the decrease likely due to specific interactions between where it is released into the vadose zone model and reductions in velocity.

6.4.6 No Low-Permeability Region in Aquifer

This case was not specified in Holdren and Broomfield (2004), and updates results of a similar assessment done after IRA modeling (Magnuson 1998), where the effect of not including the low-permeability zone in the aquifer was simulated. In the RI/FS model, the low-permeability region in the aquifer is assumed to be continuous and have substantially slow movement of water within the aquifer beneath the SDA. This slower movement results in less dilution of influxing vadose zone contaminants than would otherwise occur. Simulating only the aquifer portion of the groundwater pathway for this sensitivity simulation was necessary because the vadose zone simulation was unaffected.

Figure 6-36 shows a comparison of U-238, C-14, and nitrate concentrations between the base case and the sensitivity simulation without the low-permeability region in the aquifer. Simulated concentrations, without the low-permeability region in the aquifer, are markedly reduced. This reduction in concentration when the low-permeability region is absent demonstrates a conservative aspect of the RI/FS model.

6.4.7 Fractured Basalt Anisotropy

This case also was not specified in Holdren and Broomfield (2004). The need for this case arose when it was discovered that by using a fractured basalt anisotropy ratio of 300:1 for the horizontal-to-vertical permeability, some additional lateral water movement above the C-D interbed occurred that resulted in some water and contaminants contacting the horizontal no-flux boundary in the southeastern corner of the vadose zone simulation domain. For some short-duration periods before the end of institutional control in 2110, this lateral movement results in the peak concentration in the aquifer occurring beneath this extreme southeastern gridblock location in the vadose zone model domain.

A series of simulations were made to evaluate the effect of the selected anisotropy ratio in the fractured basalt. The RI/FS model uses an anisotropy ratio of 300:1, with horizontal permeability being 300 times greater than vertical permeability. This anisotropy ratio allows some of the water moving down through the vadose zone to migrate laterally to the extreme southeastern corner of the simulation domain, where it cannot spread further due to the lateral no-flow constraint imposed by the domain boundary.

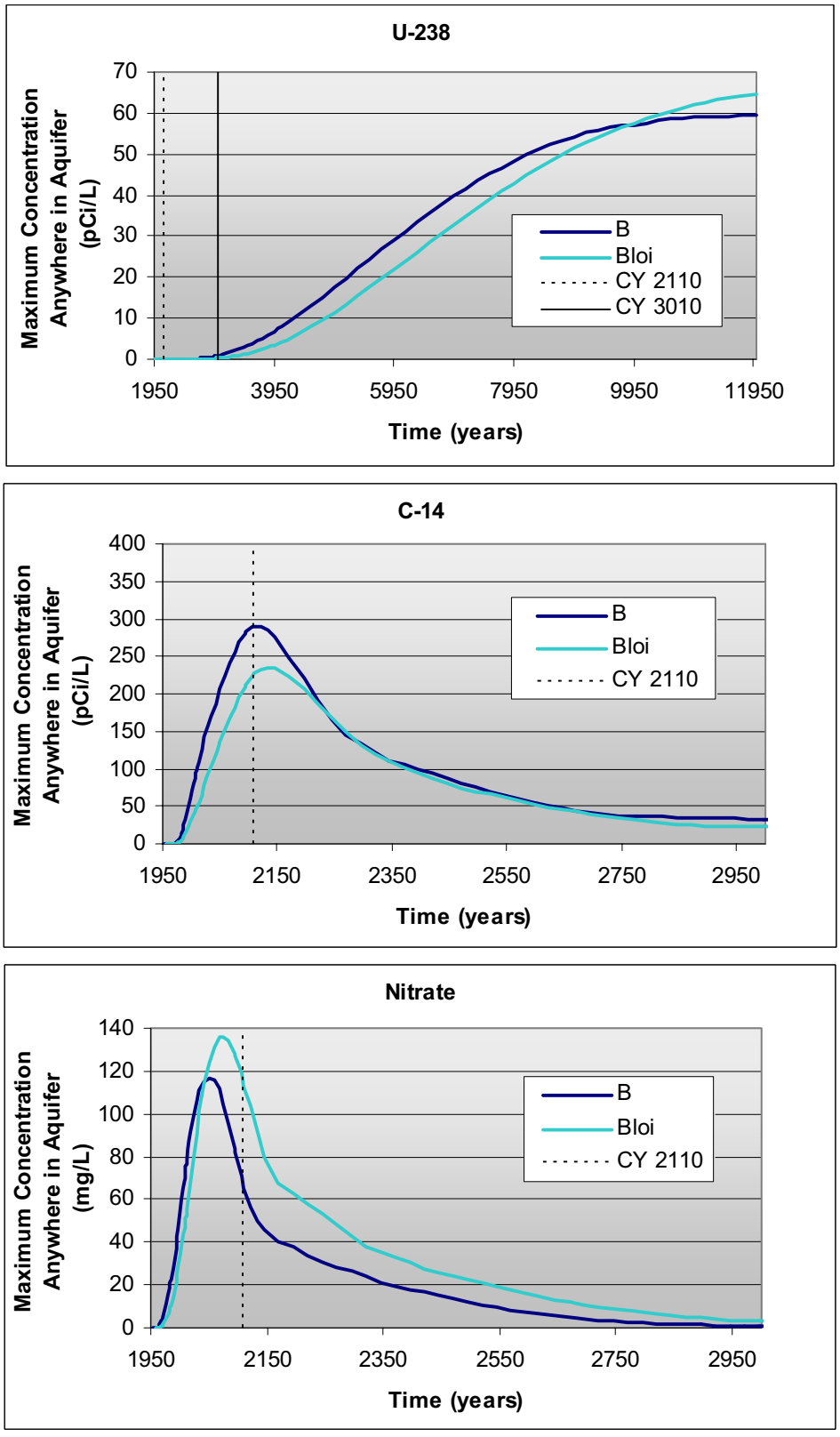

Figure 6-35. Comparison of the base (B) and low background infiltration (Bloi) maximum simulated concentration anywhere in the aquifer for uranium-238, carbon-14, and nitrate.

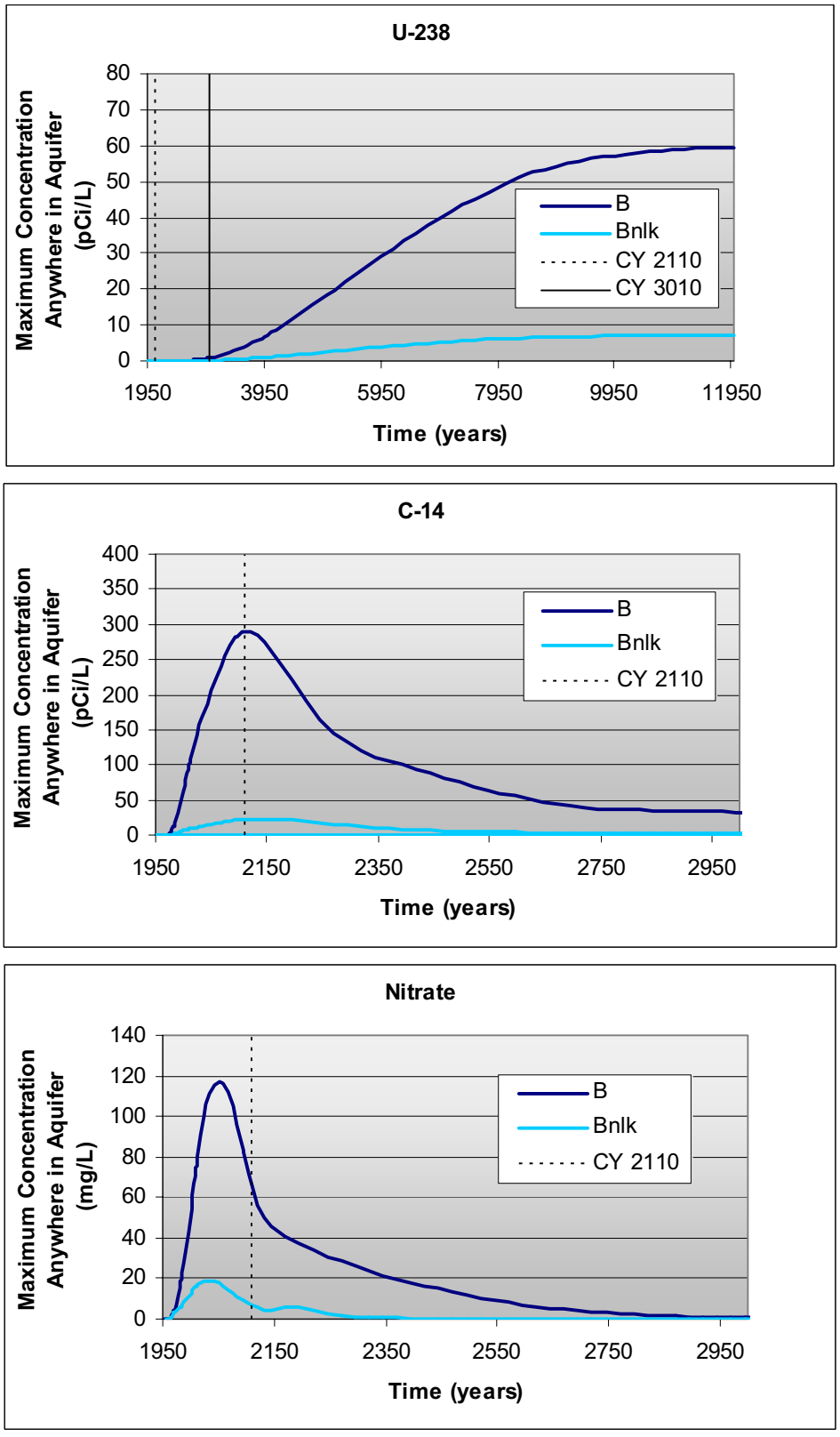

Figure 6-36. Comparison of the base (B) and no low-permeability region in aquifer (Bnlk) maximum simulated concentration anywhere in the aquifer for uranium-238, carbon-14, and nitrate.

The 300:1 ratio was a change from the 30:1 ratio that was used in the ABRA model, but was the same as the ratio that was used for the IRA model. The increase from the ABRA anisotropy value resulted from calibrating simulation results to observed CCl_4 concentrations in the vadose zone and in the aquifer, which required spreading the observed contaminant further laterally within the vadose zone domain to show better agreement between model results and monitoring results.

A possible concern with water and contaminants contacting the lateral vadose zone boundary is that resulting simulated aquifer results are inordinately affected by the boundary. In other words, if the domain extended further laterally, water and contaminants would not "pile up" at this corner of the model and potentially be forced through the interbed, thereby resulting in higher simulated aquifer concentrations than would otherwise occur.

Extending the vadose zone domain laterally, while technically feasible, could not easily be accomplished. Instead the effect of lateral movement of water and contaminants was investigated by making a series of sensitivity simulations where the anisotropy ratio was reduced. In these sensitivity simulations, water does not spread as far and behaves increasingly more like a one-dimensional simulation as the anisotropy ratio decreases and water and contaminant movement is more confined to the vertical direction.

Three different fractured-basalt anisotropy ratios were simulated in addition to the 300:1 ratio used in the RI/FS model. The ratios were 30:1, 3:1, and 1:1 with the latter case representing an isotropic condition. Cases that were simulated were the base case (B), which has no infiltration reducing cap; the modified Resource Conservation and Recovery Act Type-C barrier (FmR), with an infiltration reducing cap imposed at Calendar Year 2010; and the low-level waste performance assessment variant of the FmR run where only low-level waste contaminants were simulated (FmRpa). The contaminant group that was simulated, Group 6 (g6), included Tc-99, I-129, and Cl-36.

Comparisons of the effect of anisotropy ratios using the maximum simulated Tc-99 aquifer concentrations extracted from the second gridblock down in the aquifer are shown in Figure 6-37. For the B_g6 simulation anisotropy comparisons, the maximum concentrations are taken anywhere in the aquifer, including directly beneath the SDA, which is in contrast to locations for evaluating risk in the draft RI/BRA where the receptor location is considered to be outside the SDA fence (see Section 6.2). For the FmR_g6 and FmRpa_g6 simulations, concentration results are extracted from the same depth in the aquifer, but the area representing the SDA plus 100-m outside the SDA fence are excluded, consistent with receptor locations for the low-level waste performance assessment (see Section 6.2). For the B_g6 simulations, maximum concentrations always occur in the aquifer below the SDA or south of the SDA. Locations of the simulated maximum concentration are captured in the processing of simulation results, but are not indicated on Figure 6-37. For comparing the FmR_g6 and FmRpa_g6 simulations, maximum concentrations, for the most part, are also either beneath the SDA or south of the SDA. However, at some times up to Calendar Year 2060 in the 300:1 (base-case) simulation, the maximum concentration occurs in the extreme southeastern gridblock of the refined portion of the aquifer domain.

These results give some validity to the concern of the lateral boundary influencing the results, since there is a slight increase in the FmR and FmRpa simulated aquifer concentrations for the 300:1 anisotropy case during simulated time periods of Calendar Year 2000 to Calendar Year 2050, which is when the peak occurs in the extreme southeastern corner of the refined domain. This slight increase shows up as a "bump" in the 300:1 results. For the FmR_g6 simulation, this bump contains the overall maximum. For the FmRpa_g6 simulation, this bump does not contain the overall maximum. For the FmR_g6 simulation, however, the increase caused by this bump is still slight when compared to concentrations that occur immediately after Calendar Year 2050 along the same 300:1 anisotropy simulation result (blue diamonds). There is a local concentration maximum in this time period, which most likely represents the

peak simulated concentration if the vadose zone domain were extended to the southeast. If the chosen anisotropy ratio were appreciably higher than 300:1, which would normally further reduce simulated aquifer concentrations, the impact of the lateral boundary preventing further spreading might become more noticeable. At an anisotropy ratio of 300:1, this effect looks to be minor.

The overall effect of anisotropy on simulated aquifer concentrations appears more important than the impact of the lateral boundary. Higher anisotropy ratios spread out contaminants further in the vadose zone, and thereby reduce simulated aquifer concentrations. This result is easily seen in the B and FmR simulations, which are well-behaved with uniformly monotonic increases in the simulated aquifer concentration as the anisotropy ratio decreases. For the FmRpa case, the results are not as well behaved. The 300:1 simulation results still have the lowest overall peak concentration. The 30:1 simulation results have the highest peak overall concentration, while the 3:1 and 1:1 results have approximately the same peak concentration. Different lithologic features are controlling the peak concentrations for the 30:1, 3:1, and 1:1 cases given the difference in location where the peak occurs over time compared to the 300:1 simulation result.

Overall, the impact of changing from an anisotropy ratio of 30:1 for the ABRA to 300:1 for the current Operable Unit 7-13/14 model is to reduce simulated aquifer concentrations for all simulations performed using the RI/FS model due to dilution from additional spreading of water and contaminants in the vadose zone before they enter the aquifer model. As a reminder, the basis for this change was improved calibration for CCl_4 transport. Even with this additional dilution, the model still overpredicts concentrations compared to the observed monitoring results in the aquifer, especially for nonsorbing contaminants (see Section 6.1).

6.4.8 No Sorption in Vadose Zone Interbeds

In the RI/BRA base case, 3.7% of the Pu-239 and Pu-240 inventory for Rocky Flats Plant waste streams was mobile and moved through the surficial sediment and the A-B interbed without sorption. Sorption of the mobile plutonium did occur in the base case in the deeper, nearly continuous B-C and C-D interbeds. This section presents an extreme bounding sensitivity case that completely eliminates sorption of plutonium in both the B-C and C-D interbeds. Advective spreading during transit of the vadose zone results in some dilution as the contaminant flux is more widely spread when it enters the aquifer model domain. Other than spreading in the vadose zone model, this sensitivity case is roughly equivalent to spreading the source term laterally and leaching it directly into the aquifer. In both the RI/BRA base case and this sensitivity case, the majority of plutonium (i.e., 96.3%) undergoes sorption in the surficial sediments and interbeds with the assigned distribution coefficient of 2,500 mL/g.

Figure 6-38 shows peak simulated aquifer concentrations anywhere along the southern INL Site boundary and at the extent of the southern model domain as a function of time for the base and no sorption in the vadose zone interbeds sensitivity case. As with other results, these concentrations are extracted from the second gridblock down from the top of the aquifer domain. Simulated concentrations from the base case are very low with INL Site boundary maximums of 7E-13 pCi/L for Pu-239 and 1E-13 pCi/L for Pu-240. With the extreme bounding case of no sorption in the vadose zone, the fraction of mobile fraction of plutonium from the source model migrates past the deeper B-C and C-D interbeds and into the aquifer, resulting in simulated concentrations that are approximately fifteen orders of magnitude higher than the base case concentrations at the INL Site boundary.

Comparing simulated values through the current time to monitoring results demonstrates the lack of credibility of these results. The maximum simulated concentration results anywhere in the aquifer through 2004 for the case without sorption in the interbeds were 3E+05 pCi/L for Pu-239 and 7E+05 pCi/L for Pu-240. The detections of plutonium in the aquifer (see Section 4 of the draft RI/BRA) show an overall maximum of 4.3 pCi/L in Well M4D in 1993. Although there are other detections, they are at a low level near the minimum detectable concentration and occur very sporadically. The no-sorption sensitivity case results dramatically overpredict even the maximum monitoring results by five to six orders of magnitude. Stated another way, if the sensitivity case were at all credible, there would be easily detectible plutonium in any aquifer well in the SDA vicinity. Since this is not the case, the sensitivity simulation results are not credible as there is no basis in reality for the results.

6.5 Feasibility Study Simulations

This section briefly describes simulations to be performed for the feasibility study, which are defined in Holdren and Broomfield (2004). Contaminant groupings for the feasibility study will remain the same, except that Group 6 COPCs will be further refined. The feasibility study report will contain simulation results and additional details regarding model modifications and implementation.

Feasibility study simulations will use the base-case model, but with changes to the source release, assigned water fluxes at land surface, and other changes to reflect possible remedial alternatives. All simulations are the same as the base-case simulation until Calendar Year 2010, at which time changes are implemented.

6.5.1 Modified Resource Conservation and Recovery Act Type C Surface Barrier

In this alternative, Pad A is left in place and incorporated into a Resource Conservation and Recovery Act Type C surface barrier to be installed over the SDA. The barrier is assumed to reduce the infiltration rate to 0.1 cm/year (0.04 in./year). The background infiltration rate of 1.0 cm/year (0.4 in./year) will remain the same outside the barrier. The barrier is assumed to preclude migration of gaseous-phase contamination to the atmosphere so that shallow VVET wells will be installed adjacent to the VOC source areas and integrated into the Operable Unit 7-08 VVET units. Routine extraction from deeper wells will cease in the year 2010. The shallow extraction system will operate 10 months per year until preliminary remediation goals for CCl_4 (INEEL 2005) are achieved. This simulation will also serve as the low-level waste composite analysis simulation (see Section 6.6).

6.5.2 Evapotranspiration Surface Barrier

This alternative will include installation of an evapotranspiration surface barrier over the SDA that reduces the infiltration rate to 0.1 cm/year (0.04 in./year). The background infiltration rate of 1.0 cm/year (0.4 in./year) will remain the same outside the barrier. The barrier will include a biotic barrier and an active gas collection layer. Waste will be retrieved from Pad A and transferred to the Low-Level Waste Pit without treatment or additional engineering in the pit. The VVET system will continue routine extraction from vadose zone wells 10 months per year until preliminary remediation goals for CCl_4 (INEEL 2005) are achieved.

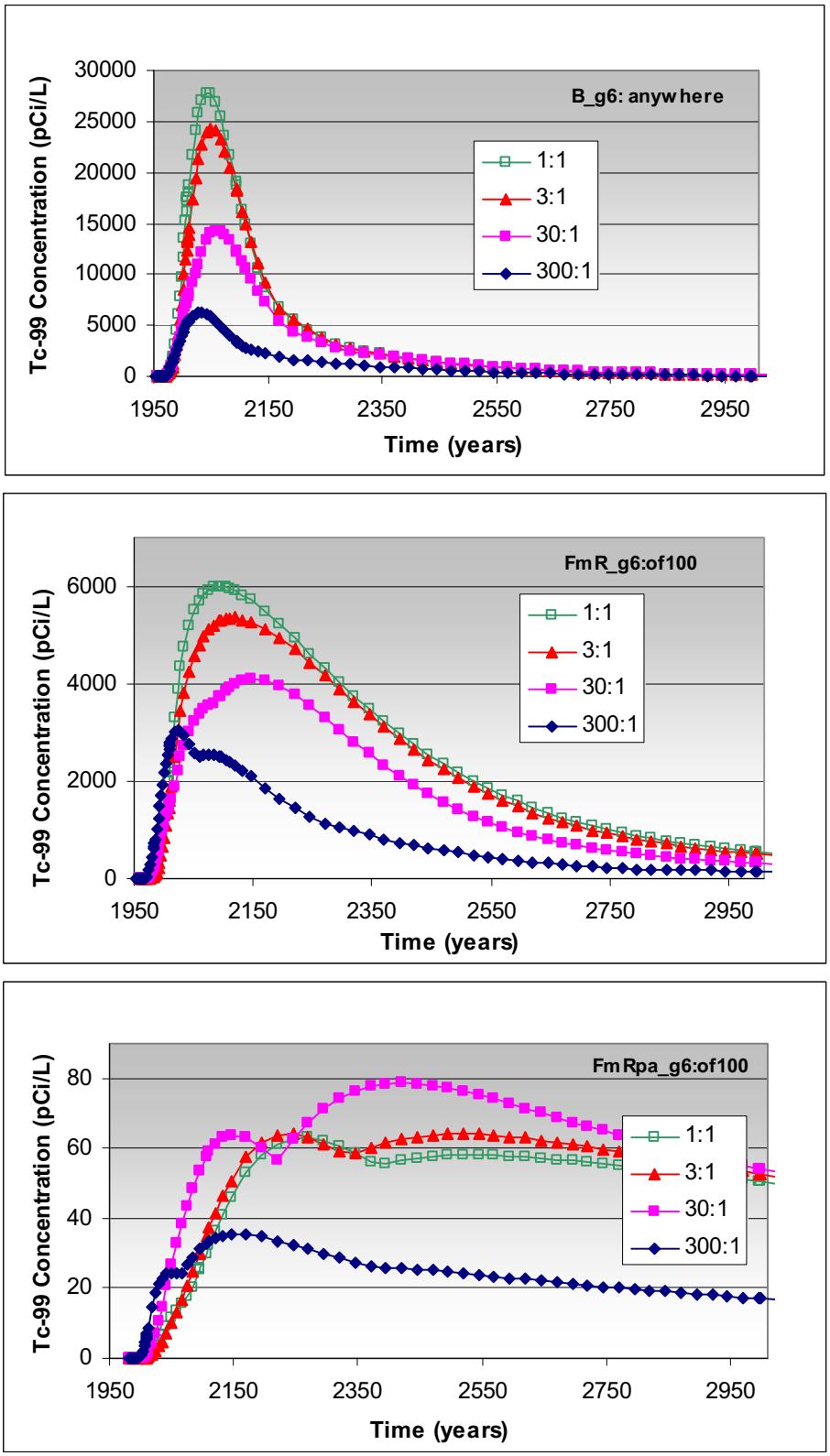

Figure 6-37. Time history of maximum simulated aquifer concentrations for a range of fractured basalt anisotropy ratios for B_g6, FmR_g6, and FmRpa_g6 simulations.

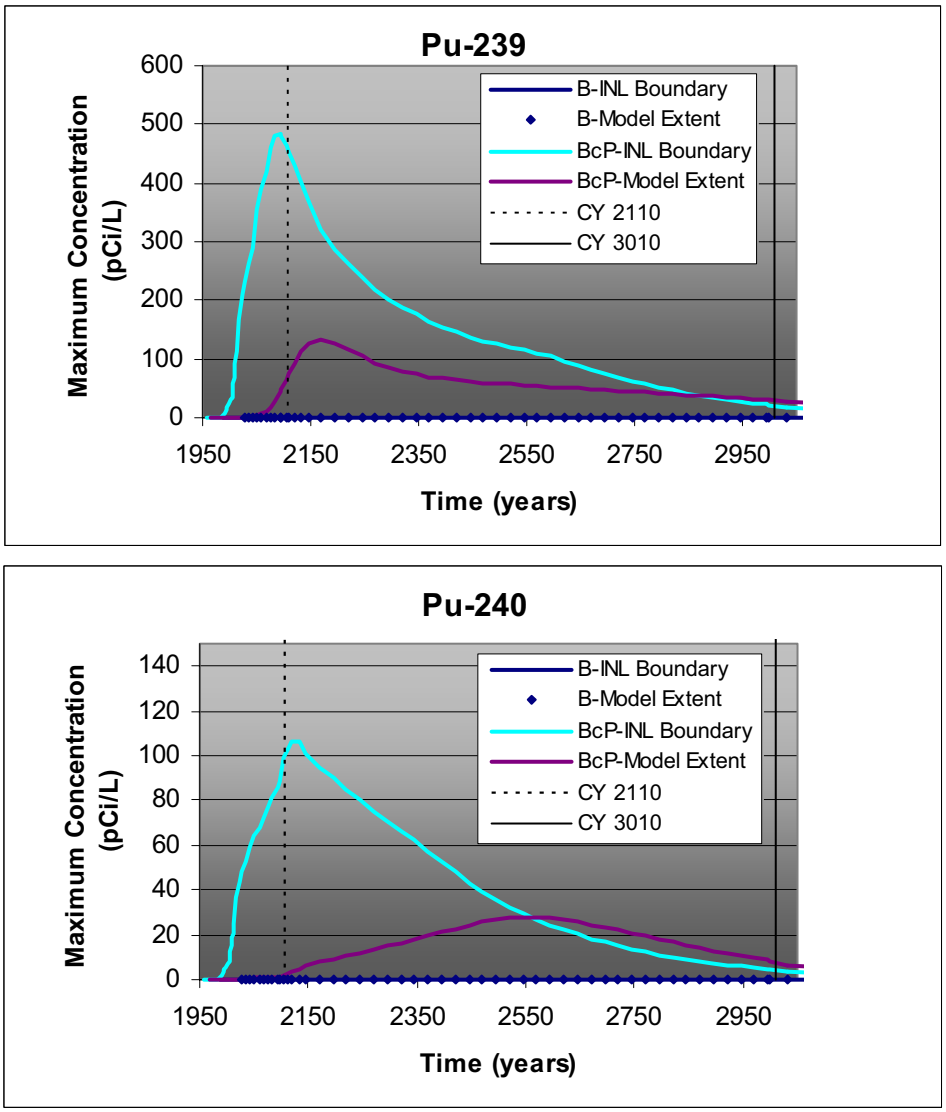

Figure 6-38. Comparison of the base (B) and the no sorption in the interbeds (BcP) maximum simulated concentration anywhere in the aquifer along the INL Site boundary and at the extreme southern extent of the model domain for plutonium-239 and plutonium-240.

6.5.3 In Situ Grouting

In this alternative, selected areas, based on contaminants of concern, will be grouted in situ. Waste from Pad A will be retrieved, treated ex situ, and returned to a pit in the SDA. The grouting only affects the release of contaminants. The waste continues to be simulated with the same hydrologic properties as surficial sediment. An evapotranspiration surface barrier that reduces the infiltration rate to 0.1 cm/year (0.04 in./year) will be installed over the SDA. The background infiltration rate of 1.0 cm/year (0.4 in./year) will remain the same outside the barrier. The barrier will include a biotic barrier and a passive gas collection layer. The VVET system will continue routine extraction from vadose zone wells 10 months per year until preliminary remediation goals for CCl_4 (INEEL 2005) are achieved.

6.5.4 Partial Retrieval, Treatment, and Disposal

This alternative will remove 1.6 ha (4 acres) of waste, targeting VOCs and transuranic waste. Waste from Pad A will be retrieved and sent to the Idaho Comprehensive Environmental Response, Compensation, and Liability Act Disposal Facility for treatment and disposal. An evapotranspiration surface barrier will be installed over the SDA that reduces the infiltration rate to 0.1 cm/year (0.04 in./year). The background infiltration rate of 1.0 cm/year (0.4 in./year) will remain the same outside the barrier. The barrier will include a biotic barrier and a passive gas collection layer. The VVET system will continue routine extraction from vadose zone wells 10 months per year until preliminary remediation goals for CCl_4 (INEEL 2005) are achieved. Results from this 1.6-ha (4-acre) partial retrieval, treatment, and disposal alternative can be scaled up or down to obtain approximations for retrievals of varying sizes as long as the same constituents are targeted.

6.5.5 Full Retrieval, Treatment, and Disposal

For this alternative, all buried waste will be removed. Waste from Pad A will also be retrieved and sent to the Idaho Comprehensive Environmental Response, Compensation, and Liability Act Disposal Facility for treatment, and then buried outside of the INL Site. An evapotranspiration surface barrier will be installed over the SDA that reduces the infiltration rate to 0.1 cm/year (0.04 in./year). The background infiltration rate of 1.0 cm/year (0.4 in./year) will remain the same outside the barrier. The barrier will include a biotic barrier and a passive gas collection layer. The VVET system will continue routine extraction from vadose zone wells 10 months per year until preliminary remediation goals for CCl_4 (INEEL 2005) are achieved.

6.5.6 Full Retrieval, Treatment, and Disposal with No Infiltration-reducing Cap

This is a feasibility study sensitivity case where all waste is removed and no infiltration reducing cap is placed over the SDA. This case mimics groundwater-pathway concentrations and the resulting risks that are attributable strictly to contaminants that have migrated into the vadose zone beyond the first basalt interface in the absence of an infiltration-reducing surface barrier.

6.5.7 Evapotranspiration Surface Barrier with 1.0-cm/year Infiltration

This is a feasibility study sensitivity case that is the same as the evapotranspiration surface barrier, but with a 1.0 cm/year (0.4 in./year) infiltration rate through the barrier (instead of 0.1 cm/year [0.04 in./year]), and an unchanged background infiltration rate of 1.0 cm/year (0.4 in./year). This simulation allows sensitivity to the infiltration rate through the barrier to be evaluated.

6.5.8 Modified Resource Conservation and Recovery Act Type C Surface Barrier with Low Background Infiltration

This is another feasibility study sensitivity case that is the same as the Modified Resource Conservation and Recovery Act Type C Surface Barrier simulation, except the background infiltration outside the SDA is assigned 0.1 cm/year (0.04 in./year) instead of 1.0 cm/year (0.4 in./year). This simulation allows sensitivity to the assigned background infiltration rate to be evaluated.

6.6 Radiological Low-Level Waste Performance Assessment Simulations

The radiological composite analysis and low-level waste performance assessment is being updated to maintain consistency with the fate and transport model used for the RI/FS. The composite analysis addresses the entire waste inventory buried in the SDA and uses radiological results from the Modified Resource Conservation and Recovery Act Type C Surface Barrier simulation defined in Section 6.5.1. A version of the Modified Resource Conservation and Recovery Act Type C Surface Barrier was also assumed for the performance assessment. For the purposes of the performance assessment and compliance with DOE O 435.1, the active low-level waste disposal facility has been defined to include Pits 17 through 20 and the soil vault rows. Additional simulations were required for the performance assessment to distinguish releases from the operating facility from contributions from the historical source terms. For all radionuclide simulations, except C-14, all source areas were nulled out, except for the soil vault rows, Pits 17 through 20, and the projected low-level waste disposal. These source areas are identified in Figure 4-21 as SVRs, P17-20, and LLW_proj. For the C-14 simulation, all source areas except Soil Vault Row 17, Soil Vault Row 20, and post-83 were nulled out. These source areas are identified in Figure 4-22. For the performance assessment simulations, only radiological COPCs were simulated.

Simulated aquifer concentrations were extracted using the same method described above and transferred to personnel conducting updates for the performance assessment and composite analysis. Simulation results were archived, along with those for the draft RI/BRA and the feasibility study.

7. SUMMARY

The groundwater-pathway flow and transport model previously used for the ABRA has been updated for use in the Operable Unit 7-13/14 RI/FS and radiological performance assessment and composite analysis. The updates consisted of the following:

1. Correcting slight errors in the ABRA

2. Using additional lithologic information from wells drilled subsequent to the ABRA modeling

3. Using additional hydrologic information from cores obtained subsequent to the ABRA modeling

4. Revising the spatially varying infiltration rate applied at the surface, including revising these same rates as they were used in the source-release modeling

5. Comparing updated model flow results to spatial trends observed with the deep tensiometer monitoring network

6. Removing the influence of additional water from the spreading areas above the C-D interbed in the vadose zone because it primarily served to dilute simulated aquifer concentrations for contaminants with long-half lives

7. Extending the aquifer domain southwestward

8. Recalibrating the CCl_4 dual-continua model, with the updated model having the larger CCl_4 inventory

9. Using the calibrated dual-continua model to simulate C-14 when it was allowed to partition into the gaseous phase and diffuse through the upper surface of the simulation domain

10. Including facilitated transport of Pu-239 and Pu-240 in the surficial sediment and A-B interbed

11. Making comparisons between simulated COPC concentrations and field-monitoring results in the surficial sediment, the vadose zone, and the aquifer. Comparisons were made for those analytes that have been identified as possibly being above background and exhibiting trends.

The RI/FS model mimics the observed large-scale trend of wetter conditions in the B-C interbed inside the SDA compared to outside. These field observations support the key conceptual model component that infiltration is higher inside the SDA than outside. For dissolved-phase transport, the results from the model are mixed. At some locations, the model underpredicts observed values, such as U-238 in the vadose zone. Some portions of this underprediction are due to gridblock averaging in the vadose zone model. In general, however, the model is conservative, because, at a larger scale, the simulated aquifer concentrations are either slightly underpredicted, in the case of chromium, or overpredicted, in the case of nitrate and Tc-99. The latter is overpredicted to the extent that the source release for Tc-99 will be revised and additional simulations performed for the feasibility study. The other contaminants that were simulated are predicted to be either not in the aquifer yet or to be present at concentrations below detectable levels. This disregards sporadic detections of plutonium isotopes and Am-241 as anomalies.

For transport of contaminants that partition between the aqueous and gaseous phases, the model generally mimics the observed spread and impact of the CCl_4 plume in the vadose zone and aquifer. The calibration to CCl_4 was successful. The impact of allowing C-14 to partition into the vapor phase was to reduce, by two orders of magnitude, the simulated groundwater-pathway concentrations. While there have been some C-14 detections in aquifer-monitoring wells, the model simulated concentrations still slightly overpredict observed values.

Considering that some portions of the modeling show representative behavior and others show conservative (e.g., overpredicting groundwater-pathway concentrations), the updated model developed to represent flow and transport in the groundwater pathway is appropriate to use in the RI/FS. This updated RI/FS model was used to simulate flow and transport of COPCs for the base case (i.e., no-action), sensitivity cases, and the feasibility study simulations. Results from the modified Resource Conservation and Recovery Act Type C surface barrier simulation also were used for comparison to the low-level waste comprehensive analysis. A variant of this simulation with only low-level waste streams provides results for the radiological low-level waste performance assessment. Some of the sensitivity cases were also simulated with just the low-level waste streams. In addition to the RI/BRA base-case and related sensitivity simulation results, the same parameterized flow and transport model was run with modifications to the infiltration rate and source release to reflect possible remedial alternatives for the feasibility study. These simulations are identified within this document.

All input files, TETRAD results files, and PV-Wave processing routines used to extract and portray the results are archived electronically. Appendix B describes this archive.

7.1 Limitations

The primary limitation of the RI/FS flow and transport model is the lack of definitive calibration targets for dissolved-phase transport of contaminants buried in the SDA down through the vadose zone. This lack of targets results from the complexity of flow and transport in the fractured basalt. On large scales with strong forcing functions, such as the Large-Scale Infiltration Test, the flow and transport has been shown to be primarily gravity-driven with little large-scale horizontal transport until an interbed was encountered. But with lower ambient infiltration conditions inside the SDA, heterogeneous waste disposal, and preferential flow in the fractured basalt, detecting large scale trends useful for model calibration has been difficult. Lower infiltration makes transport slower and, therefore, requires longer times to detect trends. Although the monitoring network in the vadose zone has been improved, preferential transport within fractured basalt makes it difficult to ensure that migrating contaminants have been or will be detected. While this lack of definitive large-scale transport for calibration is good from an overall environmental impact perspective, it does limit the ability to conclusively demonstrate that the transport represented from the model emulates the system.

Absent these calibration targets, the RI/FS model primarily still relies on comparisons between simulated and observed concentrations in the aquifer to make conclusions that the model is generally conservative. These aquifer comparisons have another limitation—uncertainty as to whether upgradient facilities, such as the Reactor Technology Complex or the Idaho Nuclear Technology and Engineering Center, contribute to contamination observed in the aquifer at the SDA. Absent this uncertainty, the model could be calibrated to mimic chromium, for example.

On a more positive note, the RI/FS model does include calibration and comparisons to measured interbed matric potentials from the deep tensiometer monitoring network and to CCl_4 transport in the vadose zone and aquifer, and can be seen to represent their general behavior. As a result, the model can be used to make predictive simulations for risk assessment with acknowledgment of uncertainty.

7.2 Uncertainty/Sensitivity

Uncertainty regarding flow and transport results is discussed qualitatively in this section, based on information obtained through performing sensitivity simulations in Section 6.4. Model uncertainty describes the degree to which a model represents the physical system being simulated. All models are simplifications of real physical systems. The issue is whether the model contains enough detail to adequately represent the physical system to the degree required, and whether the appropriate choice of inputs can be made to emulate that physical system. Quantifying model uncertainty is difficult. At best, uncertainty can be minimized by comparing results to known solutions and by calibrating the model to measured data.

Models used for this risk assessment were compared to measured data. Some components of the models had fewer available comparison data than others. The following list identifies those characteristics with the greatest effect on model uncertainty:

- Input from the source-release model—Contaminant inventories and release mechanisms are a primary source of uncertainty in the groundwater-pathway model results. Uncertainties in the flow and transport models have the potential to affect the groundwater-pathway concentrations, but not usually to the extent that the source-release modeling uncertainties do.

- Amount of water infiltrating through the waste, contacting the waste, and leaching contaminants from the waste—The current estimated infiltration rates inside the SDA, ranging from a background value of 1 cm/year (0.4 in./year) to as high as 10 cm/year (4 in./year), are reasonably conservative for the RI/FS model. These infiltration rates, applied as constants in perpetuity, should be conservative because over time natural processes of revegetation, sediment deposition, and compaction will likely reduce overall infiltration toward the lower background rate.

- Rate and direction of water and contaminant movement undergoing preferential flow through the fractured basalt portions of the vadose zone—Uncertainty is conservatively addressed through hydrologic parameterization that ensures rapid movement without any chemical interaction that would slow transport.

- Low-permeability region included in the aquifer flow and transport simulation—This low-permeability region limits dilution that may be occurring in the real system. The simulated aquifer concentrations in this region are dominated by water and contaminants entering from the vadose zone due to low horizontal velocities in the aquifer as water diverts around the low-permeability zone.

- Use of steady-state flow conditions in the vadose zone—Steady-state conditions, coupled with an assumption of linear equilibrium sorption, limits any potential influence from reactive transport that may be rate limited. While equilibrium sorption conditions are likely appropriate at depth in the vadose zone, where transient flow events get dampened, they may not be as appropriate in the near-field source area.

7.3 Areas for Improvement of the Remedial Investigation and Baseline Risk Assessment Model

Although the RI/FS model performs adequately for evaluating field-scale contaminant transport, because it provides conservative estimates of groundwater-pathway concentrations, there are still areas that could be improved. These are

- Determining whether upgradient facilities contribute to observed chromium would remove uncertainty regarding use of aquifer concentrations as calibration targets.

- Continued monitoring of the vadose zone and aquifer locations to obtain data to compare against model predictions to ensure the model remains reasonably conservative.

- Localized models, such as a two-dimensional, cross-sectional model, could better mimic chloride brine transport that results from infiltration through roadway ditches. This modeling would provide a cross check on appropriateness of the simplified treatment of flow through the fractured basalt in the RI/FS model.

- Limited quantitative evaluation of uncertainty could be accomplished using the approach developed for the low-level waste performance assessment, where a one-dimensional vadose zone model coupled with a three-dimensional aquifer model is calibrated to the results of the three-dimensional RI/FS model. The one-dimensional model is then run in a probabilistic fashion with inputs varied to assess a range of possible conditions.

8. REFERENCES

Anderson, Danny L. and Bruce H. Becker, 2006, *Source Release Modeling Report for OU 7-13/14*, ICP/EXT-05-01039, Idaho National Laboratory, Idaho Cleanup Project.

Anderson, S. R., D. J. Ackerman, M. J. Liszewski, and R. M. Freiburger, 1996, *Stratigraphic Data for Wells at and Near the Idaho National Engineering Laboratory, Idaho*, USGS Open-File Report 96 248, U.S. Department of Energy Idaho Operations Office DOE/ID-22127, U.S. Geological Survey.

Ansley, Shannon L., Catherine M. Helm-Clark, and Swen O. Magnuson, 2004, *Updated Stratigraphic Selections for Wells in the Vicinity of the Subsurface Disposal Area*, ICP/EXT-04-00207, Rev. 0, Idaho National Engineering and Environmental Laboratory, Idaho Completion Project.

Auer, L. H., N. D. Rosenberg, K. H. Birdsell, and E. M. Whitney, 1996, "The Effects of Barometric Pumping on Contaminant Transport," *Journal of Contaminant Hydrology*, Vol. 24, pp. 145–166.

Baca, R. G., S. O. Magnuson, H. D. Nguyen, and P. Martian, 1992, *A Modeling Study of Water Flow in the Vadose Zone Beneath the Radioactive Waste Management Complex*, EGG-GEO-10068, Rev. 0, Idaho National Engineering Laboratory.

Batcheller, Thomas A. and George D. Redden, 2004, *Colloidal Plutonium at the OU 7-13/14 Subsurface Disposal Area: Estimate of Inventory and Transport Properties*, ICP/EXT-04-00253, Idaho National Engineering and Environmental Laboratory, Idaho Completion Project.

Bear, J., 1972, "Dynamics of fluids in Porous Media," New York: American Elsevier Publishing Co.

Becker, B. H., J. D. Burgess, K. J. Holdren, D. K. Jorgensen, S. O. Magnuson, and A. J. Sondrup, 1998, *Interim Risk Assessment and Contaminant Screening for the Waste Area Group 7 Remedial Investigation*, DOE/ID-10569, Rev. 0, U.S. Department of Energy Idaho Operations Office.

Bishop, C. W., 1991, *Hydraulic Properties of Vesicular Basalt*, M.S. Thesis: University of Arizona, Tucson, Arizona.

Case, Marilyn J., Arthur S. Rood, James M. McCarthy, Swen O. Magnuson, Bruce H. Becker, and Thomas K. Honeycutt, 2000, *Technical Revision of the Radioactive Waste Management Complex Low-Level Waste Radiological Performance Assessment for Calendar Year 2000*, INEEL/EXT-00-01089, Idaho National Engineering and Environmental Laboratory.

Cecil, L. D., J. R. Pittman, T. M. Beasley, R. L. Michel, P. W. Kubik, P. Sharma, U. Fehn, and H. Gove, 1992, "Water Infiltration Rates in the Unsaturated Zone at the Idaho National Engineering Laboratory Estimated from Chlorine-36 and Tritium Profiles, and Neutron Logging," edited by Y. K. Kharaka and A. S. Meest, *Proceedings of the 7th International Symposium on Water-Rock Interaction*, *Park City, UT*, WRI-7, Rotterdam: Balkema.

Colwell, F. S., 1988, *Final Report: Microbial Examination of the RWMC Surface and Subsurface Soils and Biodegradation of Low Molecular Weight Hydrocarbons Using Microorganisms Indigenous to RWMC*, ST-BEG-03-88, Idaho National Engineering Laboratory.

DOE-ID, 2004, *Idaho National Engineering and Environmental Laboratory Operable Unit 10-08 Sitewide Groundwater Model Work Plan*, DOE/NE-ID-11188, Rev. 0, U.S. Department of Energy Idaho Operations Office.

DOE O 435.1, 2001, "Radioactive Waste Management," Change 1, U.S. Department of Energy.

EPA, 1999, *Understanding Variation in Partition Coefficient, K_d Values*, EPA 402-R-99-004A&B, U.S. Environmental Protection Agency.

Fabryka-Martin, J., A. Flint, and G. Gee, 1998, "Peer Review Team Report on Conceptual Models and Field Verification of Radionuclide Transport through the Vadose Zone at INEEL," Final Report, November 5, 1998, prepared for Idaho National Engineering and Environmental Laboratory.

Falta, R. W., I. Javandel, K. Pruess, and P. A. Witherspoon, 1989, "Density-Driven Flow of Gas in the Unsaturated Zone due to the Evaporation of Volatile Organic Compounds," *Water Resources Research*, Vol. 25, No. 10.

Fjeld, R. A., J. T. Coates, and A. W. Elzerman, 2000, *Final Report, Column Tests to Study the Transport of Plutonium and Other Radionuclides in Sedimentary Interbed at INEEL*, INEEL/EXT-01-00763, Rev. 0, Clemson University, Department of Environmental Engineering and Science, Clemson, South Carolina, for the Idaho National Engineering and Environmental Laboratory.

Freeze, R. A. and J. A. Cherry, 1979, *Groundwater*, Englewood Cliffs, New Jersey: Prentice-Hall.

GE, 1989, *Nuclides and Isotopes Fourteenth Edition Chart of the Nuclides*, General Electric Nuclear Energy.

Gelhar, L. W., 1986, "Water Resources Research," Vol. 22, No. 9, August 1986 Supplement, pp. 135S–145S.

Grossman, C. J., R. A. Fjeld, J. T. Coates, and A. W. Elzerman, 2001, *Task 7 Final Report: The Sorption of Selected Radionuclides in Sedimentary Interbed Soils from the Snake River Plain*, Administrative Record No. 24484, Prepared by the Department of Environmental Engineering and Sciences, Clemson University, Clemson, South Carolina, for the Idaho National Engineering and Environmental Laboratory.

Holdren, K. Jean and Barbara J. Broomfield, 2004, *Second Addendum to the Work Plan for the OU 7-13/14 Waste Area Group 7 Comprehensive Remedial Investigation/Feasibility Study*, DOE/ID-11039, U.S. Department of Energy Idaho Operations Office.

Holdren, K. Jean, Bruce H. Becker, Nancy L. Hampton, L. Don Koeppen, Swen O. Magnuson, T. J. Meyer, Gail L. Olson, and A. Jeffrey Sondrup, 2002, *Ancillary Basis for Risk Analysis of the Subsurface Disposal Area*, INEEL/EXT-02-01125, Rev. 0, Idaho National Engineering and Environmental Laboratory.

Housley, L. T., A. J. Sondrup, and M. D. Varvel, 2002, *A Compilation of Results from Shallow Soil-Gas Surveys of the Subsurface Disposal Area for Operable Unit 7-08*, INEEL/EXT-01-00026, EDF-ER-263, Rev. 1, Idaho National Engineering and Environmental Laboratory.

Hubbell, J. M., 1993, *Elevation of Surficial Sediment/Basalt Contact in the Subsurface Disposal Area, Idaho National Engineering Laboratory*, EGG-ER-10794, Idaho National Engineering Laboratory.

Hubbell, J. M., M. J. Nicholl, J. B. Sisson, and D. L. McElroy, 2004, "Application of a Darcian Approach to Estimate Liquid Flux in a Deep Vadose Zone," *Vadose Zone Journal*, Vol. 3, pp. 560-569.

Hull, Larry, Idaho National Engineering and Environmental Laboratory, to K. Jean Holdren, Idaho National Engineering and Environmental Laboratory, September 25, 2003, "Plutonium Kd Post Tally Jenkin's Comment."

Hull, Larry C. and Carolyn W. Bishop, 2003, *Fate of Magnesium Chloride Brine Applied to Suppress Dust from Unpaved Roads at the INEEL Subsurface Disposal Area*, INEEL/EXT-01-01173, Rev. 0, Idaho National Engineering and Environmental Laboratory.

INEEL, 2005, *Data Quality Objectives Summary Report for the Operable Unit 7-08 Post-Record of Decision Sampling*, INEEL/EXT-2000-00814, Rev. 2, Idaho National Engineering and Environmental Laboratory, Idaho Completion Project.

Jolley, Wendell, 2003, "Fiscal Year 2003 Pumping Test Results from Wells Located at the Radioactive Waste Management Complex," EDF-3777, Rev. 0, Idaho National Engineering and Environmental Laboratory.

Knobel, L. L., B. R. Orr, and L. D. Cecil, 1992, "Summary of Background Concentrations of Selected Radiochemical and Chemical Constituents in Groundwater from the Snake River Plain Aquifer, Idaho: Estimated from an Analysis of Previously Published Data," *Journal of the Idaho Academy of Science*, Vol. 28, No. 10.1, pp. 48.

Koeppen, L. Don, Gail L. Olson, Alva M. Parsons, Mitch A. Plummer, Paul D. Ritter, and A. Jeffrey Sondrup, 2005, *Fiscal Year 2004 OU 7-13/14 Environmental Monitoring Report for the Radioactive Waste Management Complex*, ICP/EXT-05-00795, Idaho National Laboratory, Idaho Cleanup Project.

Leecaster, Molly K., 2004, *Fiscal Year 2004 Geostatistical Modeling of Lithologic Characteristics in the Radioactive Waste Management Complex for OU 7-13/14*, ICP/EXT-04-00494, Idaho National Engineering and Environmental Laboratory, Idaho Completion Project.

Leecaster, Molly K., 2002, *Geostatistic Modeling of Subsurface Characteristics in the Radioactive Waste Management Complex Region, Operable Unit 7-13/14*, INEEL/EXT-02-00029, Rev. 0, Idaho National Engineering and Environmental Laboratory.

Leecaster, Molly K. and Laurence C. Hull, 2004, *Spatial Distribution of Neptunium and Uranium Partition Coefficient (K_d) for Interbed Sediments at a Radioactive Waste Subsurface Disposal Area*, ICP/EXT-03-00088, Idaho National Engineering and Environmental Laboratory, Idaho Completion Project.

Lerman, A., 1988, *Geochemical Processes: Water and Sediment Environments*, New York: John Wiley & Sons.

Lowe, Darren, Wayne Downs, Sheldon Smith, and W. Vincent Wilding, 2003, *Mass Release of Chlorinated Solvents through Oil, Adsorbent, and Polyethylene Bagging at the Radioactive Waste Management Complex*, ICP/EXT-03-00057, Rev. 0, Idaho National Engineering and Environmental Laboratory, Idaho Completion Project.

Magnuson, S. O., 1998, *Sensitivity of the SDA Flow and Transport Simulator to the Low Permeability Region in the Aquifer*, INEEL/INT-01066, Idaho National Engineering and Environmental Laboratory.

Magnuson, S. O., 1995, *Inverse Modeling for Field-Scale Hydrologic and Transport Parameters of Fractured Basalt*, INEL-95/0637, Idaho National Engineering Laboratory.

Magnuson, S. O. and D. L. McElroy, 1993, *Estimation of Infiltration from In Situ Moisture Contents and Representative Moisture Characteristic Curves for the 30', 110', and 240' Interbeds*, EG&G Engineering Design File #RWM-93-001.1, Idaho National Engineering Laboratory.

Magnuson, S. O. and A. J. Sondrup, 1998, *Development, Calibration, and Predictive Results of a Simulator for Subsurface Pathway Fate and Transport of Aqueous- and Gaseous-Phase Contaminants in the Subsurface Disposal Area at the Idaho National Engineering and Environmental Laboratory*, INEEL/EXT-97-00609, Rev. 0, Idaho National Engineering and Environmental Laboratory.

Martian, P., 2003, "Simulation of Carbon-14 Transport in a Mesoscale Experiment," MCP-3394, Rev. 0, Idaho National Engineering and Environmental Laboratory.

Martian, P., 1995, *UNSAT-H Infiltration Model Calibration at the Subsurface Disposal Area, Idaho National Engineering Laboratory*, INEL-95/0596, Idaho National Engineering Laboratory.

McCarthy, J. M., B. H. Becker, S. O. Magnuson, K. N. Keck, and T. K. Honeycutt, 2000, *Radioactive Waste Management Complex Low-Level Waste Radiological Composite Analysis*, INEEL/EXT-97-01113, Rev. 0, Idaho National Engineering and Environmental Laboratory.

McCarthy, J. M., R. C. Arnett, R. M. Neupauer, M. J. Rohe, and C. Smith, 1995, *Development of a Regional Groundwater Flow Model for the Area of the Idaho National Engineering Laboratory, Eastern Snake River Plain Aquifer*, INEL-95/0169, Rev. 1, Idaho National Engineering Laboratory.

McElroy, Deborah L. and Joel M. Hubbell, 2003, *Advanced Tensiometer Monitoring Results from the Deep Vadose Zone at the Radioactive Waste Management Complex*, INEEL/EXT-02-01276, Rev 0, Idaho National Engineering and Environmental Laboratory.

Mendoza, C. A. and E. O. Frind, 1990a, "Advective-Dispersive Transport of Dense Organic Vapors in the Unsaturated Zone, 1, Model Development," *Water Resources Research*, Vol. 26, No. 3, pp. xxx.

Mendoza, C. A. and E. O. Frind, 1990b, "Advective-Dispersive Transport of Dense Organic Vapors in the Unsaturated Zone, 2, Sensitivity Analysis," *Water Resources Research*, Vol. 26, No. 3, pp. xxx.

Miller, Eric C. and Mark D. Varvel, 2005, *Reconstructing the Past Disposal of 743-Series Waste in the Subsurface Disposal Area for Operable Unit 7-08, Organic Contamination in the Vadose Zone*, INEEL/EXT-01-00034, Rev. 1, Idaho National Laboratory, Idaho Completion Project.

Millington, R. J., 1959, "Gas Diffusion in Porous Media," *Science*, Vol. 130.

Mualem, Y., 1976, "A New Model for Predicting the Hydraulic Conductivity of Unsaturated Porous Media," *Water Resources Research*, Vol. 12, No. 3, pp. 513-522.

Nalla, Gopi, 2004, *Near-Field Simulation of Carbon-14 and Tritium Migration from Buried Beryllium Blocks in the Subsurface Disposal Area*, ICP/EXT-04-00321, Rev. 0, Idaho National Engineering and Environmental Laboratory, Idaho Completion Project.

Nimmo, J. R., K. S. Perkins, P. A. Rose, J. P. Rousseau, B. R. Orr, B. V. Twining, and S. R. Anderson, 2001, "2001 Kilometer-Scale Rapid Flow in a Fractured-Basalt Unsaturated Zone at the Idaho National Engineering and Environmental Laboratory," edited by B. H. Kueper, K. S. Novakowski, and D. A. Reynolds., *2001 Conference Proceedings*, *Toronto*, *March 26-28, 2001*.

Olson, G. L., 2004, *OU 7-13 and 7-14 Field Representative Glovebox Excavator Method Logbook – December 15, 2003 – February 24, 2004 (12/15/03 – 02/24/04) – Excavator Book*, ER-039-2004, Idaho National Engineering and Environmental Laboratory, Idaho Completion Project.

Parker, J. C., R. J. Lenhard, and T. Kuppusamy, 1987, "A Parametric Model for Constitutive Properties Governing Multiphase Flow in Porous Media," *Water Resource Research*, Vol. 23, No. 4, pp. 618-624.

Plummer, M. A., L. C. Hull, and D. T. Fox, 2004, "Transport of Carbon-14 in a Large Unsaturated Column," *Vadose Zone Journal*, Vol. 3, No. 1, pp. 109–121.

Roback, R. C., T. M. Johnson, T. L. McLing, M. T. Murrell, Shangde Luo, and Teh Lung Ku, 2001, "Uranium Isotopic Evidence for Groundwater Chemical Evolution and Flow Patterns in the Eastern Snake River Plain Aquifer," *Idaho-Geological Society of America Bulletin*, Vol. 113, No. 9, pp. 1133-1141.

Robertson, J. B., R. Schoen, and J. T. Barraclough, 1974, *The Influence of Liquid Waste Disposal on the Geochemistry of Water at the National Reactor Testing Station, Idaho, 1952-1970*, USGS Open-File Report IDO-22053, U.S. Geological Survey.

Rodriguez, R. R., A. L. Schafer, J. M. McCarthy, P. Martian, D. E. Burns, D. E. Raunig, N. A. Burch, and R. L. Van Horn, 1997, *Comprehensive RI/FS for the Idaho Chemical Processing Plant OU 3-13 at the INEEL--Part A, RI/BRA Report*, DOE/ID-10534, U.S. Department of Energy Idaho Operations Office.

Rood, A. S., 1999, *GWSCREEN: A Semi-Analytical Model for Assessment of the Groundwater Pathway from Surface or Buried Contamination, Theory and User's Manual Version 2.5*, INEEL/EXT-9800750, Idaho National Engineering and Environmental Laboratory.

Rousseau, Joseph P., Edward R. Landa, John R. Nimmo, L. DeWayne Cecil, LeRoy L. Knobel, Pierre D. Glynn, Edward M. Kwicklis, Gary P. Curtis, Kenneth G. Stollenwerk, Steven R. Anderson, Roy C. Bartholomay, Clifford R. Bossong, and Brennan R. Orr, 2005, *Review of the Transport of Selected Radionuclides in the Interim Risk Assessment for the Radioactive Waste Management Complex, Waste Area Group 7 Operable Unit 7-13/14, Idaho National Engineering and Environmental Laboratory, Idaho*, USGS Scientific Investigations Report 2005-5026, prepared in cooperation with the U.S. Department of Energy, DOE/ID-22192, U.S. Geological Survey.

Shook, G. Michael, J. Hope Forsmann, M. Elena Velasquez, and Swen O. Magnuson, 2003, "Improving Numerical Model Efficiency of an Existing, In-House Simulation Model," *Laboratory-Directed Research and Development, FY-2003 Annual Report*, INEEL/EXT-04-01772, Idaho National Engineering and Environmental Laboratory, pp. 197-199.

Smith, R. P., 2002, *Variability of the Aquifer Thickness Beneath the Idaho National Engineering and Environmental Laboratory (INEEL)*, INEEL/EXT-02-01022, Idaho National Engineering and Environmental Laboratory.

Sondrup, A. J., 1998, *Preliminary Modeling of VOC Transport for Operable Unit 7-08, Evaluation of Increased Carbon Tetrachloride Inventory*, INEEL/EXT-2000-00849, Rev. 0, Idaho National Engineering and Environmental Laboratory.

Sondrup, A. Jeffrey, Eric C. Miller, Edward H. Seabury, and Nick Josten, 2004, *Estimating Carbon Tetrachloride and Total Volatile Organic Compound Mass Remaining in Subsurface Disposal Area Pits*, ICP/EXT-04-00396, Idaho National Engineering and Environmental Laboratory, Idaho Completion Project.

van Genuchten, M. Th., 1980, "A Closed-form Equation for Predicting the Hydraulic Conductivity of Unsaturated Soils," *Soil Science Society of America Journal*, Vol. 44, pp. 892-898.

Vejvoda, Edward, 2005, *Summary of Rocky Flats Plant Waste Buried in the Subsurface Disposal Area*, ICP/EXT-04-00717, Idaho National Laboratory, Idaho Completion Project.

Vigil, M. J., 1988, *Estimate of Water in Pits During Flooding Events*, EDF-BWP-12, Idaho National Engineering Laboratory.

Vinsome, P. K. W. and G. M. Shook, 1993, "Multi-Purpose Simulation," *Journal of Petroleum Science and Engineering*, Vol. 9, pp. 29-38.

Visual Numerics, Inc., 2001, PV-WAVE User's Guide, unpublished work, 1990-2001.

Warren, J. E., and P. J. Root, 1963, "The Behavior of Naturally Fractured Reservoirs," *Transactions Society of Petroleum Engineers AIME*, Vol. 228, pp. 245-255.

Whitmire, D. L., 2001, *Summary Report: Simulation of Groundwater Flow near the Subsurface Disposal Area at the Idaho National Engineering and Environmental Laboratory,* INEEL/EXT-01-01643, Rev. 0, prepared by North Wind Environmental for Idaho National Engineering and Environmental Laboratory.

Wylie, A. H. and J. M. Hubbell, 1994, *Aquifer Testing of Wells M1S, M3S, M4D, M6S, M7S, and M10S at the Radioactive Waste Management Complex*, ER-WAG7-26, Rev. 1, Idaho National Engineering Laboratory.

Zitnik, James F., Aran T. Armstrong, Brian K. Corb, Mark H. Edens, Douglas B. Holsten, Patricia M. O'Flaherty, Janet Rodriguez, Tamara N. Thomas, Russell L. Treat, Wayne Schofield, and Kira L. Sykes, 2002, *Preliminary Evaluation of Remedial Alternatives for the Subsurface Disposal Area*, INEEL/EXT-02-01258, Rev. 0, prepared by CH2MHILL for the Idaho National Engineering and Environmental Laboratory.